Inaugural dissertation

for

obtaining the doctoral degree

of the

Combined Faculty of Mathematics, Engineering and Natural Sciences

of the

Ruprecht - Karls - University

Heidelberg

Presented by

Franziska Falk, M.Sc.

born in: Eberbach

Oral examination: 21.03.2022

Translation control in *Trypanosoma brucei* by mRNA cap-binding proteins and their interaction partners

Referees: Prof. Dr. Christine Clayton

Prof. Dr. Dr. Georg Stoecklin

„Wessen wir am meisten im Leben bedürfen ist jemand,

der uns dazu bringt, das zu tun,

wozu wir fähig sind.“

Ralph Waldo Emerson

Acknowledgements

I would like to express my deepest gratitude to my PhD supervisor **Prof. Dr. Christine Clayton** for the opportunity to conduct my PhD in her laboratory, for mentoring and motivating me throughout.

Many thanks to my Thesis Advisory Committee members **Prof. Dr. Luise Krauth-Siegel** and **Prof. Dr. Dr. Georg Stoecklin** for their advice, guidance, and helpful discussions. Furthermore, I am thankful that they will also take the last steps with me and review my final thesis. I really appreciate that **Prof. Dr. F. Nina Papavasiliou** will be part of the thesis committee as an expert of trypanosome biology.

I am thankful for the support by all former and current members of the Clayton Lab with whom I shared ideas and discussions throughout all achievements and setbacks. I would like to express my special gratitude to **Albina** and **Tania**, my partners in crime, as well as to **Ute** and **Claudia** for technical support and advice. I would also like to thank **Rafael** for supporting me during the final phase of my PhD project.

Apart from those, I would like to thank **Thomas Ruppert** and **Sabine Merker** from the Mass Spectrometry Core Facility, **David Ibberson**, head of the RNA Sequencing Facility, as well as **Kevin Leiss** for the help with bioinformatics tools.

Zuletzt möchte ich mich außerdem bei meinem Mann **Lukas**, meinem Papa **Michel** und meiner Mama **Uschi**, meinen Geschwistern **Ronja, Tim, Alex** und **Leonie**, sowie meiner Tante **Claudia** für ihre bedingungslose Liebe, Unterstützung und ihr Verständnis bedanken. Ganz besonders dankbar bin ich meiner Oma **Monika**, die immer für mich da war und mich mit ihrer positiven Art immer aufzuheitern vermochte.

Table of contents

List of abbreviations

Abbreviation	Description
3’-UTR	3’ untranslated region
5’-UTR	5’ untranslated region
AD	activating domain
ALBA	acetylation lowers binding affinity
BD	binding domain
BSF	bloodstream form
CAT	chloramphenicol acetyltransferase
CBC	cap-binding complex
CDK	cyclin-dependent kinase
CDS	coding sequence
DNA	deoxyribonucleic acid
DTT	dithiothreitol
EDTA	ethylenediaminetetraacetic acid
ER	endoplasmic reticulum
ES	expression site
ESAG	expression site-associated gene
FBS	fetal bovine serum
gDNA	genomic DNA
IF	immunofluorescence
kDNA	kinetoplast DNA
KO	knockout
mRNA	messenger RNA
mRNP	messenger ribonucleoprotein
MS	mass spectrometry
ORF	open reading frame
PABP	poly(A)-binding protein
PAC	puromycin N-acetyltransferase
PAD	protein associated with differentiation
PCF	procyclic form
PCR	polymerase chain reaction
qPCR	quantitative PCR
RBP	RNA-binding protein
RIP-Seq	RNA immunoprecipitation followed by next-generation sequencing
RNA	ribonucleic acid
RNAi	RNA interference
RRM	RNA recognition motif
rRNA	ribosomal RNA
RT-qPCR	reverse transcription quantitative PCR
SDS	sodium dodecyl sulfate
SIF	stumpy induction factor
SL	spliced leader
TAP	tandem affinity purification
Tet	tetracycline
VSG	variant surface glycoprotein
WT	wildtype
Y2H	yeast-two-hybrid
ZPFM	Zimmerman’s post fusion medium

List of figures

List of tables

Summary

Gene expression in *Trypanosoma brucei* lacks regulatory mechanisms at the level of RNA polymerase II transcription. The initiation step of translation is therefore a critical point for controlling gene expression. Despite being unicellular eukaryotes, the parasites are equipped with a large repertoire of EIF4E cap-binding proteins to adjust the gene expression program according to the different environments encountered in the bloodstream of a mammalian host and the tsetse fly vector, where they multiply as so-called bloodstream forms (BSFs) and procyclic forms (PCFs), respectively.

EIF4E3 and EIF4E4 are considered canonical translation initiation factors that associate with EIF4G4 and EIF4G3, respectively, to form EIF4F-like complexes that initiate bulk translation. Loss of any of the two proteins is not compatible with normal cellular life at both BSF and PCF stages. EIF4E1 and EIF4E2 act independently of EIF4G proteins, and are thus hypothesized to have regulatory functions. EIF4E1 was previously shown to act as a translational repressor by interacting with 4EIP, while EIF4E2 associates with a homolog of the histone mRNA stem-loop-binding protein, SLBP2, in PCFs. Possible functions of the two smallest members, EIF4E5 and EIF4E6, which do in turn interact with different EIF4G proteins, point towards a role in cellular integrity and motility, as evidenced by knockdown experiments in PCFs.

The aim of this work was to dissect the roles of the non-canonical EIF4E proteins in BSFs and/or PCFs, as well as during differentiation processes. Previously obtained data suggested that the functions are unlikely to be identical, but the level of redundancy was to be addressed in this study. Loss-of-function phenotypes were assessed, protein interaction partners were analyzed by quantitative mass spectrometry and yeast-2-hybrid experiments, and associated mRNAs were examined by qPCR and RNA sequencing.

Despite accumulating evidence in *Leishmania*, a translation-promoting function of EIF4E1 without 4EIP could not be confirmed. EIF4E1 was shown to associate with similar mRNA subsets in the presence and absence of 4EIP in PCFs, where it is essential. In contrast, its binding partner 4EIP is required for BSF to PCF differentiation, which proceeds normally without EIF4E1. The mechanisms of action of EIF4E1/4EIP are reminiscent of 4EHP/GIGYF2 complexes in mammals, which initiate translation-coupled mRNA decay. Accordingly, 4EIP-dependent associations with the terminal uridylyl transferase 3 (TUT3) and the CAF-NOT deadenylation complex were uncovered, but the uridylase activity of TUT3 was not required for 4EIP-dependent repression.

EIF4E2 was found to serve an essential role in the regulation of S-phase mRNAs in BSFs, which are known to be stabilized by the RNA-binding protein PUF9. There is evidence that the latter interacts directly with EIF4E2/SLBP2 complexes. EIF4E2 further appeared to be involved in allelic exclusion, which ensures expression of a single variant surface glycoprotein (VSG) variant at a time. The latter covers the BSF in a dense glycoprotein coat and constitutes approximately 10% of total cellular protein. Loss of EIF4E2 resulted in promiscuous expression of numerous, otherwise silenced *VSG* genes, which could be rescued by reconstitution of EIF4E2 expression.

EIF4E6 was revealed to be dedicated to promoting *VSG* mRNA translation by cooperating with activating MKT1 complexes. The latter were previously shown to be directed to target mRNAs by RNA-binding proteins. This was accomplished by the F-box-containing protein CFB2 in the case of EIF4E6. Depletion of *EIF4E6* led to a global translational shutdown in BSFs. Evidence in support of EIF4E3 providing additional translational initiation at *VSG* mRNAs was obtained, likely to help the parasite cope with the high demand for VSG proteins. Collectively, the results presented highlight the independent roles of the different cap-binding proteins in *T. brucei*, and loss of a particular cap-binding protein can generally not be compensated for by others at particular life cycle stages.

Zusammenfassung

Der Genexpression in *Trypanosoma brucei* fehlt es an Regulationsmechanismen auf der Ebene der RNA-Polymerase-II-vermittelten Transkription. Folglich ist die Initiation der Translation ein ausschlaggebender Ansatzpunkt für die Kontrolle der Genexpression. Obwohl sie einzellige Eukaryoten sind, besitzen sie ein großes Repertoire an Kappe-bindenden EIF4E-Proteinen zur Anpassung des Genexpressions-Programms an die verschiedenen Wirtsumgebungen, denen sie im Blutstrom eines Säugerwirtes und in einem Tsetse-Fliegen-Vektor ausgesetzt sind, wo sie sich als sogenannte Blutstrom-Formen bzw. prozyklische Formen vermehren.

EIF4E3 und EIF4E4 gelten als kanonische Translationsinitiationsfaktoren, die mit EIF4G4 bzw. EIF4G3 assoziieren, um EIF4F-ähnliche Komplexe zu bilden, die den Großteil an Translation initiieren. Der Verlust eines der beiden Proteine ist sowohl in der Blutstromform als auch in der prozyklischen Form nicht mit dem normalen zellulären Leben vereinbar. EIF4E1 und EIF4E2 hingegen wirken unabhängig von EIF4G-Proteinen und erfüllen vermutlich regulatorische Funktionen. Es wurde zuvor gezeigt, dass EIF4E1 als translationaler Repressor wirkt, indem es mit 4EIP interagiert, während EIF4E2 mit einem Homolog des Histon-mRNA-Stemloop-bindenden Proteins, SLBP2, in prozyklischen Zellen assoziiert. Mögliche Funktionen der beiden kleinsten Mitglieder EIF4E5 und EIF4E6, die wiederum mit verschiedenen EIF4G-Proteinen interagieren, weisen auf eine Rolle bei der zellulären Integrität und Motilität hin, wie Knockdown-Experimente in prozyklischen Formen belegen.

Das Ziel dieser Arbeit war es, die Rolle der nicht-kanonischen EIF4E-Proteine in Blutstromformen und/oder prozyklischen Formen sowie bei Differenzierungsprozessen zu analysieren. Zuvor generierte Daten deuteten darauf hin, dass ihre Funktionen wahrscheinlich nicht identisch sind, aber der Grad der Redundanz sollte in dieser Studie adressiert werden. Dazu wurden Funktionsverlust-Phänotypen bewertet, Protein-Interaktionspartner durch quantitative Massenspektrometrie und Hefe-2-Hybrid-Experimente analysiert und mRNAs, die mit ausgewählten EIF4E-Proteinen assoziiert sind, durch qPCR und RNA-Sequenzierung untersucht. Im Gegensatz zu einer Ansammlung von Daten aus *Leishmania* konnte eine translationsfördernde Funktion von EIF4E1 ohne 4EIP nicht bestätigt werden. EIF4E1 assoziierte mit ähnlichen mRNA-Untergruppen in Gegenwart und Abwesenheit von 4EIP in prozyklischen Formen, für welche es essentiell ist.

Im Gegensatz dazu wird sein Bindungspartner 4EIP für die Differenzierung von der Blutstromform zur prozyklischen Form benötigt, welche normal ablaufen kann ohne EIF4E1. Die Wirkmechanismen von EIF4E1/4EIP erinnern an 4EHP/GIGIF2-Komplexe in Säugetieren, die den translationsgekoppelten mRNA-Abbau initiieren. Dementsprechend wurden 4EIP-abhängige Assoziationen mit der terminalen Uridylyltransferase 3 (TUT3) und dem CAF-NOT-Deadenylierungskomplex aufgedeckt, aber die Uridylaseaktivität von TUT3 war für die 4EIP-abhängige Repression nicht erforderlich. Es wurde festgestellt, dass EIF4E2 eine wesentliche Rolle bei der Regulation von S-Phase-mRNAs in Blutstromformen spielt, von denen bekannt ist, dass sie durch das RNA-bindende Protein PUF9 stabilisiert werden. Es gibt Hinweise darauf, dass letzteres direkt mit EIF4E2/SLBP2-Komplexen interagiert. EIF4E2 schien ferner am Allel-Ausschluss beteiligt zu sein, der die Expression einer einzelnen Variante des Oberflächenglykoproteins (VSG) zu einem gegebenen Zeitpunkt sicherstellt. Letzteres bedeckt die Blutstromform mit einer dichten Glykoproteinhülle und macht daher etwa 10% des gesamten zellulären Proteins aus. Der Verlust von EIF4E2 führte zu einer vermischten Expression zahlreicher, ansonsten stummgeschalteter *VSG*-Gene, die durch Rekonstitution der EIF4E2-Expression gerettet werden konnten. Es wurde gezeigt, dass EIF4E6 die Translation der *VSG*-mRNA vermittelt, indem es mit aktivierenden MKT1-Komplexen kooperiert. Für letztere wurde zuvor gezeigt, dass sie durch verschiedene RNA-bindende Proteine zu Ziel-mRNAs geleitet werden. Dies

wurde im Fall von EIF4E6 durch das F-Box-enthaltende Protein CFB2 erreicht. Dementsprechend führte der Verlust der EIF4E6-Expression zu einem globalen translationalen Shutdown in Blutstromformen. Es gibt Hinweise darauf, dass EIF4E3 zusätzlich die translationale Initiation an *VSG*-mRNAs ermöglicht, was dem Parasiten wahrscheinlich hilft, den hohen Bedarf an VSG-Protein zu decken. Insgesamt heben die präsentierten Ergebnisse die unabhängigen Rollen der verschiedenen Cap-bindenden Proteine in *T. brucei* hervor, und der Verlust eines bestimmten Cap-bindenden Proteins in bestimmten Lebenszyklusstadien kann im Allgemeinen nicht durch andere kompensiert werden.

1. Introduction

1.1 Kinetoplastida

Protozoan parasites of the order Kinetoplastida are flagellated unicellular organisms that feature a unique structure, the kinetoplast. It is composed of thousands of interlocked circular DNA molecules within the mitochondrion and is located at the base of the flagellum [1].

Organisms of the order Kinetoplastida include species of the genera *Leishmania* and *Trypanosoma*, which include intra- and extracellular parasites known to cause infectious diseases in humans and animals [2]. These are usually transmitted by arthropods [3]. In the case of *Trypanosoma brucei,* the tsetse fly (*Glossina* spp.) serves as a vector. Parasites of the *T. b. gambiense* subspecies are most prevalent in central and Western Africa, causing chronic human African trypanosomiasis (HAT, or sleeping sickness), which generally progresses slowly over several years. The subspecies *T. b. rhodesiense*, which is common in Eastern Africa, is responsible for fast-onset HAT, which usually lasts several weeks to months, and accounts for around 3% of HAT cases [4].

During the early stage, parasites multiply in the skin, lymph, and blood of infected individuals, causing rather unspecific symptoms, including itching, headaches, fever, as well as muscle and joint pain. Once the parasite has crossed the blood-brain barrier, the disease progresses to the late stage as parasites populate the central nervous system. It then causes altered sleeping cycles, deep sensory disturbances, psychiatric disorders, seizures, coma, and usually death in the absence of treatment [5, 6].

During the early stage, infections with *T. b. rhodesiense* and *T. b. gambiense* are treated with suramin and pentamidine, respectively. Later stages are treated with melarsoprol (*T. b. rhodesiense* and *gambiense*) or nifurtimox-eflornithine combination therapy (*T. b. gambiense*). The drugs used to treat HAT require long administration periods, high doses, and are generally toxic, causing numerous side effects, such as melarsoprol-induced encephalopathy (5-10% of patients) [5, 7, 8].

Animal trypanosomiasis or nagana is caused by several *Trypanosoma* species, predominantly by *T. congolense* and *T. vivax,* representing a high socio-economic burden by decimating the number of livestock and domestic animals. Furthermore, *T. brucei brucei* parasites are responsible for a minor fraction of nagana cases. However, the human immune system can efficiently eliminate parasites associated with nagana-causing subspecies, making *T. b. brucei* parasites a valuable model organism commonly cultured in the laboratory for studying trypanosome biology, including this work [2, 9].

American trypanosomiasis (or Chagas disease), on the other hand, is caused by *Trypanosoma cruzi*, which cycles between triatomines and humans [10]. Kinetoplastids of the *Leishmania* genus are causative agents of cutaneous, mucocutaneous, or visceral Leishmaniasis in tropical or subtropical countries [11].

1.2 Trypanosomes as model organisms for biological studies

Trypanosomes are spindle-shaped unicellular eukaryotes ranging from 8 to 50 µm in length and 1.5 to 3.5 µm in diameter, depending on the life cycle stage [12, 13]. Furthermore, all classical eukaryotic organelles can be identified, including a nucleus, lysosomes, endo- and exocytosis systems, a Golgi apparatus, and an endoplasmic reticulum (ER), as well as a single flagellum that runs along the trypanosome axis (**Figure 1.1**). The latter is important for cell polarity and segregation during cell division, and also allows the cell to swim with the flagellum tip leading. An invagination of cell membrane around the base of the flagellum, the so-called flagellar pocket, is the only known site of endo- and exocytosis [14].

The two major forms cultured in the laboratory are the procyclic form (PCF) that is naturally found in the digestive system of tsetse flies, and the bloodstream form (BSF) that multiplies extracellularly in mammalian blood and tissue fluids. BSFs are grown in a high glucose environment, as glycolysis constitutes the main pathway of energy production by generating ATP from substrate-level phosphorylation. Most glycolytic enzymes are localized within a specialized microbody-like organelle, the glycosome, constituting another peculiarity of trypanosomes [15, 16]. At the BSF stage, the function of the mitochondrion is largely repressed. In contrast, amino acids are used as substrates for energy production through oxidative phosphorylation in the PCF [17].

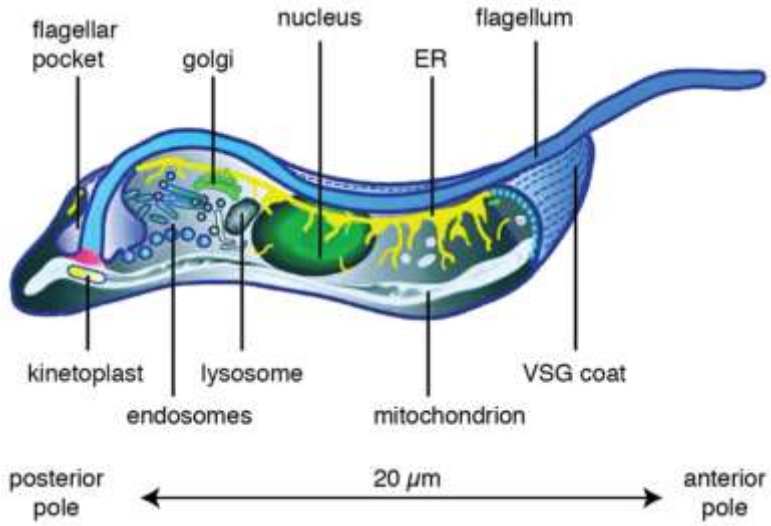

Figure 1.1 Trypanosome morphology. Schematic representation of trypanosome morphology (bloodstream form). Adapted from Grünfelder et al., 2003 [18]

1.3 The life cycle of *T. brucei*

The digenic life cycle of *T. brucei* involves multiplication of different developmental stages in both the mammalian host and blood-feeding tsetse fly (**Figure 1.2**). Posterior and anterior positioning of the kinetoplast allows for differentiation between trypomastigote and epimastiogte morphologies, respectively. In a mammalian host, trypomastigote BSFs are multiplying in the blood and tissue fluids. At this stage, the parasite is characterized by a long slender morphology and a dense surface coat of the glycosylphosphatidylinositol (GPI)-anchored major surface protein, variant surface glycoprotein (VSG) [19, 20].

The VSG coat is highly immunogenic, allowing the host organism to mount a strong adaptive immune response. Trypanosomes escape clearance by a mechanism called antigenic variation, during which a small percentage of a given population switches to a different variant, which occurs at a frequency of about 1 event per 10^3-10^5 cells, depending on the surrounding conditions [21]. At the same time, monoallelic exclusion ensures expression of only one VSG variant at a time from a large repertoire. Nearly 30% of the genome are dedicated to *VSG* sequences, including ca. 2000 genes, fragments, and pseudogenes, which can be recombined to create an unlimited repertoire of variants [22, 23]. As a consequence, waves of parasitemia are characteristic of an infection with *T. brucei*, as they are always one step ahead of the host's immune response. At peak parasitemia of long slender BSFs, a threshold level of a quorum sensing molecule, the so-called stumpy induction factor (SIF), is reached. This leads to developmental stage transition of a fraction of the population to the stumpy stage. This

is presumed to (i) serve as a means to control the parasite load within the host and (ii) lead to a pre-adapted state for successful infection of a tsetse fly [24, 25].

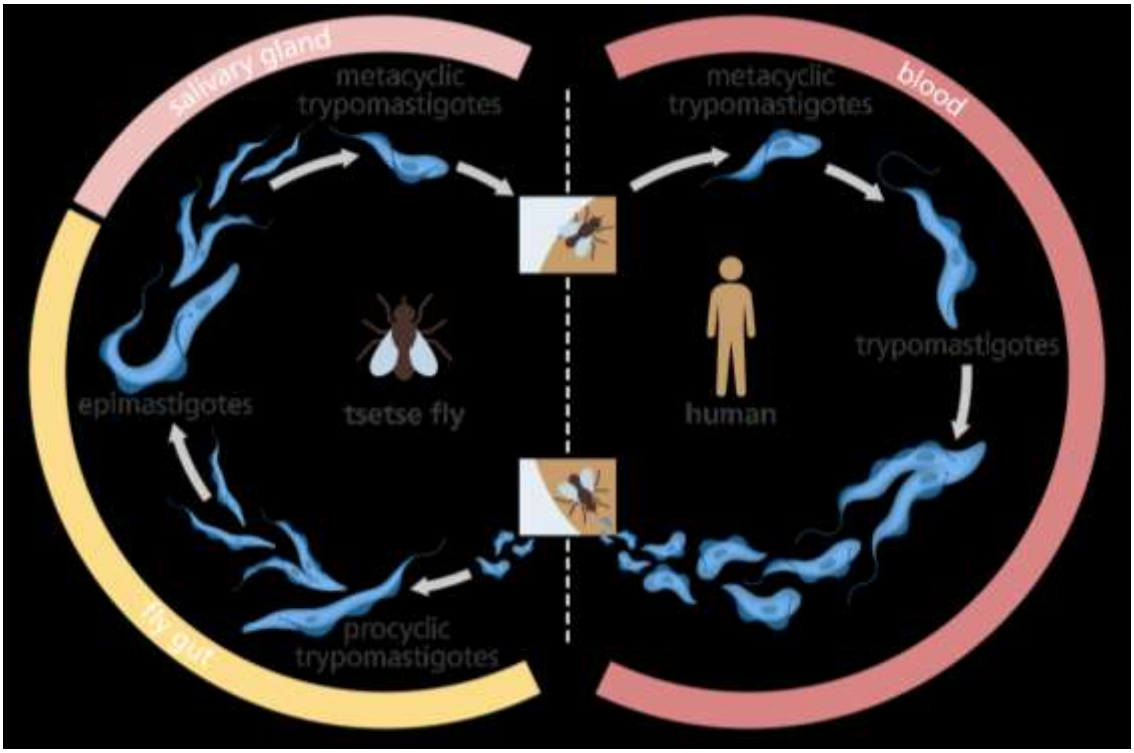

Figure 1.2 The digenic life cycle of *Trypanosoma brucei*. Schematic representation of the *Trypanosoma brucei* life cycle within the human and tsetse fly host. Adapted from https://www.yourgenome.org/facts/what-is-african-sleeping-sickness

The identity of SIF has been the subject of extensive research in the past. It is now presumed that parasite load correlates with secreted protease activity, generating high levels of extracellular oligopeptides, presumably serving as SIF. This oligopeptide cocktail is thought to be sensed by BSFs through *Tb*GPR89 receptors (**Figure 1.3**). High SIF levels then lead to signaling cascades that induce stumpy formation, while low levels repress stumpy formation by activating alternative pathways [26, 27]. Once stumpy formation has been induced, a short, stumpy morphology can be observed, along with a G1/G0-phase arrest, and a shut-down of global translation. However, expression of selected factors is ensured, such as the carboxylate transporter proteins of the PAD (proteins associated with differentiation) family, of which PAD1 is expressed exclusively at this life cycle stage, therefore qualifying as a stumpy form marker [28, 29]. Lysosome relocalization to a position anterior to the nucleus was further described as a stumpy-form specific event by Vanhollebeke and colleagues [30]. Additionally, lysosome repositioning was found to occur in association with the mitochondrion, which is known to become more elaborate at this stage [30].

Other characteristics of stumpy forms include tolerance to low pH and proteolysis, presumably representing a pre-adaptation for survival in the tsetse midgut, where they, once taken up by a blood meal, differentiate into the PCF and resume growth [31, 32]. This is further characterized by kinetoplast repositioning and replacement of the VSG coat with a less dense coat composed of procyclins: GPEET and EP, which are found on early and late PCFs, respectively. Both GPEET and EP are extensively modified by phosphorylation and glycosylation, respectively. Under natural conditions, GPEET is repressed after six days, and EP becomes the major surface protein [33].

Changes in culturing conditions in the laboratory can skew expression towards re-expression of GPEET in late PCFs through treatment with glycerol or, alternatively, suppression of GPEET

expression by addition of glucose [34-36]. The so-called glycerol-responsive element (GRE), which is present in the 3'-UTR, allows for regulation of GPEET expression independently of EP [35]. The PCF then migrates along the foregut until it reaches the proventriculus, where it undergoes an asymmetric division event, resulting in long and short epimastigotes, which are characterized by cell-surface expression of BARP [19, 37]. Only short epimastigotes continue to migrate into the salivary glands to form pre-metacyclics, and, eventually, non-dividing metacyclic trypomastigotes that do already express a dense VSG coat. Upon the next blood meal, they can be transmitted to a mammalian host to complete the life cycle by differentiating into long slender trypomastigotes.

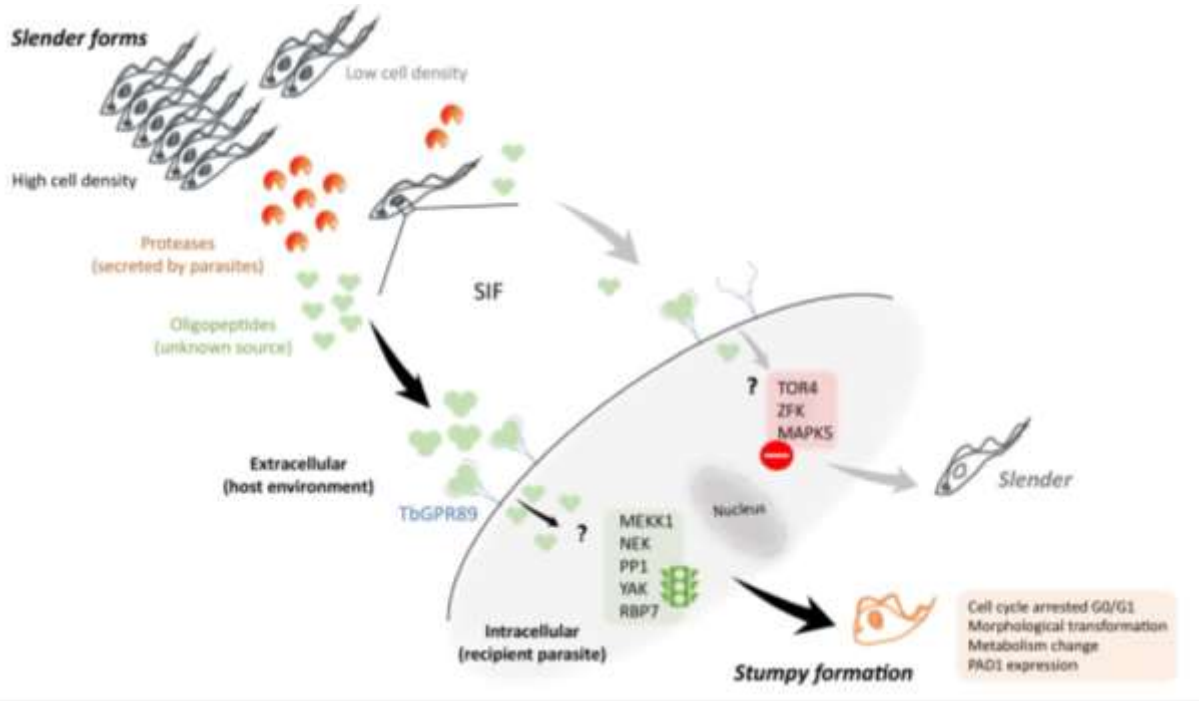

Figure 1.3 Model of long slender to stumpy bloodstream form differentiation. High cell densities lead to high protease levels in the extracellular environment, leading to increased levels of oligopeptides. The latter are presumed to serve as stumpy induction factor (SIF) when internalized by recipient parasites through *Tb*GPR89 receptors. Activated signaling pathways, including MEEK1, NEK1, PP1, YAK, and RBP, together induce differentiation to the stumpy form, which is characterized by G0/G1-phase arrest and PAD1 expression. Oligopeptide sensing at low cell density results in an activation of alternative pathways, such as TOR4, ZFK, and MAPK, leading to repression of stumpy formation. Adapted from Sollelis and Marti, 2018 [38]

Recently, this "traditional" view of the trypanosome life cycle has been called into question by the group of Markus Engstler. They discovered that long slender BSFs could establish infections of tsetse flies at efficiencies similar to those observed with growth-arrested stumpy forms. These cells could then successfully differentiate into the PCF without undergoing a cell cycle arrest *in vitro*, but they were still characterized by expression of PAD1 [39].

1.4 The cell cycle in *T. brucei* and its regulation

The eukaryotic cell cycle can be divided into G0/G1-, S-, G2-, and M-phases. The cells are growing and preparing for another round of cell division during the first gap phase (G0/G1). Afterwards, the DNA is duplicated during the so-called synthesis phase or S-phase. During the second gap phase (G2), which can be very short or even absent, the cells grow rapidly and feature high rates of protein

synthesis, in preparation for mitosis. The latter phase describes the segregation of the nuclear content and the division of the cell body (cytokinesis) [40].
The cell cycle of *T. brucei* parasites can be described by this universal model, but is additionally characterized by unique features. Apart from the nucleus, the kinetoplast contributes to the nucleic acid content, and needs to be duplicated and subsequently segregated accurately between the daughter cells. As a consequence, kinetoplast and nuclear S-phases need to be spatially and temporally coordinated and require unique and novel solutions [41]. Prior to DNA synthesis, the formation of a second flagellum is initiated by the recruitment of γ-tubulin, which can be morphologically described by an elongation of the basal body [42]. Kinetoplast S-phase starts before and is immediately followed by nuclear S-phase. Before the onset of mitosis, segregation of the kinetoplast genome is already completed. Based on this, the DNA content allows for a discrimination between different cell cycle stages in the *T. brucei* life cycle upon visualization of the DNA content, e.g., by DAPI staining. During early G2-phase, separation of the basal bodies, and concurrently the kinetoplast DNA, occurs in a microtubule-dependent manner [42, 43].
The nuclear spindle is formed inside the nucleus during M-phase, as the nuclear envelope is not disassembled. How chromosomal segregation occurs precisely still remains obscure, as the number of the microtubules formed is too small to allow for individual microtubule-kinetochore interactions. Finally, cytokinesis occurs along the longitudinal axis of the dividing parasite from the anterior to the posterior pole [41, 43].

1.5 Genome organization and regulation of gene expression

The 35-Mb genome (haploid) of *T. brucei* parasites is divided into two units, i.e., kinetoplast and nuclear genomes. The latter can be subdivided into 11 pairs of Mb-sized chromosomes, as well as intermediate- and mini-chromosomes, based on their sizes. At present, approximately 9000 genes have been predicted, of which 900 and 1700 are pseudogenes and *T. brucei*-specific genes, respectively [44].
Trypanosomes are exposed to vastly different environments in the two hosts in terms of temperature, nutrient sources, pH, and host immune responses. Hence, the ability to sense these differences and regulate gene expression in a life-cycle stage-specific manner is crucial for trypanosome survival.
Life of a eukaryotic mRNA classically starts with transcription by RNA polymerase II in the nucleus, which is accompanied/followed by mRNA processing and export from the nucleus. Once in the cytoplasm, machineries responsible for mRNA translation, storage, and degradation take over [45].

1.5.1 Transcription

Despite the high demand for flexibility and adaptation, there is virtually no regulation of transcription at the level of individual genes, which needs to be compensated for by post-transcriptional mechanisms. More specifically, initiation of transcription by RNA polymerase II (pol II) is regulated by histone variants and modifications rather than combinations of specific promoters and transcription factors [46]. Pol II transcription proceeds uniformly and is polycistronic, generating transcripts from clusters of tens to hundreds of intron-less genes (**Figure 1.4**). Open reading frames (ORFs) are typically arranged in a head-to-tail fashion across transcription units that are up to 100 kb long. Proteins encoded in up to 100 ORFs on a given transcription unit are generally unrelated in levels of expression and function. Genes encoding abundant mRNAs are often present in multiple copies on the genome as a way of ensuring high levels of expression [47].

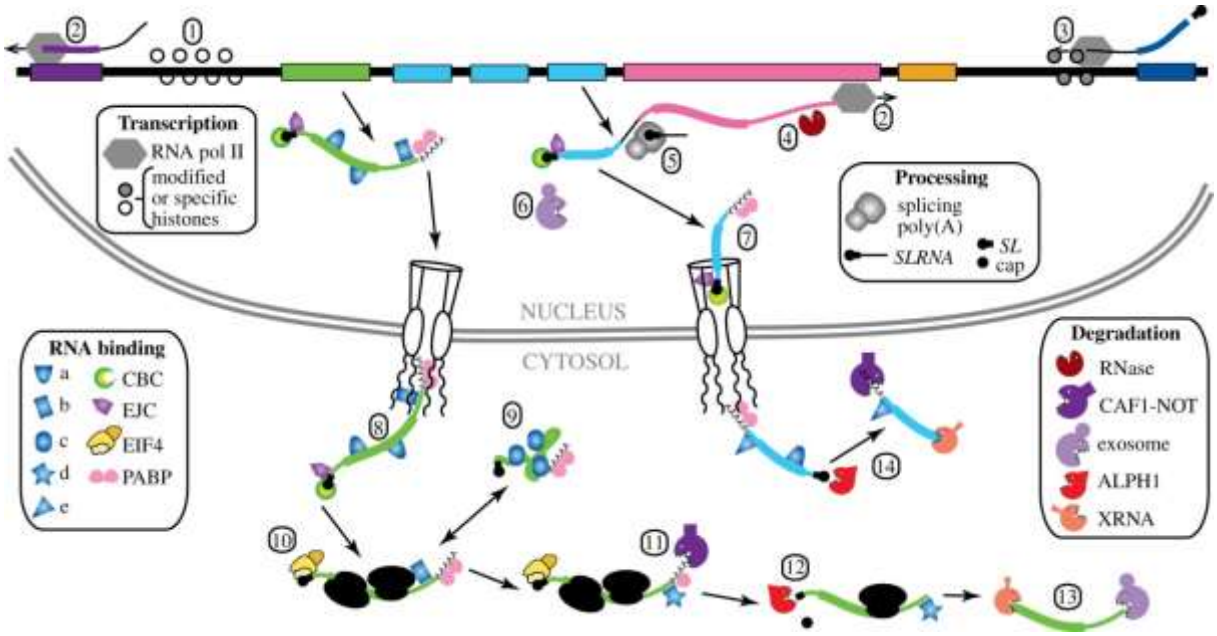

Figure 1.4 Gene expression in *Trypanosoma brucei*. Transcription by RNA polymerase II is polycistronic. Individual mRNAs are liberated by *trans*-splicing, upon which the spliced leader (SL) sequence with a cap structure is attached to the 5'-end. Afterwards, mRNAs are bound by different RNA-binding proteins, such as the nuclear cap-binding complex (CBC) and poly(A)-binding proteins (PABPs), and exported from the nucleus through nuclear pore complexes. In the cytosol, the CBC is replaced by cytoplasmic cap-binding proteins (EIF4E proteins) to initiate translation. Deadenylation by the CAF1-NOT complex generally marks the first step during RNA decay. The mRNAs without poly(A) tails are targets for decapping by ALPH1 and 5'-3'-degradation by XRNA, as well as for 3'-5'-degradation by the exosome. Adapted from Clayton, 2019 [45]

The gene cluster encoding the 142 nt spliced leader (SL) is an exception among the pol II transcripts, as its transcription is driven by a discrete promoter sequence that acts in concert with specific transcription factors. This results in high synthesis rates [48].
Transcription units are separated by so-called strand switch regions (SSRs), where transcription is presumed to initiate and terminate. These are marked by modified histones and/or specific histone variants [49].
Genes encoding rRNAs and cell surface proteins, such as VSGs and procyclins, are transcribed by RNA pol I, which is ten times more active than RNA pol II, to ensure production of large quantities. RNA pol III, on the other hand, mediates transcription of tRNAs, 7SL RNA, and U-rich snRNA genes [50].
Post-transcriptional mechanisms, such as pre-mRNA processing, mRNA transport, localization, stability, and translation, have to be tightly regulated and fine-tuned to regulate gene expression. Based on this, trypanosomes constitute excellent models for studying post-transcriptional control mechanisms.

1.5.2 mRNA processing and export

Individual mRNAs are liberated from polycistronic transcription units through *trans*-splicing of the SL mini-exon at the 5'-end and polyadenylation at the 3'-end, whereas *cis*-splicing is rare [51, 52]. As a consequence, mRNAs share the same 39 nt SL RNA sequence and a cap4 structural element. Polyadenylation occurs around 100-300 nt upstream of the splice site. The latter is marked by a polypyrimidine tract. Signals within this region as well as those in the 5'-UTR serve to regulate splicing efficiency and thus mature mRNA abundance [53-55].
Ribonucleoprotein particles (RNPs) are formed by binding of various RNA-binding proteins (RBPs) to nascent transcripts and change throughout an RNA's life to determine its fate. The cap-binding

complex (CBC) is bound to the hypermethylated cap inside the nucleus. For transport into the cytosol, mRNPs are exported by a RanGTP-dependent mechanism. While the heterodimeric nuclear export receptor Mex67-Mtr2 of the export complex is conserved in all eukaryotes, some components are unique to trypanosomes [56-58].

1.5.3 RNA-binding proteins

Each mRNA is bound by multiple RBPs at a given time in order to control its expression. These RBPs display a varying degree of sequence specificity and are recruited through regulatory *cis*-elements, the majority of which are found within the 3'-UTR of a target mRNA.
Based on characteristic structural domains, which mediate mRNA binding, RBPs can be categorized into several subclasses, which are described below in more detail. Additionally, more than 125 RBPs that do not feature canonical RNA-binding domains have been described [59].

Proteins containing an RNA recognition motif (RRM)

The *T. brucei* genome encodes more than 75 RRM domain-containing proteins. An RRM consists of two α-helices and a four-stranded β-sheet, which can reportedly bind sequences around 2-8 nt in length present on ssRNA. RRM domain-containing proteins are exemplified by poly(A)-binding proteins (PABPs) 1 and 2, both of which bind to the poly(A) tails of mRNAs, and are expected to interact with translation initiation factors bound to the cap, thereby shielding the mRNA ends from degradation machineries. Furthermore, this interaction presumably allows for faster re-initiation of translation [60, 61].
RBP6 and RBP10 are RRM domain proteins essential for life cycle stage-specific gene expression control. Although the targets of RBP6 remain to be determined, ectopic expression of this protein was shown to trigger the differentiation of PCFs to epimastigotes [62-64]. Reportedly, RBP6 expression is highest at this life cycle stage. RBP10, on the other hand, is presumed to be a master regulator of BSF-specific gene expression profiles. Transient, ectopic expression of RBP10 in PCFs in combination with a shift in temperature (37 °C to 27 °C) and energy sources is sufficient for promoting development into proper BSFs. Accordingly, depletion of *RBP10* by RNAi was shown to result in reduced expression of BSF-specific genes [62, 65].

Zinc finger proteins

T. brucei has about 40-50 RBPs with $CX_8CX_5CX_3H$ zinc finger domains [66]. Of those, ZFP1 and ZFP2 are involved in differentiation of the BSF to the PCF, whereas ZFP3 has been described to bind mRNAs increased in stumpy forms [67, 68].
ZC3H11 is a zinc finger protein that binds to chaperone mRNAs to stabilize them. In line with this, it is essential for BSF survival [69]. In PCFs, on the other hand, it is dispensable for growth at 27 °C, but is needed at 37 °C and during transient heat shock conditions at 41 °C, where it is required for protein re-folding after heat-denaturation. Heat shock leads to a rapid increase in ZC3H11 expression, while it is nearly undetectable under normal growth conditions. Mechanistically, ZC3H11 is known to exert its functions by interaction with 5'-*UAU*-3' repeats in the 3'-UTR and subsequent recruitment of the so-called MKT1 complex, which is described in more detail below [69, 70].

Alba domain proteins

Four small acetylation lowers binding affinity (ALBA) domain proteins, ALBA1, 2, 3, and 4, have been described, each of which is present at 10,000-20,000 molecules per procyclic trypanosome against the background of 40,000 mRNAs. Binding of ALBA proteins to RNAs is regulated by acetylation/deacetylation processes [71]. Furthermore, these proteins are known to form homo- and heterodimers in the cytoplasm, of which both ALBA1/2 and ALBA3/4 complexes are associated with poly(A) RNA in starvation stress granules [72]. Furthermore, ALBA2/3 dimers were found in association with the cap-binding protein EIF4E4 and polysomes. Another study reported ALBA3/4 co-localization with the DEAD-box RNA helicase DHH1 and poly(A) RNA in stress granules. Presumed functions include regulation of chromatin modifications, translation, as well as differentiation processes [72, 73].

Pumilio-Fem3 (PUF) domain proteins

There are at least 12 PUF domain proteins encoded in the *T. brucei* genome. These are characterized by eight tandemly repeated α-helices, each of which contacts another base of the RNA-binding sequence [74]. PUF9 was found to stabilize a small subset of mRNAs from late G1-phase throughout S-phase by binding to its (putative) binding motif, 5'-*UUGUAC*-3', which is essential for regulation by PUF9 [75]. PUF7 and PUF10 are nucleolar proteins required for rRNA maturation processes and bind to a nucleolar regulator of GPEET 1 (NRG1) [76, 77]. Accordingly, knockdown of those factors resulted in reduced 5.8S rRNA levels, but at the same time caused an increase in abundance of the mRNAs encoding the GPEET procyclin surface protein at life cycle stages at which it is usually repressed [77].

Non-canonical RBPs

Of note, the current knowledge on RBPs is largely restricted to proteins containing predicted RNA-binding domains. It is presumed that a large variety of non-canonical RBPs lacking these particular motifs add to the complexity of RBP regulation circuits and cross-talks.

1.5.4 mRNA storage and localization

Control of mRNA storage and localization add to a trypanosome's repertoire to regulate gene expression at the post-transcriptional level [78]. Accordingly, different types of non-membranous aggregates of proteins and mRNAs, so-called mRNPs, have been described in trypasonomes, including P-bodies and stress granules.

Due to the presence of proteins involved in RNA metabolism, such as decapping enzymes, the 5'-3' exoribonuclease XRNA, and the deadenylase CAF1, P-bodies are thought to be the sites of mRNA storage and/or degradation. They are permanently present in the cells and have been shown to increase in size upon translational repression [79]. Interestingly, only one of the six cap-binding proteins, EIF4E1, has been identified in trypanosomal P-body structures [80].

Different types of stress can additionally induce the formation of so-called stress granules, which are presumed to contain mRNAs that are temporarily stalled at the initiation step of translation. Accordingly, three of the six cap-binding translation initiation factors (EIF4E1-3) and polyadenylated mRNAs have been detected in starvation stress granules [80]. These mRNAs are stable, even if transcription is inhibited for an extended period of time. Once the stress has been resolved, translation of these mRNAs can resume immediately. In contrast to stress granules in mammalian

cells, those of trypanosomes do not contain ribosomal subunits or EIF4G scaffold proteins. Stress granules further contain several cytoplasmic RBPs, such as DHH1, XRNA, PABP2, and ALBA1-4 [80].

1.5.5 Translation control

General concepts in eukaryotes

In order to be efficiently translated, ribosomes need to assemble near the 5' end of an mRNA to initiate protein synthesis at the first start codon. To achieve this, the cap-binding protein eIF4E associates with the cap and in turn recruits a large scaffold protein, eIF4G, which is able to interact with various initiation factors, including the helicase eIF4A. The latter is responsible for unwinding RNA secondary structures. Traditionally, this tripartite protein complex is referred as eIF4F complex [81]. The small ribosomal subunit loaded with met-tRNA, eIF1, eIF1A, eIF3, and eIF3 is referred to as 43S pre-initiation complex, and is recruited to the mRNA through eIF4G-eIF3 binding. After that, the small ribosomal subunit is assumed to slide along the mRNA until the start codon is recognized with the help of the anticodon loop of the initiator-tRNA. At the same time, PABPs bound to the poly(A) tail can interact with eIF4G to circularize the mRNA. Subsequent to scanning and recognition of the first AUG by the small ribosomal subunit, the interaction with the eIF4F complex is lost and the large ribosomal subunit joins to catalyze the formation of the first peptide bond of the nascent peptide [81-83].

Cap structure of **T. brucei** *mRNAs*

The cap structure of *T. brucei* is composed of the classical 7-methylguanine (m7GTP) cap that is heavily modified on the four nucleotides that immediately follow, 5-*'AACU*-3' [84, 85]. The ribose moieties of these residues are 2'-O-methylated, and the first adenine and fourth uridine are additionally characterized by unusual base-methylations, i.e., m_2^6A and m_3U. Together, the m7GTP cap plus the modifications are referred to as cap4 structure, which is found exclusively in trypanosomatids. The SL precursor is modified co-transcriptionally, as the cap4 structure is required for efficient *trans*-splicing and polyadenylation [85, 86].

Cap-binding proteins

Generally speaking, cap binding by eIF4E proteins is enabled by the typical "cupped-hand" tertiary structure that is composed of eight antiparallel β-sheets and three α-helices, and is conserved from yeast to mammals. Contacts between the cap and the concave side of an eIF4E protein are established by two conserved tryptophan residues through π-π stacking. Electrostatic interactions and hydrogen bonding further contribute to cap binding. Interactions with eIF4G classically involve the canonical $Y(X)_4L\Phi$ motif in the eIF4G N-terminus, which is shared with eIF4E-binding proteins (4E-BPs), causing competition for eIF4E binding [87-89]. As binding of 4E-BP and eIF4G proteins is mutually exclusive, 4E-BPs prevent eIF4F complex assembly at the cap [90].
Furthermore, certain eIF4E homologs are not responsible for promoting "global" translation initiation, but instead serve as translational repressors. While mammalian eIF4E1 promotes general translation activation, mammalian 4EHP (also called eIF4E2) acts to suppress the translation of a specific subset of mRNAs under steady-state conditions. Accordingly, it mainly localizes to processing bodies [91]. Proteins of the 4EHP-type do not associate with eIF4G proteins [92]. These further include *Drosophila* d4EHP/EIF4E-8, which plays a major role during early development. The suppressive functions of these proteins depend upon binding of specialized partner proteins, such as

GIGYF in mammals and bicoid in the case of *Drosophila* [93, 94]. Interestingly, these factors further display intrinsic RNA-binding activities.

The genome of *T. brucei* encodes six EIF4E proteins, suggesting that translation control might be exerted at the level of differential mRNA selection by different EIF4E proteins, which assemble functionally distinct initiation complexes (**Figure 1.5**) [85]. A repertoire of five EIF4G proteins and two different EIF4A helicases further contributes to the complexity. Furthermore *T. brucei* and *Leishmania* parasites possess two and three homologs of the PABP, respectively [95, 96].

Trypanosomal EIF4E proteins have been categorized into three subclasses based on their structural properties. EIF4E1 and EIF4E2, both of which are approximately 26-28 kDa in size and of relatively low abundance, belong to group 1. Group 2 comprises EIF4E3 and EIF4E4, which associate with EIF4G4 and EIF4G3, respectively, to form EIF4F-like complexes to promote translational activation. EIF4E5 and EIF4E6 were most recently identified and fall into group 3. These two EIF4E proteins are the smallest found in trypanosomes, but nonetheless share the common EIF4E core structure that allows for cap recognition and EIF4G binding. The three groups are described in more detail below. Of note, reported cap binding affinities were mainly determined using m7GTP-binding assays, but authentic data on cap4 binding affinities are scarce. Therefore, cap binding affinities are not referred to in the following sections [85, 97-99].

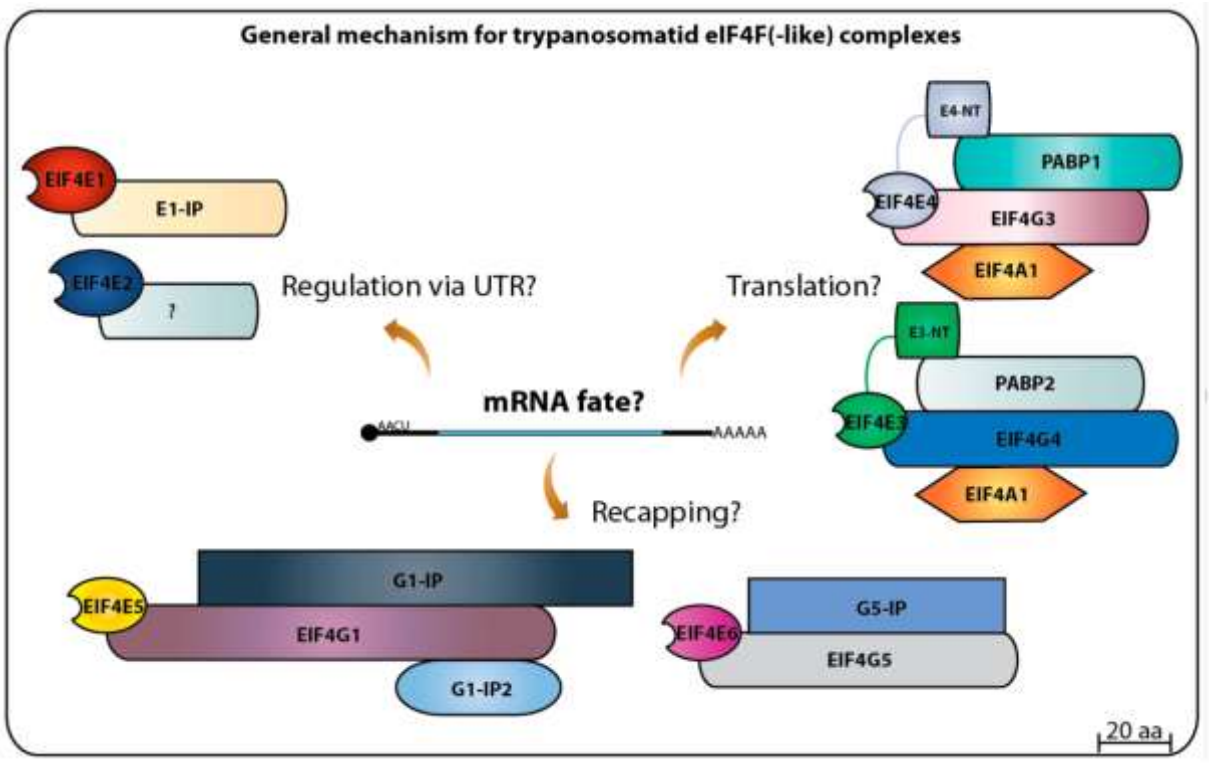

Figure 1.5 Overview of EIF4F(-like) complexes in *Trypanosoma brucei*. Different EIF4F(-like) complexes assembling at mRNA cap structures around the six EIF4E proteins described in *T. brucei.* PABP, poly(A)-binding protein; 4E-IP, 4E-interacting protein; G1-IP, G1-interacting protein; G5-IP, G5-interacting protein; NT, N-terminus; UTR, untranslated region. Adapted from Freire et al., 2017 [85]

EIF4E1 and 4EIP

Quantification approaches by Freire revealed that EIF4E1 is present at 3-8 × 10^3 and 2.5-5 × 10^3 molecules/cell in the PCF and BSF, respectively [97]. This is in the range of 0.0001-0.001% of total

protein. EIF4E1 does not pair with an EIF4G protein, but rather associates with 4EIP, an mRNA-binding protein. Upon artificial tethering of λN-4EIP or λN-EIF4E1, fusion proteins with a box-B element-binding λN-peptide, to a reporter mRNA with a box-B element encoded in the 3'-UTR, both could induce reporter mRNA degradation and translational repression [100]. In a *4EIP* knockout background, EIF4E1 failed to downregulate reporter expression, whereas 4EIP was shown to repress independently of EIF4E1 [100]. BSF and PCF parasites can grow almost normally in the absence of 4EIP. In contrast, during differentiation from the BSF to the PCF, 4EIP is essential for translational repression in the growth-arrested stumpy form. Differentiation competence can be rescued by expressing a truncated version of 4EIP that does not interact with EIF4E1 [100].

EIF4E1 from *Leishmania* has been reported to associate directly with EIF3A by binding to the C-terminus of EIF3A. Furthermore, EIF3A was able to pull down EIF4E1 *in vitro*, suggesting that EIF4E1 may be able to initiate translation independent of an EIF4G protein [101]. According to this model, the translation-promoting activity of EIF4E1 is blocked by 4EIP. Structural analyses by Meleppattu et al. supported this hypothesis. Binding of 4EIP to EIF4E1 was shown to allosterically destabilize the binding between the cap structure and EIF4E1 protein *in vitro*, leading to the assumption that fewer mRNAs are associated with EIF4E1 in the absence of 4EIP [102].

EIF4E2

Like EIF4E1, the group 1 member EIF4E2 has not been found in association with an EIF4G protein under all conditions and life cycle stages analyzed so far. Furthermore, there is no evidence linking EIF4E2 function to promoting translational activation in *T. brucei*. Instead, a homolog of the histone mRNA stem-loop-binding protein, SLBP2, has been identified as a binding partner of EIF4E2 in PCFs [103]. Binding is mediated through a conserved central region that is missing in other known SLBP homologs. In metazoans, the major histone mRNA-binding protein (SLBP/SLBP1) is involved in most steps of histone mRNA metabolism, including histone pre-mRNA processing in the nucleus, transport to and translation, stability, and degradation in the cytoplasm [104]. Metazoan histone mRNAs lack a poly(A) tail, but feature a characteristic stem-loop structure in the 3'-UTR that serves as a binding platform for SLBPs. In some metazoans, a second homolog, SLBP2, is expressed exclusively at the oocyte stage, where it suppresses histone pre-mRNA processing until SLBP1 takes over [105]. In yeast and plants, sequences predicted to encode SLBP homologs appear to be absent from the genome. Accordingly, histone mRNAs are polyadenylated and lack the stem-loop structure [106]. Histone levels are regulated rather at the transcriptional level and through protein degradation in these organisms. Interestingly, histone mRNAs in trypanosomatids possess both a poly(A) tail and the stem-loop structure that allows for SLBP binding. However, the exclusive localization of SLBP2 in the cytoplasm argues against a similar role in histone mRNA processing in these parasites [103]. So far, the role of the EIF4E2/SLBP2 complex remains unknown, but binding to specific stem-loop structures in mRNA targets other than histone mRNAs has been suggested. In procyclic cells, the expression of both EIF4E2 and SLBP2 is highest during early log-phase, and is drastically reduced as the cells reach a stationary growth phase [103]. In contrast, *Tb*SLBP1 expression is constant during all growth and cell cycle phases analyzed in *T. brucei*.

EIF4E3 and EIF4E4

Group 2 includes EIF4E3 and EIF4E4, which are abundant in the cytoplasm and have so far been assumed to be the main initiators of translation. Accordingly, there are 10× more EIF4E3 and EIF4E4

than EIF4E1 or EIF4E2 molecules. Both EIF4E4 and EIF4E3 are about equimolar with mRNA levels [107].
Both were shown to form classical EIF4F complexes; EIF4E3 preferentially associates with EIF4G4, whereas EIF4E4 binds to EIF4E3. Knockdown in the BSF was shown to lead to growth impairment or even cell death. A growth defect was also observed after RNAi targeting *EIF4E3* PCFs, but knockdown of *EIF4E4* had no effect at this particular life cycle stage, suggesting that they have specialized to a certain degree [97]. While protein synthesis inhibition was observed upon knockdown of *EIF4G3*, depletion of *EIF4G4* could not inhibit global protein synthesis [108].
In comparison with other trypanosomatid EIF4Es, EIF4E3 and EIF4E4 are characterized by a very long N-terminal extension, resulting in an overall size of approximately 46-48 kDa each. In support of a translation-promoting function, EIF4E3, EIF4E4, EIF4G3, and EIF4G4 were shown to lead to increased reporter expression upon tethering to a reporter mRNA using the aforementioned box-B/λN system [109]. Furthermore, all of these proteins are reportedly present in polysomes [110]. Interestingly, EIF4E4 was shown to bind to both PABPs, but exhibits a preference for PABP1 [95, 111].

EIF4E5 and EIF4E6

Group 3 is formed by EIF4E5 and EIF4E6, which are comparably small in size, i.e., 22 kDa and 21 kDa, respectively. Still, both of them associate with EIF4G proteins to form EIF4F-like complexes, the roles of which during translation are to be determined. They may aid progression through different developmental stages or help overcome different kinds of cellular stress. It has further been shown that both EIF4E5 and EIF4E6 are essential in the PCF [98, 99]. Data obtained by label-free mass spectrometry indicated that EIF4E6 is actually more abundant than previously thought. In the BSF, EIF4E6 levels were slightly higher than that of EIF4E3 [112]. Both proteins appeared to be equally abundant in PCFs [112].
Analyses by mass spectrometry revealed that EIF4E5 could associate with two of the five EIF4G proteins in PCFs to form two distinct subcomplexes: EIF4E5/EIF4G1 and EIF4E5/EIF4G2. Furthermore, association with EIF4G1 led to the recruitment of 14-3-3 I only, while complexes containing EIF4G2 contained both 14-3-3 protein isoforms. In PCFs, EIF4F complexes around EIF4E6 comprise EIF4G5 protein, which in turn interacts with G5-interacting protein (G5-IP) [98].
EIF4E5 RNAi in PCFs elicited a so-called “settling” phenotype, where cells could be found at the bottom of the flask instead of being in suspension. This was accompanied by a loss of social motility upon plating on semisolid culture plates [98]. Similarly, knockdown of *EIF4E6* resulted in a social motility defect, which was not associated with the “settling” phenotype observed upon depletion of *EIF4E5*. In addition, flagellar abnormalities, primarily flagellar detachment, could be detected when *EIF4E6* was depleted, which were particularly pronounced after centrifugation [99].
A large-scale tethering screen aimed at identifying regulators of mRNA expression in *T. brucei* led to the identification of a novel protein, which acted as one of the strongest promoters of reporter expression when artificially tethered to the 3’ UTR of the mRNA encoding the reporter protein. Based on this observation, it was termed eXpression ACtivator 1 (XAC1) [109]. XAC1 is essential for growth of *T. brucei*. Subsequent studies served to identify the proteins found in a complex with XAC1, which included MKT1, PBP1, LSM12, and PABP (mostly PABP2). This so-called MKT1 complex had previously been identified as the mediator of ZC3H11 activity [70].
Artificial tethering of λN-PABP1/2, λN-PBP1, λN-LSM12, λN-MKT1, or λN-ZC3H11, all caused increases in the expression of a reporter mRNA that encoded a box-B element in the 3’-UTR. Additionally, the EIF4G-component of the cap-binding translation initiation complex EIF4E6/EIF4G5 was also identified in the XAC1-bound proteome [113]. Recruitment of the complex to target mRNAs has been proposed

to occur through interactions between MKT1 and numerous RNA-binding proteins, including ZC3H11 [113].
XAC1 is also present in an alternative complex containing PBP1, LSM12, as well as MKT1-Like (MKT1L) protein, which shares large sequence homology with MKT1 at the C-terminus, but additionally contains an N-terminal extension [113]. Furthermore, MKT1L does not associate with mRNAs or RNA-binding proteins. It was thus hypothesized that MKT1L scavenges protein binding partners of MKT1 to modulate the activity of MKT complexes.
According to the aforementioned tethering screen, artificial tethering of EIF4G1 resulted in increased reporter expression, whereas tethering of EIF4G2 had no effect [109]. EIF4E5 also displayed translation-promoting activities upon examination in the tethering screen [109].

1.5.6 mRNA decay

The half-lives of most mRNAs in both BSFs and PCFs are in the range of 5 to 20 min, although highly stable mRNAs with half-lives of more than 120 min can be found as well [114].
In general, mRNA degradation is initiated by deadenylation. In the course of this process, PABP dissociates and therefore exposes the cap of the previously circularized mRNA. Consequently, decapping occurs, which is followed by degradation catalyzed by the 5'-exoribonuclease XRNA. At the 3' end, the exosome is taking over once the poly(A) tail has been removed. Both degradation pathways are described in more detail below.

Deadenylation and 3'-5' degradation

Removal of the poly(A) tail through deadenylation by CAF1/NOT or PAN2/PAN3 complexes is central to initiation of mRNA degradation. All NOT complex subunits except for a CCR4 homolog are present in kinetoplastids, with CAF1 serving as the major deadenylase responsible for global mRNA decay [47, 115]. Accordingly, loss of CAF1 resulted in an increase in average poly(A) tail length, which was accompanied by a delay in the degradation of constitutively expressed mRNAs. Activity and targeting of the degradation machinery can be regulated via sequence-specific RBPs, such as the zinc finger proteins ZC3H15 and ZC3H5, and the RRM-containing proteins DRBD5 and RBP31, which were shown to interact with CAF1. Removal of the poly(A) tail is accompanied by the loss of PABP binding, ultimately exposing both ends of the mRNA. At this point, other degradation machineries can take over. At the 3'-end, this role is realized by the exosome. Eight of the ten complex components known from yeast could be identified in *T. brucei*, seven of which are essential for parasite survival [116]. However, the *T. brucei* exosome was shown to be characterized by greater simplicity, as only five components were found in the cytosolic exosomal complex, highlighting that it has become more elaborate in the course of eukaryotic evolution [116].

Decapping and 5'-3'degradation

The removal of the poly(A) tail also initiates the hydrolysis of the mRNA cap, leading to a decapped, free 5'-end. This renders the mRNA as a target for 5'-3'-degradation by the exonuclease XRNA [117]. Although these processes are conserved, trypanosomal homologues to the decapping complex subunits could not be identified. A major breakthrough was the identification of an ApaH-like phosphatase 1 (ALPH1) as major mRNA decapping enzyme by Susanne Kramer [118]. Furthermore, ALPH1 was found to co-localize with XRNA near the posterior end of the parasite. In line with the presumed role of ALPH1, depletion leads to an accumulation of deadenylated mRNAs that have not undergone 5'-3'-degradation. Knockdown of *XRNA*, on the other hand, could inhibit the degradation

of certain unstable mRNAs, whereas a reduction in exosome complexes resulted in minor delays in the degradation of particular mRNAs with intermediate half-lives in the range of 20 to 60 min [116, 117].

Terminal uridylation

T. brucei possesses five enzymes with terminal uridylyl transferase activity. Most of them are located in the mitochondrion, where they edit RNA molecules. TUT3 and TUT4, however, have been described to be cytoplasmic enzymes, but their functions *in vivo* remain obscure [119]. In an *in vitro* assay, recombinant *Tb*TUT3 was indeed acting as an enzymatically active 3'-terminal RNA uridylyltransferase [120].

In a large-scale tethering screen, λN-TUT3 neither acted as an activator nor a repressor when artificially bound to the 3'-UTR of a reporter mRNA through a box-B element. Furthermore, it was shown not to bind polyadenylated RNA [59]. Recently obtained data indicated that 4EIP and TUT3 interact with each other. This interaction was relatively weak [100].

Based on data obtained in other organisms, it is presumed that cytoplasmic uridylation serves to mark selected mRNAs for degradation [121]. So far, the highly abundant *GPEET* mRNA is the only verified cytoplasmic uridylation target in trypanosomes, but whether this is catalyzed by TUT3 remains to be determined [33]. In this instance, rapid control of *GPEET* mRNA levels could facilitate the progression from early to late PCFs, which are characterized by expression of different types of procyclins, i.e., GPEET and EP, respectively.

1.6 Aim of this study

T. brucei is equipped with an exceptionally large repertoire of cap-binding EIF4E proteins. However, their individual, transcriptome-wide roles remain largely elusive. The functions of the translation-promoting EIF4E isoforms could be fully redundant, but presumably vary among different life cycle stages. Alternatively, each EIF4E could be responsible for the translation regulation of a highly specific pool of mRNAs. Likely, the actual roles *in vivo* are somewhere between these two extremes. To shed light on this, the main goal of my project was to determine the roles of the regulatory cap-binding translation initiation factors EIF4E1, EIF4E2, EIF4E5, and EIF4E6 of *T. brucei* during translation initiation, focusing on the level of redundancy in comparison with other, canonical or regulatory EIF4Es by

1. characterizing knockout phenotypes
2. analyzing their roles in differentiation regulation
3. identifying protein binding partners and bound mRNA targets
4. determining the effects on translation initiation

2. Materials and methods

2.1 Trypanosome cell culture and manipulation

The experiments in this study were carried out using pleomorphic EATRO1125 (Antat1.1) BSFs or PCFs. The only exceptions were TUT3 studies, for which monomorphic Lister 427 BSFs and PCFs were used. All of these cell lines were characterized by constitutive expression of the Tn10 tet repressor.

2.1.1 BSF culture

BSF parasites were maintained at densities between 0.1-0.5 × 10^6 cells/mL in HMI-9 medium with or without 1.1% methylcellulose in a humid environment at 37 °C with 5% CO_2. To allow for gas exchange, the screw caps were only loosely fixed.

Table 1. Composition of HMI-9 medium

Component	Final concentration
Iscove's modified Dulbecco's medium	17.66 g/L
$NaHCO_3$	3.024 g/L
Hypoxanthine	136 mg/L
Sodium pyruvate	110 mg/L
Thymidine	39 mg/L
Bathocuprono disulfonic acid disodium salt	28 mg/L

HMI-9 medium was filter sterilized (0.22 µm) and stored in 450 mL aliquots at 4 °C. Prior to use, each aliquot was supplemented with 10% (v/v) heat-inactivated (56 °C, 30 min) fetal bovine serum (FBS), 100 U/mL penicillin/streptomycin, 1.5 mM L-cysteine, and 0.14% (v/v) β-mercaptoethanol.

To prepare a 2.5% methylcellulose stock solution, 15 g of methylcellulose were dissolved in 500 mL of H_2O by constant stirring at 4 °C for 1-2 days. After autoclaving, the methylcellulose solution was filled up to 600 mL with sterile H_2O and stirred at 4 °C for another 1-2 days until it was completely dissolved.

Table 2. Composition of HMI-9 containing 1.1% methylcellulose (1 L)

Component	Amount
2× concentrated HMI-9	440 mL
2.5% methylcellulose	440 mL
Heat-inactivated FBS	100 mL (10%, v/v)
Penicillin/streptomycin	10 mL (100 U/mL)
L-cysteine	10 mL (1.5 mM)
β-mercaptoethanol	14 µL (0.14%, v/v)

2.1.2 PCF culture

PCFs were cultured at densities between 0.5-5 × 10^6 cells/mL in supplemented MEM-Pros medium at 27 °C.

Table 3. Composition of MEM-Pros medium

Component	Final concentration
MEM-pros mixture	16.55 g/L
MEM non-essential amino acids	1% (v/v)
MEM vitamins	1% (v/v)
NaOH	pH adjustment to 7.4

MEM-Pros medium was filter sterilized (0.22 µm) and stored in 450 mL aliquots at 4 °C. Prior to use, each aliquot was supplemented with 10% (v/v) FBS (heat-inactivated at 56 °C for 30 min), 100 U/mL penicillin/streptomycin, and 7.5 mg/L hemin.

Table 4. Selective drugs

Antibiotic	BSF	PCF
Blasticidin	5 µg/mL	10 µg/mL
Neomycin	5 µg/mL	15 µg/mL
Hygromycin	5 µg/mL	50 µg/mL
Phleomycin	0.2 µg/mL	0.5 µg/mL
Puromycin	0.2 µg/mL	1 µg/mL
Tetracycline	100 ng/mL	100 ng/mL

2.1.3 Transfection of BSFs and PCFs

Approximately 1-2 × 10^7 cells were collected upon reaching a density of 5 × 10^5 cells/mL and subjected to a washing step using the corresponding transfection buffer (cytomix for BSFs and ZPFM for PCFs). The cells were then resuspended in an appropriate volume of the respective, ice-cold transfection buffer (150 µL for BSFs, 400 µL for PCFs), transferred to an electroporation cuvette, and mixed with 10-12 µg of linearized plasmid DNA. Transfection of BSFs was performed using the Amaxa Nucleofector system (program X-001), whereas PCFs were electroporated with a BTX electroporation apparatus (1.5 kV, resistance setting R2), and the cells were transferred to the respective pre-warmed culture medium without selective drugs immediately after transfection. The cells were allowed to recover for 6-12 h, after which selective drugs were added. The cells were then plated on 24-well plates in serial dilution. Clones were identified and expanded 6-10 days after plating, and the desired genotypes and phenotypes were tested by gDNA extraction in combination with PCR and by western blotting, respectively.

Table 5. Composition of cytomix, pH 7.6

Component	Final concentration
EGTA	2 mM
KCl	120 mM
$CaCl_2$	0.15 mM
K_2HPO_4/KH_2PO_4, pH 7.6	10 mM
HEPES	25 mM
$MgCl_2$	5 mM
Glucose	0.5% (w/v)
BSA	100 µg/mL
Hypoxanthine	1 mM

Table 6. Composition of Zimmerman's post fusion medium (ZPFM), pH 7.0

Component	Final concentration
NaCl	132 mM
KCl	8 mM
Na_2HPO_4	8 mM
KH_2PO_4	1.5 mM
MgAc	1.5 mM
$Ca(OAc)_2$	90 µM

2.1.4 Freezing and thawing of trypanosomes

To freeze the parasites, 5 mL of a growing culture at 0.5 × 10^6 cells/mL for BSFs and 2-5 × 10^6 for PCFs were harvested by centrifugation (2300 rpm, 8 min) and resuspended in 500 µL of the corresponding culture medium. The cells were transferred to a cryotube and mixed with 500 µL of medium containing 20% (v/v) glycerol. The cryotubes were then wrapped in tissues and frozen at -80 °C. For long-term storage, the tubes were transferred to liquid nitrogen. To thaw an aliquot of cells, the cryotubes were left at 25 °C until the content was thawed, and the cells were washed once in 25 mL of pre-warmed media to remove the glycerol. The cells were subsequently resuspended in an appropriate volume of the corresponding culture medium and left to recover for 24 h before selective drugs were added.

2.1.5 Trypanosome differentiation

With stumpy formation (regular protocol)

In order to generate stumpy BSFs, pleomorphic cells were cultured to high densities (2-3 × 10^6 cells/mL) in HMI-9 medium with 1.1% methylcellulose. To reach this stationary state, a starting culture at 0.5 × 10^6 cells/mL was left to grow without dilution for 3-4 days. Upon reaching high densities, the cells were counted every 2 h and collected as the densities had declined again to 1 × 10^6 cells/mL due to cell death. For sample collection, the cells in methylcellulose were diluted 1:5 using pre-warmed PBS containing 25 mM glucose, filtered through MN616 ¼ filter papers (Macherey Nagel), and eventually harvested by centrifugation at 1400 × *g* for 10 min. The cells were resuspended in HMI-9 medium without methylcellulose and 6 mM *cis*-aconitate was added to induce differentiation. After 24 h of incubation at 27 °C, the cells were harvested by centrifugation and resuspended in the same volume of MEM-pros medium for long-term cultivation at 27 °C.

Without stumpy formation (fast protocol)

Alternatively, stumpy formation was omitted, and cells grown at 1 × 10^6 cells/mL in HMI-9 medium were incubated with 6 mM *cis*-aconitate at 27 °C for 24 h. On the following day, the medium was exchanged for MEM-pros medium and the cells were cultured at 27 °C afterwards.

2.2 DNA methods and cloning

Primers used for PCR and RT-qPCR reactions were ordered from Biomers.net. Obtained amplification products were digested with the appropriate restriction enzymes (NEB or Fermentas) and ligated into a dephosphorylated plasmid backbone (2.2.4) digested with the same enzymes. Constructs generated by ligation with T4 DNA ligase were then transformed into competent *E.coli* DH5α cells (2.2.5). Positive clones were identified by colony PCR using Taq DNA polymerase or by plasmid

isolation (Macherey-Nagel mini prep kit) followed by restriction digests. Selected clones were analyzed by Sanger DNA sequencing (MicroSynth SeqLab).

2.2.1 Agarose gel electrophoresis

DNA fragments and constructs were analyzed by separation on a 1% (w/v) agarose gel containing ethidium bromide, and images were acquired using a UV imager.

Table 7. Composition of TAE buffer, pH 8.0

Component	Final concentration
Tris-HCl	40 mM
EDTA	1 mM
Acetic acid	0.11%

2.2.2 Polymerase chain reaction (PCR)

Gene/UTR amplification

Sequences of interest were amplified by PCR using Phusion® High Fidelity DNA Polymerase and the corresponding buffer according to the manufacturer's instructions (NEB).

Table 8. PCR reaction setup

Component	Volume/final concentration
5x phusion buffer	10 µL
Fwd primer	2.5 µL (0.5 µM)
Rev primer	2.5 µL (0.5 µM)
10 mM dNTPs	1 µL
DNA template	plasmid: < 10 ng genomic: < 250 ng
Phusion DNA polymerase	0.5 µL (1 U)
H_2O	ad 50 µL

Table 9. PCR program

Step	Temperature	Time	Cycles
Initial denaturation	95 °C	30 sec	1×
Denaturation	95 °C	5 sec	30×
Annealing	60-70 °C	15 sec	
Elongation	72°C	30 sec/kb	
Final extension	72 °C	5 min	1×

2.2.3 Colony PCR

To perform PCR reactions directly on bacterial lysates without prior isolation of the plasmid DNA, individual bacterial colonies were picked from LB plates containing the respective antibiotic, dipped into 10 µL of H_2O first, and into LB media afterwards. PCR reactions were set up as described above, for which 1 µL of the bacterial solution was employed instead of purified plasmid DNA. Furthermore, a prolonged denaturation step of 5 min at 95 °C was conducted to ensure proper lysis of the bacteria

and concomitant release of the plasmid DNA to be analyzed. Inocula of positive clones were then incubated at 37 °C for 16 h, after which the plasmid DNA was isolated and analyzed by sequencing.

2.2.4 Restriction endonuclease digestion, 5'-dephosphorylation, and ligation of DNA fragments

For setting up restriction endonuclease digestions, an appropriate amount of DNA (cloning: 1-5 µg, transfections: 12 µg) was treated according to the following protocol:

Table 10. Restriction endonuclease digestions

Component	Final concentration
10× buffer	5 µL
DNA	1-12 µg
Restriction endonuclease	10 U
H_2O	ad 50 µL

After 1 h at 37 °C, vector DNA to be used in ligation reactions was dephosphorylated by incubation with calf intestinal alkaline phosphatase (CIP) for another 30 min at 37 °C in the recommended buffer system. Digestion reactions were then cleaned up using the NucleoSpin® Gel and PCR clean-up kit (Macherey-Nagel) according to the manufacturer's instructions. Ligation reactions were setup at a molar ratio of 1:3 vector to insert DNA according to the following scheme:

Table 11. DNA ligation reactions

Component	Final concentration
10× ligase buffer	2 µL
DNA	up to 100 µg
T4 DNA ligase	1 µL
H_2O	ad 20 µL

Ligation reactions were incubated at 16 °C for 12-18 h and subsequently transformed into competent *E.coli,* as described below.

2.2.5 Transformation of bacteria and plasmid preparations

A mixture of 50 µL of competent bacteria (DH5α) and 100-500 ng of plasmid DNA was incubated on ice for 20 min. The bacteria were then heat shocked for 90 s at 42 °C using a water bath, after which they were incubated on ice for another 2 min. Subsequently, 200 µL of LB medium were added, and the cells were grown at 37 °C for 30-60 min without selective drugs. Afterwards, the bacteria were plated on selective plates to obtain single clones, which were then inoculated overnight in liquid cultures of LB media containing the respective selective drug. Plasmids were isolated from transformed bacteria using the Nucleospin Plasmid kit (Macherey Nagel) according to the manufacturer's instructions.

Table 12. Composition of Luria Bertani (LB) medium

Component	Final concentration
Tryptone	10 g/L
Yeast extract	5 g/L
NaCl	10 g/L

Table 13. Composition of LB agar plates (1 L)

Component	Final concentration
LB medium	1 L
Bacto-agar	15 g
Ampicillin/kanamycin	100 µg/mL and 50 µg/mL

2.2.6 Preparation of genomic DNA from trypanosomes

5×10^8 parasites were harvested and lysed in 0.5 mL of EB buffer. RNase A was added at a final concentration of 25 µg/mL, and the mixture was then incubated at 37 °C for 1 h. Subsequently, 200 µL of ice-cold 5 M ammonium acetate were added and the mixture was incubated on ice for 1 min. Cell debris was pelleted by centrifugation for 5 min at 6000 × *g* and the supernatant was transferred to a fresh tube. This was followed by addition of 0.7× the volume of isopropanol to precipitate the DNA. The latter was then pelleted by centrifugation for 15 min at 16,700 x *g* and 4 °C, and subsequently washed with 70% ethanol to remove residual salts. Another washing step was performed with 100% ethanol and 5 min centrifugation at 16,700 × *g*, the supernatant was taken off, and the pellet was dried for 10 min at 25 °C. Afterwards, 200 µL of TE buffer were added to the pellet, which was then allowed to dissolve at 37 °C for 1 h and was ultimately stored at 4 °C.

Table 14. Composition of extraction buffer (EB) for DNA isolation, pH 8.0

Component	Final concentration
Tris-HCl	10 mM
NaCl	10 mM
EDTA	10 mM
SDS	0.5% (w/v)

Table 15. List of plasmids

Plasmid name	Description	Resistance marker	Backbone
Plasmids for *in situ* tagging			
pHD3039	triple myc-tag replaced by PTP-tag	NeoR	pHD2876
pHD3054	C-terminal *in situ* tagging of EIF4E1 (PTP)	NeoR	pHD3039
pHD3055	C-terminal *in situ* tagging of EIF4E2 (PTP)	NeoR	pHD3039
pHD3068	C-terminal *in situ* tagging of EIF4E3 (PTP)	PurR	c-PTP-4E5
pHD3056	C-terminal *in situ* tagging of EIF4E4 (PTP)	NeoR	pHD3039
pHD3076	expression of GFP-PTP	HygroR	pHD330
pHD3091	*in situ* tagging of EIF4E6 (myc)	NeoR	c-PTP-4E6
pHD3128	*in situ* tagging of EIF3A (V5)	BlaR	BlaV5
pHD3129	*in situ* tagging of EIF3A (V5)	HygroR	BlaV5
pHD2211	*in situ* tagging of CAF1 (V5)	BlaR	BlaV5
pHD1973	*in situ* tagging of MKT1 (V5)	BlaR	BlaV5
pHD2730	*in situ* tagging of MKT1-Like (V5)	BlaR	BlaV5
Plasmids for gene knockouts and RNAi			
pHD2994	single knockout of *EIF4E1*	PuroR	pHD1747
pHD2995	single knockout of *EIF4E1*	BlaR	pHD1748
pHD3090	single knockout of *EIF4E1*	HygroR	pHD2995
pHD3057	single knockout of *EIF4E2*	BlaR	pHD1748
pHD3067	single knockout of *EIF4E2*	PuroR	pHD3057
pHD3040	single knockout of *EIF4E3*	BlaR	pHD1748

pHD3041	single knockout of *EIF4E4*	BlaR	pHD1748
pHD3327	single knockout of *EIF4E5*	HygroR	PKO-4E5
pHD2897	single knockout of *4EIP*	PuroR	pHD1747
pHD2898	single knockout of *4EIP*	BlaR	pHD2897
pHD3074	single knockout of *4EIP*	HygroR	pHD2898
pHD2880	RNAi of *TUT3*	HygroR	pHD1146
pHD2463	RNAi of *EIF4E1*	HygroR	p2T7
pHD3326	RNAi of *EIF4E6*	HygroR	P2T7
Plasmids for reconstitution of expression			
pHD3066	EIF4E1 addback	HygroR	pHD330
pHD3089	EIF4E2 addback	HygroR	pHD330
pHD3075	EIF4E5 addback	PuroR	pHD330
pHD2533	4EIP(-myc) addback (full-length)	HygroR	pHD1700
pHD2529	4EIP(-myc) addback (dN mutant)	HygroR	pHD2424
Plasmids for Y2H screening			
pGADT7	AD/library (HA)	AmpR	
pGBKT7	DNA/bait (c-myc)	KanR	
pGADT7-T	AD/T-antigen (HA)	AmpR	pGADT7
pGBKT7-53	BD/p53 (c-myc)	KanR	pGBKT7
pGBKT7-Lam	BD/lamin C (c-myc)	KanR	pGBKT7
pGADT7-4EIP	Y2H screening	AmpR	pGADT7
pGBKT7-4EIP	Y2H screening	KanR	pGBKT7
pGADT7-TUT3	Y2H screening	AmpR	pGADT7
pGBKT7-TUT3	Y2H screening	KanR	pGBKT7
pGADT7-Dis3L2	Y2H screening	AmpR	pGADT7
pGBKT7-Dis3L2	Y2H screening	KanR	pGBKT7
pGADT7-SLBP2	Y2H screening	AmpR	pGADT7
pGBKT7-SLBP2	Y2H screening	KanR	pGBKT7
pGADT7-EIF4E2	Y2H screening	AmpR	pGADT7
pGBKT7-EIF4E2	Y2H screening	KanR	pGBKT7
pGADT7-PUF9	Y2H screening	AmpR	pGADT7
pGBKT7-PUF9	Y2H screening	KanR	pGBKT7
Plasmid name	**Description**	**Resistance marker**	**Origin**
c-PTP-EIF4E5	C-terminal *in situ* tagging of EIF4E5	PurR	kindly provided by O. de Melo Neto
c-PTP-EIF4E6	C-terminal *in situ* tagging of EIF4E6	NeoR	kindly provided by O. de Melo Neto
PKO-EIF4E5	single knockout of *EIF4E5*	PurR	kindly provided by O. de Melo Neto
PKO-EIF4E6	single knockout of *EIF4E6*	HygR	kindly provided by O. de Melo Neto

Table 16. List of oligonucleotides

Oligo no.	Description	Restriction site	Sequence (5'→3')	Function
cz5154	fwd-puro		caccagggcaagggtctg	PCR
cz5155	rev-puro		agttcttgcagctcggtgac	PCR
cz5725	fwd-spliced leader	-	acgctattattagaacagtttctgtac	PCR/qPCR
cz6166	fwd-hygro	HindIII	tattaagcttgatgaaaaagcctgaactca	change of resistance

cz6167	rev-hygro	SphI	tatagcatgcctattccttgccctcggac	change of resistance
cz6168	rev-α-tubulin	-	cagcctgaccaatgtggatgcagat	PCR/qPCR
cz6863	fwd-EIF4E1 5'UTR	XhoI	tatactcgaggctgaggcatgcagggtcg	gene knockout
cz6864	rev-EIF4E1 5'UTR	HindIII	tataaagcttaaactatctccttgg	gene knockout
cz6865	fwd-EIF4E1 3'UTR	EcoRI	tatagaattcctagcaaggcctaaagag	gene knockout
cz6866	rev-EIF4E1 3'UTR	SacII	tataccgcgggctgtaagtcgtctgac	gene knockout
cz6883	fwd-EIF4E1 5'UTR		cggttgtccagcaatgttatcc	PCR
	rev-EIF4E1 5'UTR	AscI	gatcggcgcgccatggccaagcctttgtct	knockout
cz6893	rev-blasticidin	PacI	gatcttaattaattagccctcccacacataac	PCR
cz6924	fwd-EIF4E5	-	catccctcaactcacgacag	PCR
cz6925	rev-EIF4E5	-	cttgccgtatgtctgatcgc	PCR
cz6946	fwd-EIF4E4-PTP	ApaI	gatcgggccccgtatggactgcatctcttc	PTP-tagging
cz6947	rev-EIF4E4-PTP	NotI	gatcgcggccgcgccaaagccgacgattg	PTP-tagging
cz6948	fwd-EIF4E2 5'UTR	XhoI	gatcctcgagacaatgaacattaggcccag	gene knockout
cz6949	rev-EIF4E2 5'UTR	HindIII	gatcaagcttcttgtgtgtgggagctttg	gene knockout
cz6950	fwd-EIF4E2 3'UTR	EcoRI	gatcgaattcaaggcccatgcctactgt	gene knockout
cz6951	rev-EIF4E2 3'UTR	SacI	gatcgagctcgggaaactaaacgaacgcaa	gene knockout
cz6952	fwd-EIF4E3 5'UTR	XhoI	gatcctcgaggtgccgtgtcacattggt	gene knockout
cz6953	rev-EIF4E3 5'UTR	HindIII	gatcaagctttgcctgtttgctactctccc	gene knockout
cz6954	fwd-EIF4E3 3'UTR	EcoRI	gatcgaattcgcttgcgtacacgtaccgta	gene knockout
cz6955	rev-EIF4E3 3'UTR	SacI	gatcgagctcatgcactagcggactcgag	gene knockout
cz6956	fwd-EIF4E4 5'UTR	XhoI	gatcctcgagcgaactgttttaagggtcac	gene knockout
cz6957	rev-EIF4E4 5'UTR	HindIII	gatcaagcttcgatcagatgaaggtcacta	gene knockout
cz6958	fwd-EIF4E4 3'UTR	EcoRI	gatcgaattcccaacaccatcactcattta	gene knockout
cz6959	rev-EIF4E4 3'UTR	SacI	gatcgagctctaatgcacgtttctccaac	PCR
cz6995	fwd-EIF4E2 5'UTR	-	gtatgacaagtgacgaggtcg	PCR
cz7031	rev-PTP	-	aatttgttgtccacggcttca	change of tag
cz7034	fwd-PTP	XhoI	gatcctcgaggaagatcaggtggatcctcg	change of tag
cz7035	rev-PTP	SalI	gatcgtcgactcaggttgacttccccg	change of tag
cz7036	fwd-EIF4E1-PTP	KpnI	gatcggtaccggtggcggaaagacgagaa	PTP-tagging
cz7037	rev-EIF4E1-PTP	XhoI	gatcctcgagggccttgctagcgccatg	PTP-tagging
cz7038	fwd-EIF4E1 3'UTR2	BspE1	gatctccggaaagaggagaggagaggagga	PTP-tagging
cz7039	rev-EIF4E1 3'UTR2	NotI	gatcgcggccgctctcctctatccctcgcag	PTP-tagging
cz7040	fwd-EIF4E2-PTP	KpnI	gatcgggccccatgtacactcaatccttcg	PTP-tagging
cz7041	rev-EIF4E2-PTP	XhoI	gatcgcggccgcgcaattgatacaagggtggga	PTP-tagging
cz7118	fwd-hygro	HindIII	gatcaagcttatgaaaaagcctgaactcaccg	change of resistance
cz7119	rev-hygro	XbaI	gatctctagactattcctttgccctcggac	change of resistance
cz7120	fwd-EIF4E1+	HindIII	gatcaagcttatgatggctgaatcaagcgc	reconstitution of exression

cz7121	rev-EIF4E1+	XmaI	gatccccgggtgttttctccccttcccctc	reconstitution of exression
cz7122	fwd-EIF4E5+	SacI	gatcgagctcatggaggaggagagtcacgcg	reconstitution of exression
cz7123	rev-EIF4E5+	XmaI	gcatcccgggtgacatttga	reconstitution of exression
cz7160	EIF4E1 3‘UTR	XbaI	gatctctagactagcaaggcctaaagag	gene knockout
cz7162	rev-EIF4E3-PTP	NotI	gatcgcggccgcaaaagcgtgaagtcgggtgtta	PTP-tagging
cz7163	fwd-EIF4E3-PTP	KpnI	gatcggtaccgagcatccaacaccgtttg	PTP-tagging
cz7193	fwd-GFP	HindIII	gatcaagcttatggtgagcaagggcga	GFP-PTP control
cz7194	rev-GFP	XbaI + BamHI	gatcggatccgatctctagacttgtacagctcgtccatgcc	GFP-PTP control
cz7195	fwd-PTP	XbaI	gatctctagagaagatcaggtggatcctc	GFP-PTP control
cz7196	rev-intergenic region	XmaI	gatccccgggaagctagcaattcgtttgaacta	GFP-PTP control
cz7210	fwd-EIF4E2+	HindIII	gatcaagcttatgcagaccttactgagacccc	reconstitution of exression
cz7211	rev-EIF4E2+	XmaI	gatccccgggcacgcgtagtttgcaacca	reconstitution of exression
cz7244	fwd-myc	SacII	gatcccgcggctaacgagcaaaagctcatttc	myc-tagging
cz7245	rev-myc	SacII	gatcccgcggttacaagtcctcttcagaaatgag	myc-tagging
cz7283	fwd-EIF3A 5‘UTR	SacII	gatcccgcgggtgggaggatcgttcact	V5-tagging
cz7284	rev-EIF3A 5‘UTR	XbaI	gatctctagaccttcctttctcgtttgttc	V5-tagging
cz7285	fwd-EIF3A ORF	XhoI	gatcctcgagatgttgcaagcggaagtaa	V5-tagging
cz7286	rev-EIF3A ORF	ApaI	gatcgggcccagctttagtttcatcaaccttatc	V5-tagging
cz7359	fwd-CFB2 ORF	NcoI	tataccatggggtccttggaggagggaagc	Recombinant expression
cz7360	rev-CFB2 ORF	BamHI	tataggatccctacatctcagcgtaatccactt	Recombinant expression
cz7512	rev-VSG	-	gttttcgatgctggcttgcg	PCR/qPCR
cz5265	fwd-4EIP	XhoI	gatctcgagagaactacaattcgatac	PCR/qPCR
cz5266	rev-4EIP	KpnI	gatgggcccgtacccctcttcgaatgc	PCR/qPCR
cz7628	fwd-NOT1	-	ctactgacatcgggagctcc	PCR/qPCR
cz7629	rev-NOT1	-	agccgtgcctaattcatcaatg	PCR/qPCR
cz7626	fwd-histone H3	-	aaaccgccaggacgaagaag	PCR/qPCR
cz7627	rev-histone H3	-	ggtgaatgtcctttggttggat	PCR/qPCR
cz7514	fwd-EIF4E6 RNAi	XhoI	tatactcgagatggccgctgaggctact	RNAi
cz7515	rev-EIF4E6 RNAi	BamHI	tataggatcccttcgcctcctcccttcc	RNAi
cz7516	fwd-EIF4E6 5‘UTR	SacII	tataccgcggccttacttacaaccggtaacc	
cz7517	rev-EIF4E6 5‘UTR	XbaI	tatatctagaatctcctttctgttaaataaccctt	
cz7518	fwd-EIF4E6 ORF	XhoI	tatactcgagatggccgctgaggctactg	PCR
cz7519	rev-EIF4E6 ORF	ApaI	tatagggcccaacacgagcggtacagcctg	PCR
cz7560	fwd-TUT3AB	XmaI	tatacccgggaatgttcacatcggtgcctgtag	Y2H (AD, BD)
cz7561	rev-TUT3A	SacI	tatagagctcctagtttttctgacagttgtacgcc	Y2H (AD)
cz7562	fwd-Dis3L2AB	BamHI	tataggatccaaatggatgaaacaccgaatgctgt	Y2H (AD, BD)
cz7563	rev-Dis3L2A	SacI	tatagagctctcaaacgagacttgtgggtattgc	Y2H (AD)
cz7564	rev-TUT3B	NotI	tatagcggccgcctagtttttctgacagttgtacgcc	Y2H (BD)
cz7565	rev-Dis3L2	NotI	tatagcggccgctcaaacgagacttgtgggtattgc	Y2H (BD)
cz7920	fwd-EIF4E2	Sfi	cagtggccatggaggccatgcagaccttactgagacc	Y2H
cz7921	rev-EIF4E2	BamHI	cagtggatcctcacaattgatacaagggtg	Y2H
cz7922	fwd-SLBP2	Sfi	cagtggccatggaggccatgcaaactccgctacgtcc	Y2H
cz7923	rev-SLBP2	BamHI	cagtggatccttactctgtgaataatatc	Y2H
cz7924	fwd-PUF9	Sfi	ggccatggaggccatggaagtacgcgatgtgaa	Y2H
cz7925	rev-PUF9	BglII	cagtagatctctaacactctccgccatcac	Y2H

2.2.7 Southern blotting

For analysis of trypanosomal DNA by Southern blotting, 5 µg of genomic DNA were digested using appropriate restriction enzymes, and subsequently separated by agarose gel electrophoresis. The gel was then incubated with hydrolysis buffer (0.25 M HCl) for 15 min, followed by treatment with denaturing buffer (1.5 M NaCl, 0.4 M NaOH) for 15 min. The latter was then exchanged for neutralizing buffer (1.5 M NaCl, 0.5 M Tris-Cl, pH7.5) and incubated with the gel for 15 min before blotting onto a nylon membrane by downward capillary forces for at least 4 h. The DNA was then UV cross-linked to the membrane using a Stratagene® UV cross-linker. The blot was blocked with pre-hybridization buffer (5× SSC, 0.5% sodium dodecyl sulfate (SDS), 5× Denhardt's solution, 100 µg/mL of salmon sperm DNA) at 65 °C prior to probing. Probes were prepared by incorporation of radioactive nucleotides into PCR products corresponding to the DNA sequence of interest employing the Prime-It kit (Stratagene). Probes (> 2×10^6 cpm/mL) were then incubated with the blot at 65 °C for 16 h. After two sequential washing steps (2× SSC, 0.1 % SDS), 10 min each at 25 °C, followed by another washing step at 65 °C for 15 min, the blot was exposed to a phosphorimaging film before developing the autoradiographs with a phosphorimager (Fugifilm FLA-3000).

2.3 RNA methods

2.3.1 RNA isolation

For preparation of total RNA, samples frozen in TriFast™ were allowed to thaw and incubated for another 5 min at 25 °C to permit the complete dissociation of nucleoprotein complexes. Subsequently, 0.2 mL of chloroform were added, after which the samples were shaken vigorously by hand for 15 s and left at 25 °C for 2-3 min. Samples were centrifuged at 12,000 rpm for 10 min at 4 °C. The upper, aqueous phase was transferred to a fresh tube without disturbing the protein interphase. To precipitate the RNA present in the samples, 7 µL of a 10 mg/mL glycogen solution and 500 µL of isopropanol were added. Samples were mixed briefly by vortexing, incubated at 25 °C for 10 min, and then centrifuged at 12,000 rpm for 15 min at 4 °C. The supernatant was removed, and the cell pellet was washed using 70% ethanol and 5 min centrifugation at 10,000 rpm and 4 °C. The supernatant was removed and the pellets were then subjected to a second washing step with 100% ethanol. After removing the supernatant, the pellets were air-dried for 10 min at 25 °C and subsequently dissolved in 20 µL of RNase-free H_2O by 5 min of incubation at 55 °C.

2.3.2 rRNA depletion

Ribosomal RNAs present in both unbound and bound samples were depleted using an RNase H-based protocol. For this, up to 5 µg of RNA were mixed with hybridization buffer (1× final concentration) and an anti-rRNA oligo mix (131 oligos of approximately 50 bases in 3.275 µL of the mix, corresponding to a final concentration of 0.5 µM of each oligo). Following hybridization according to the program below, equal amounts of 2× RNase H digestion buffer and 5 U of RNase H were added to the reaction, which was then allowed to proceed at 37 °C.

Table 17. Composition of hybridization buffer (5×)

Component	Final concentration
Tris-HCl, pH 7.4	500 mM
NaCl	1 M

Table 18. Composition of RNase H digestion buffer (10×)

Component	Final concentration
Tris-HCl, pH 7.4	500 mM
NaCl	1 M
$MgCl_2$	200 mM

Table 19. Hybridization program

Step	Temperature	Time	
Denaturation	95 °C	2 min	
Hybridization	37 °C	2 min	
	37 °C	pause	Addition of RNase H mix
Digestion	37 °C	30 min	
	4 °C	pause	

Finally, oligonucleotide DNA was removed by addition of Turbo DNase I (Ambion).

Table 20. DNase I treatment

Component	Amount
Turbo DNase I buffer (10×)	5 µL
RNA sample	10 µL
Turbo DNase I	1 µL
H_2O	34 µL

Depleted RNA was then cleaned up using RNA clean-up & concentrator columns (Zymo Research, R1015) according to the manufacturer's instructions, and eluted in 15 µL of RNase-free H_2O for RNA sequencing.

2.3.3 RNA sequencing

After determining the concentrations of the RNAs to be sequenced using a NanoDrop® or a Qubit® spectrophotometer, RNA sequencing was carried out by David Ibberson at the Deep Sequencing Core Facility (Bioquant, Heidelberg).

For RNA sequence analysis, fastq files were used as input for TrypRNAseq, an RNA Seq data analysis pipeline developed in-house (https://github.com/klprint/TrypRNAseq). First, sequencing data underwent a quality control step, adapters were trimmed, and the sequences were aligned to the *T. brucei* genome (TREU927). Read counts were typically normalized to reads per million (RPM). Average RPMs of the bound fractions were compared against the average RPMs of the unbound fractions. Genes with a fold change ≥2 (or ≥1.5, depending on the set of samples) were considered as targets/affected genes.

2.3.4 Quantitative reverse transcription polymerase chain reaction (qRT-PCR)

RNA extracted from trypanosomes according to the procedure described in 2.3.1 was reverse transcribed into cDNA using the Maxima First Strand cDNA synthesis kit (Thermo Scientific, K1671), as described below.

Table 21. cDNA synthesis setup

Component	Amount
5× Maxima reaction mix	4 µL
Maxima enzyme mix	2 µL
Template RNA	up to 5 µg
H_2O	ad 20 µL

Subsequently, qPCR reactions were set up using the Luna Universal qPCR Master Mix (NEB, #M3003S) according to the manufacturer's instructions.

Table 22. qPCR setup

Component	Amount
Luna universal qPCR master mix	10 µL
Fwd primer	0.5 µL
Rev primer	0.5 µL
Template (c)DNA	up to 100 ng
H_2O	ad 20 µL

All samples were measured in triplicates, and expression of VSG or tubulin was used for normalization. Data were analyzed by the $2^{-\Delta\Delta Ct}$ method and plotted using GraphPad Prism software.

2.3.5 RNA separation by polyacrylamide gel electrophoresis

To separate RNAs by polyacrylamide gel electrophoresis, 1×10^8 cells were collected by centrifugation at 3000 rpm for 5 min. The supernatant was replaced by 1 mL of TriFast™ reagent and RNA was extracted according to the standard protocol (2.3.1). The RNA was then mixed with 2x bromophenol loading dye and separated on a polyacrylamide gel by 2.5 h of electrophoresis at 100 V.

Table 23. Tris-borate-EDTA (TBE) buffer (10×)

Component	Amount
Tris-HCl	108 g
Boric acid	55 g
Na_2EDTA	9.3 g
H_2O	ad 1 L

Table 24. Polyacrylamide gel (15%) for separation of RNAs

Component	Amount
Urea	21 g
Polyacrylamide mix	12.5 mL
TBE (10×)	5 mL
H_2O	ad 50 mL

Afterwards, the RNAs were stained with methylene blue for 1 h and the rest of the gel was subsequently destained for 3 h using H_2O.

2.3.6 Analysis of circular RNAs

This method has been published in Falk et al. (2021) with slight modifications [122]: "For this purpose, 1×10^8 PCFs were harvested after growth with or without glucose, and total RNA was extracted according to the standard protocol. Afterwards, 30 µg of RNA were treated with 20 U of

DNase I in 200 µL in the presence of RNaseIN for 30 min at 25 °C. The reaction was terminated by phenol-chloroform extraction and ethanol precipitation of the RNA. The pellet was dissolved in 32 µL of RNase-free water and incubated with 100 pmol of an oligonucleotide complementary to the first 15 nt of the spliced leader (5'-*TCTAATAATAGCGTT*-3') at 37 °C for 5 min. RNase H buffer was added to reach a concentration of 1×, along with 5 U of RNase H, and the reaction was then incubated for 1 h at 37 °C. The RNA was then purified and precipitated with ethanol according to the standard protocol. Subsequently, 10 µg of RNA were circularized by incubation at 16 °C for 16 h in a reaction volume of 400 µL containing 40 U of T4 RNA and 80 U of RNaseIN. For reverse transcription, ~2 µg of RNA were incubated with 50 pmol of *GPEET*-specific reverse primer, 200 U SuperScript III RT (Invitrogen), and 40 U RNase inhibitor in a 20 µL reaction volume.
PCR amplification was performed in a 50 µL reaction using 1 µL of cDNA (5%), 10 pmol each of forward and reverse primers, and 2.5 U Taq DNA polymerase in the corresponding buffer system (program: 30 s at 95 °C, 30 s at 52 °C, and 45 s at 72 °C). The PCR products were gel-purified and cloned into EamI-digested p2T7 vector. Clones were randomly selected and analyzed by sequencing."

2.3.7 Ribosome profiling

For isolation of ribosome-protected fragments, 3×10^9 BSF parasites were harvested by centrifugation (8 min, 2300 rpm). The pellet was resuspended in 50 mL of fresh media supplemented with 100 µL of cycloheximide (stock: 50 µg/µL) and incubated at 37 °C for 10 min. The cells were harvested and subjected to a washing step using PBS supplemented with cycloheximide. After another round of centrifugation, the cell pellet was lysed in 300 mL of lysis buffer by pipetting 20× up and down. For removal of cellular debris, the lysate was centrifuged for 10 min at 13,000 × *g* and 4 °C. The supernatant was subsequently transferred to a fresh 1.5 mL tube and the concentration of the lysate was determined spectrophotometrically. For each 5 OD recorded in this fashion, 20 U of RNAseI were added and the samples were mixed by pipetting. After 1 h of incubation at 25 °C, the reaction was stopped by addition of 15 µL of SUPERaseIN. In the meantime, two S400 columns per sample were re-equilibrated with 4 mL of ribosome profiling buffer by washing them repeatedly with ribosome profiling buffer. Half of the digestion reaction was added per pre-equilibrated column, which was followed by 2 min centrifugation at 600 x *g.* For subsequent RNA extraction, 850 µL of TriFast™ reagent were added and the ribosome-protected fragments were isolated as per the instructions in 2.3.1. The elution step was performed using 12.5 µL of H_2O, and split samples were re-combined to 25 µL per replicate.
Isolated RNA fragments were then separated on a 15% PAA gel, which was run at 20 mA by gradual adjustment of the voltage from 100-200 V. For staining of the RNA, the gel was transferred to 50 mL of TBE buffer with SYBRGold dye and incubated for 10 min while gently rocking. A UV-imager served to visualize the stained RNA fragments, with the reference RNAs allowing the identification and isolation of the desired fragment sizes. More specifically, the region between the two reference bands was cut in each sample and transferred to a fresh 0.5 mL tube into which a hole had been pinched with a needle. This tube was then placed into a 1.5 mL tube to force the gel through the opening upon centrifugation at 8000 rpm for 5 min. To extract the RNA from the gel, 400 µL of 300 mM NaOAc with 1.0 mM EDTA were added to each sample. After incubation at -80 °C overnight, the samples were thawed and incubated at 25 °C for 2 h. To separate the gel from the buffer containing the RNA fragments, the samples were centrifuged at 10,000 rpm for 5 min. The supernatant was transferred to a fresh tube and the RNA was precipitated by addition of an equal volume of isopropanol and 5 µL of glycogen. To increase the yield, the RNA was allowed to precipitate overnight at -20 °C.

On the following day, the RNA was pelleted by centrifugation at 13,000 x *g* and 4 °C for 20 min. The pellet was washed with freshly prepared 80% ethanol, subsequently allowed to dry for 10 min at 25 °C, and resuspended in 10 µL of H_2O. For dephosphorylation of the RNA fragments, 33 µL of H_2O were added, followed by denaturation at 80 °C for 1.5 min. Afterwards, 5 µL of 10× PNK buffer, as well as 1 µL of SUPERaseIn and 1 µL of T4 PNK were added to the RNA samples. The reactions were incubated at 37 °C for 1 h, subsequently heat-inactivated at 70 °C for 10 min, and cleaned up using the Zymo RNA clean and concentrator kit according to the manufacturer's instructions. The RNA was eluted in 10.5 µL of H_2O to then proceed with the library preparation for sequencing using the NEXTFLEX® Small RNA-Seq Kit v3 according to the manufacturer's instructions (gel-free size selection and cleanup option). Sequencing was carried out by David Ibberson (Deep Sequencing Core Facility, Bioquant, Heidelberg).

Table 25. Composition of lysis buffer for ribosome profiling, pH 7.4

Component	Final concentration
Tris-HCl	20 mM
NaCl	250 mM
$MgCl_2$	15 mM
DNase I	24 U/mL
Triton X-100	0.05%
DTT	1 mM
Cycloheximide	100 µg/mL

Table 26. Composition of ribosome profiling buffer, pH 7.4

Component	Final concentration
Tris-HCl	20 mM
NaCl	250 mM
$MgCl_2$	15 mM

2.3.8 Polysome profiling

Prior to cell harvest, 15-50% sucrose gradients were made using polysome buffer according to the instructions on the machine (TRIAx™ Flow Cell, Biocomp Instruments). Per gradient, 5×10^8 BFSs without (-tet) or with (+tet) induction of *EIF4E6* RNAi for 24 h were harvested by 15 min centrifugation at 4 °C and 2000 × *g*. The cell pellet was resuspended in 50 mL of serum-free HMI-9 medium and again collected by centrifugation at 4 °C and 1000 × *g* for 7 min. After removal of the supernatant, the pellet was resuspended in 1 mL of ice-cold PBS and subjected to another centrifugation step at 4 °C and 1000 × *g*. The cells were lysed in 350 µL of lysis buffer by repeated passage through 21 and 27 gauge needles using a 1 mL syringe. Subsequently, the lysate was cleared by centrifugation at 15,000 × *g* for 10 min at 4 °C. The salt concentration was then adjusted to 120 mM KCl. Afterwards, the lysate was loaded onto the linear sucrose gradient and ultracentrifuged at 164,326 × *g* for 2 h at 4 °C in a Beckmann SW60 centrifuge using a swinging bucket rotor. This was followed by collection of 16 fractions of 500 µL each upon fractionation on a UV/VIS detector (TRIAx™ Flow Cell, Biocomp Instruments).

Table 27. Composition of lysis buffer for polysome profiling, pH 7.5

Component	Final concentration
Tris-HCl	20 mM
KCl	20 mM
$MgCl_2$	2 mM
DTT	2 mM
RNasin	500 U/mL
Leupeptin	10 µg/mL
IGEPAL	0.2%
Sucrose	200 mM
Cycloheximide	100 µg/mL

Table 28. Composition of polysome buffer, pH 7.5

Component	Final concentration
Tris-HCl	20 mM
KCl	120 mM
$MgCl_2$	2 mM
DTT	1 mM
Leupeptin	10 µg/mL
Cycloheximide	100 µg/mL

2.4 Protein methods

2.4.1 SDS polyacrylamide gel electrophoresis (PAGE)

Sample collection: Trypanosomes

For this, 1-5 × 10^6 trypanosomes were harvested by centrifugation (10 min at 2300 rpm) and washed once with 1× PBS. For cell lysis, Laemmli buffer was added to the cell pellet, which was then resuspended and boiled for 10 min at 95 °C. Of note, samples that were analyzed for PAD1 expression were not subjected to heat denaturation and SDS-PAGE was performed at 4 °C to prevent degradation of the unstable PAD1 protein.

Table 29. Composition of Laemmli buffer (6×)

Component	Final concentration
Tris-HCl, pH 6.8	375 mM
SDS	12%
EDTA	45 mM
β-mercaptoethanol	30%
Glycerol	60%
Bromophenol blue	0.01%

Sample collection: Yeast

For analysis by SDS-PAGE, 500 µL of an overnight culture were subjected to centrifugation (1000 × *g*, 5 min). The supernatant was removed and the cells were resuspended in 100 µL of supercracking buffer. To lyse the cells and denature the proteins, samples were boiled for 10 min at 95 °C.

Table 30. Composition of yeast supercracking buffer

Component	Final concentration
Urea	8 M
SDS	5% (w/v)
Tris-HCl, pH 6.8	40 mM
EDTA	0.1 mM
Bromophenol blue	0.4 mg/mL
β-mercaptoethanol	1% (v/v)

Gels

Proteins were concentrated using 5% SDS polyacrylamide stacking gels at 80 V, whereas percentages of separating gels ranged from 8% to 15% and were run at 120 V in running buffer. The gels were then subjected to either Coomassie staining (2.4.2) or western blotting (2.4.3.).

Table 31. Stacking gel, 5% (10 mL)

Component	Amount
Polyacrylamide (30%)	1.7 mL
Tris-HCl, pH 6.8 (1 M)	1.25 mL
SDS (10%)	100 µL
APS (10%)	100 µL
TEMED	10 µL
H_2O	ad 10 mL

Table 32. Separation gel, 8-15% (20 mL)

Component	Amount
Polyacrylamide (30%)	5.3-10 mL
Tris-HCl, pH 8.8 (1.5 M)	5 mL
SDS (10%)	200 µL
APS (10%)	200 µL
TEMED	8 µL
H_2O	ad 20 mL

Table 33. Composition of running buffer (1 L)

Component	Amount
Tris	3.03 g
Glycine	14.42 g
SDS	1 g
H_2O	ad 1 L

2.4.2 Coomassie staining

Proteins separated by SDS-PAGE were fixed by incubation in destaining solution I for 30-60 min and subsequently stained with Coomassie (0.2% in 95% ethanol) for 1-6 h at 25 °C. To destain the gel, it was shortly rinsed with destaining solution II and subsequently incubated with destaining solution I until the bands were clearly distinguishable.

Table 34. Composition of destaining solution I

Component	Amount
Ethanol	40 mL
Acetic acid	10 mL
H_2O	50 mL

Table 35. Composition of destaining solution II

Component	Amount
Ethanol	10 mL
Acetic acid	10 mL
H_2O	80 mL

2.4.3 Protein detection by western blotting

Proteins separated by SDS-PAGE were subsequently transferred to a 0.45 µm nitrocellulose blotting membrane (Neolabs). To verify efficient protein transfer, the membrane was stained using Ponceau S (SERVA). The membrane was then blocked for 1 h at 25 °C using 5% (w/v) milk in TBS-Tween. Overnight incubation with the desired primary antibody in 5% milk in TBS-Tween was then followed by three sequential washing steps (10 min each) using TBS-Tween. Afterwards, the corresponding secondary antibody was incubated with the membrane for 1 h at 25 °C. The Western Lightning Ultra® (Pekin Elmer) system was used for detection of chemiluminescent signals on an LAS-4000 machine (GE Healthcare) with a CCD camera (Fujifilm™).

Table 36. Composition of blotting buffer (1 L)

Component	Amount
Tris	3.03 g
Glycine	14.42 g
Methanol	200 mL
H_2O	ad 1 L

Table 37. Composition of TBS-Tween

Component	Amount
Tris	50 mM
NaCl	150 mM
Tween-20	0.05%

Table 38. Primary antibodies used for protein detection by western blotting

Antibody	Dilution	Supplier	Origin
Anti-aldolase	1:50,000	Antiserum	Rabbit
Anti-EIF4E1	1:2000	Antiserum	Rabbit
Anti-HPC4	1:1000	Cell Signaling Technology	Rabbit
Anti-myc (9E10)	1:2000	Santa Cruz Biotechnology	Mouse
Anti-PAD1	1:000	Antiserum	Rabbit
Anti-V5	1:2000	Biorad (MCA1360)	Mouse
Anti-pGPEET	1:2000	Cedarlane	Mouse
Anti-EP1	1:2000	Cedarlane	Mouse
Anti-DHH1	1:5000	Antiserum	Rabbit
Anti-CAT	1:2000	Antiserum	Rabbit
Anti-CFB2	1:2000	Antiserum	Rabbit

Peroxidase-anti-peroxidase (PAP)	1:20,000	Sigma	Rabbit
Anti-HA	1:1000	Roche	Rat
Anti-S9	1:2000	Antiserum	Rat

Table 39. Secondary antibodies used for protein detection by western blotting

Antibody	Dilution	Supplier	Origin
ECL anti-mouse IgG	1:2000	GE Healthcare	Sheep
ECL anti-rabbit IgG	1:2000	GE Healthcare	Donkey
ECL anti-rat IgG	1:2000	GE Healthcare	Goat
ECL anti-mouse IgG true blot	1:2000	Rockland	Goat

2.4.4 Protein purification of recombinant CFB2 for antibody production

Recombinant protein expression

Ten individual colonies of bacteria transformed with an expression vector encoding a fusion product of CFB2 and a carrier protein (NusA) were inoculated in 5 mL of LB^{Kan} each and grown for 16 h at 37 °C. After that, OD measurements were performed every hour, until the cultures had reached an OD_{600} of 0.8. After that, 1 mL of each inoculum was collected by centrifugation (2 min, 16,000 × *g*), and the supernatant was removed. The pellet was resuspended and lysed in Laemmli buffer ("uninduced" sample) and stored at -20 °C until further processing. IPTG at a final concentration of 1 mM was added to the remaining 4 mL of the culture to induce recombinant protein expression. Additionally, another 1 mL of LB^{Kan} was added before the samples were incubated at 27 °C for 14 h. As an OD_{600} of 2.5-3 was reached, 300 µL were collected per sample by centrifugation at 16,000 × *g* for 2 min. "Induced" samples were processed and lysed in a similar way as the "uninduced" samples. All samples were boiled at 95 °C for 10 min and the proteins were separated using 10% SDS-polyacrylamide gels, which were then stained with Coomassie blue.

Analysis of soluble and insoluble fractions

Recombinant protein expression was induced as described above. Instead of subjecting the bacteria to lysis by addition of Laemmli buffer, the pellet was resuspended in 350 µL of bacterial lysis buffer. Additionally, 25 µL of freshly prepared lysozyme solution (stock: 10 mg/mL in Tris-HCl, pH 8.0) were added. The samples were then vortexed and incubated at 4 °C for 4 h on a rotor. The samples were subjected to three freeze-thaw cycles using liquid nitrogen. Soluble and insoluble fractions were separated by centrifugation for 10 min at 16,000 x *g*. Liquid and solid phases were then analyzed by SDS-PAGE and Coomassie staining to determine which fraction contained the recombinant protein of interest.

Table 40. Composition of bacterial lysis buffer

Component	Amount/concentration
Tris, pH 7.5	50 mM
NaCl	100 mM
EDTA	1 mM
DTT	1 mM
Aprotinin	1 µg/mL
Leupeptin	1 µg/mL

Purification of inclusion bodies

For this purpose, IPTG-induced bacteria were incubated overnight at 27 °C in 1 L of LB medium until an OD_{600} of 0.8 was reached. The bacteria were harvested by 20 min of centrifugation at 5000 rpm. The pellet was washed with PBS and stored at -80 °C until further processing. It was then thawed and resuspended in 500 µL of bacterial lysis buffer supplemented with 50 µL of freshly prepared lysozyme solution (stock: 10 mg/mL in Tris-HCl, pH 8.0). Lysis was performed by rotation for 4 h at 4 °C, followed by three freeze-thaw cycles using liquid nitrogen. Inclusion bodies were collected by 20 min of centrifugation at 15,000 rpm and 4 °C. The pellet was then washed once with bacterial lysis buffer containing 1% Triton-X100, followed by centrifugation for 20 min at 15,000 rpm and 4 °C to pellet inclusion bodies. The latter were then resuspended in 10 mL of 8 M urea and left to dissolve overnight at 4 °C with constant rotation.

2.4.5 Affinity purification of proteins

Coupling of magnetic beads

Magnetic beads (Dynabeads™ M-280 Tosylactivated, Thermo Fisher Scientific) were resuspended by vortexing for 30 s, and 165 µL were transferred to an RNase-free tube. This tube was then placed into a magnetic stand (DynaMag™-2 Magnet), and the beads were allowed to concentrate on one side. The supernatant was discarded and 1 mL of buffer A was added. Again, the beads were collected using a magnet, after which a second washing step was performed using 165 µL of buffer A. After placing the tube in a magnet and removing the supernatant, 100 µg (10 µL) of rabbit IgG were added to the beads, filled up to 150 µL using buffer A, and vortexed for approximately 30 s. Subsequently, 100 µL of buffer C were added and mixed by vortexing. The beads were incubated with the antibodies at 37 °C for 12-18 h while rotating (20 rpm). On the following day, the tube was placed in a magnetic stand and the supernatant was removed. This was followed by two sequential washing steps with an excess of PBS-Tween (0.05%). The beads were washed twice with PBS (pH 7.4) and eventually resuspended in 240 µL of PBS to achieve a final bead concentration of 20 mg/mL.

Table 41. Composition of buffer A, pH 7.4 (1 L)

Component	Amount
NaH_2PO_4	2.62 g
Na_2HPO_4	13.42 g
H_2O	ad 1 L

Table 42. Composition of buffer C, pH 7.4 (0.1 L)

Component	Amount
$(NH_4)_2SO_4$	39.64 g
Buffer A	ad 0.1 L

Cell lysis and protein/RNP capture

This method has been published in Falk et al. (2021) with slight modifications [122]: “For cell harvest, 2×10^9 (MS/RNA-IP) or 1×10^8 (IP followed by WB) cells at a concentration of 5×10^5 cells/mL were centrifuged at 3000 rpm for 13 min at 4 °C. The pellet was resuspended in 50 mL of ice-cold PBS and centrifuged at 2300 rpm for 8 min. After removal of the supernatant, the pellet was snap-frozen in liquid nitrogen and stored at -80 °C until further processing. All of the following steps were performed in the cold room (4 °C). Cell pellets were thawed on ice and resuspended in 0.5 mL of lysis

buffer (see below). For releasing protein contents, the cells were passaged 20× through a 21G×1½'' needle and 20× through a 27G×¾ needle using a 1 mL syringe. In order to pellet the cell debris, samples were centrifuged at 10,000 × *g* for 15 min, and the supernatant was transferred to a fresh tube. The salt concentration was then adjusted to 150 mM KCl. Magnetic IgG-coupled beads were adjusted by three sequential washes with wash buffer (see below). Depending on the cell number, 10-100 µL of the beads were then added to each sample. To allow binding, cell lysate and beads were incubated for 1 h at 4 °C while rotating (20 rpm)."

Sample preparation

For western blotting

The beads were boiled in Laemmli buffer for 10 min at 95 °C.

For mass spectrometry

The beads were washed four times with wash buffer and subjected to TEV protease cleavage in 0.5 mL of wash buffer for 90 min at 20 °C. For removal of His-tagged TEV, IgG magnetic beads were collected on one side and the supernatant was transferred to a new tube. Afterwards, 10 µL of equalization buffer and 30 µL of Ni-NTA-magnetic beads were added and incubated for 30 min at 20 °C while rotating (20 rpm). Ni-NTA magnetic beads were retained by a magnetic stand and the supernatant was transferred to a fresh tube and stored in Laemmli buffer at -80 °C.

For RNA sequencing

Unbound samples were transferred to a new tube, three volumes of peqGOLD TriFast™ FL reagent were added, and the samples were stored at -80 °C until further processing. The beads were washed four times with wash buffer and subjected to TEV protease cleavage in wash buffer for 90 min at 20 °C. The beads were concentrated on one side of the tube to collect the elution fractions, and three volumes of peqGOLD TriFast™ FL reagent were added to the supernatant. The samples were stored at -80 °C until further processing.

Table 43. Composition of lysis buffer for affinity purification

Component	Final concentration
Tris, pH 7.5	20 mM
$MgCl_2$	5 mM
IGEPAL	0.05%
DTT	1 mM
RNasin	100U/mL
Aprotinin	10 µg/mL
Leupeptin	10 µg/mL

Table 44. Composition of wash buffer for affinity purification

Component	Final concentration
Tris, pH 7.5	20 mM
$MgCl_2$	5 mM
IGEPAL	0.05%
DTT	1 mM
RNasin	100U/mL
KCl	150 mM

Table 45. Composition of equalization buffer (2×)

Component	Final concentration
Na_3PO_4	200 mM
NaCl	600 mM
Imidazole	60 mM
Tween-20	0.1% (v/v)
NaOH	to pH 8.5

2.4.6 Mass spectrometry

Proteins co-purifying with PTP-tagged EIF4E1, EIF4E2, EIF4E3, EIF4E5, and EIF4E6 were analyzed by LC/MS at the ZMBH Mass Spectrometry Facility. Experiments were performed in duplicates or triplicates, and trypanosomes expressing GFP-PTP served as a control.

For that purpose, the proteins were separated by SDS-PAGE (2 cm into a 1.5 mm NuPAGE™ Novex™ 4-12% Bis-Tris protein gel (Thermo Fisher Scientific)) and subjected to Coomassie blue staining, destained with destaining solution (10% acetic acid, 50% methanol), and cut from the gel. This gel area was then quantitatively analyzed by mass spectrometry.

Raw files were processed using MaxQuant (version 1.5.3.30) for peptide identification and quantification. MS2 spectra were searched against the TriTrypDB-8.1TREU927-AnnotatedProteins-1 database (containing 11567 sequences), contaminants of Maxquant were included. The maximum false discovery rate for proteins and peptides was 0.01 and a minimum peptide length of 7 amino acids was required. Analysis was done in LFQ mode; all other parameters are default parameters of MaxQuant. Data provided by the facility were further processed using Perseus software [123].

2.4.7 Targeted yeast-2-hybrid assays

This method has been published in Falk et al. (2021) with slight modifications: “For testing direct protein-protein interactions, the Matchmaker Yeast Two-Hybrid System (Clontech) was used according to the manufacturer’s instructions. To that end, the genes of interest (*TUT3*, *4EIP*, *Dis3L2*, *EIF4E2*, *SLBP2*, and *PUF9*) were PCR-amplified from genomic DNA and cloned into both pGBKT7 and pGADT7 plasmids. Prey and bait plasmids were co-transformed pairwise into AH109 yeast strains, and selected initially on double drop-out (DDO) plates (i.e., SD medium lacking Trp and Leu) or quadruple drop-out (QDO) plates (i.e., lacking Trp, Leu, His, and Ade). Growth on QDO plates indicated positive interactions. The interaction between p53 and SV40 large T-antigen and the combination of LaminC and SV40 large T-antigen served as positive and negative controls, respectively. Western blotting was used to confirm expression of c-myc-tagged BD-domain proteins and HA-tagged AD-domain proteins.”

Table 46. Composition of dropout solution (10×)

Component	Final concentration
L-isoleucine	300 mg/L
L-valine	1500 mg/L
L-arginine HCl	200 mg/L
L-lysine HCl	300 mg/L
L-methionine	200 mg/L
L-phenylalanine	500 mg/L
L-threonine	2000 mg/L
L-tyrosine	300 mg/L
L-uracil	200 mg/L

Table 47. Composition of SD medium (5 L), sterile-filtered

Component	Amount
Yeast nitrogen base without amino acids	33.5 g
Dropout solution (10×)	500 mL
Glucose	100 g

3. Results

3.1 *Tb927.11.2260* - Eukaryotic translation initiation factor 4E1 (EIF4E1)

3.1.1 EIF4E1 is expressed and stabilized through direct interactions with 4EIP in BSFs and PCFs

While EIF4E3 and EIF4E4 are considered canonical translation initiation factors, EIF4E1 is presumed to exert specific roles at particular life cycle stages. There is growing evidence from *Leishmania* species that EIF4E1 is a translational activator that is inhibited by 4EIP [101]. The latter was previously shown to be essential during stumpy formation by being a main effector of this translationally suppressed stage [100].

In *T. brucei*, 3-8 × 10^3 and 1.5-5 × 10^3 molecules of EIF4E1 are present in PCFs and BSFs, respectively, according to quantitative western blotting with samples from the Lister 427 strain [97]. In this study, experiments were performed with differentiation-competent EATRO1125 cells. To investigate the roles of EIF4E1 during different life cycle stages, expression was analyzed in EATRO1125 strain BSFs and PCFs by western blotting using specific antiserum. As shown in **Figure 3.1A**, EIF4E1 was expressed during both life cycle stages analyzed, with slightly higher relative levels in the BSF.

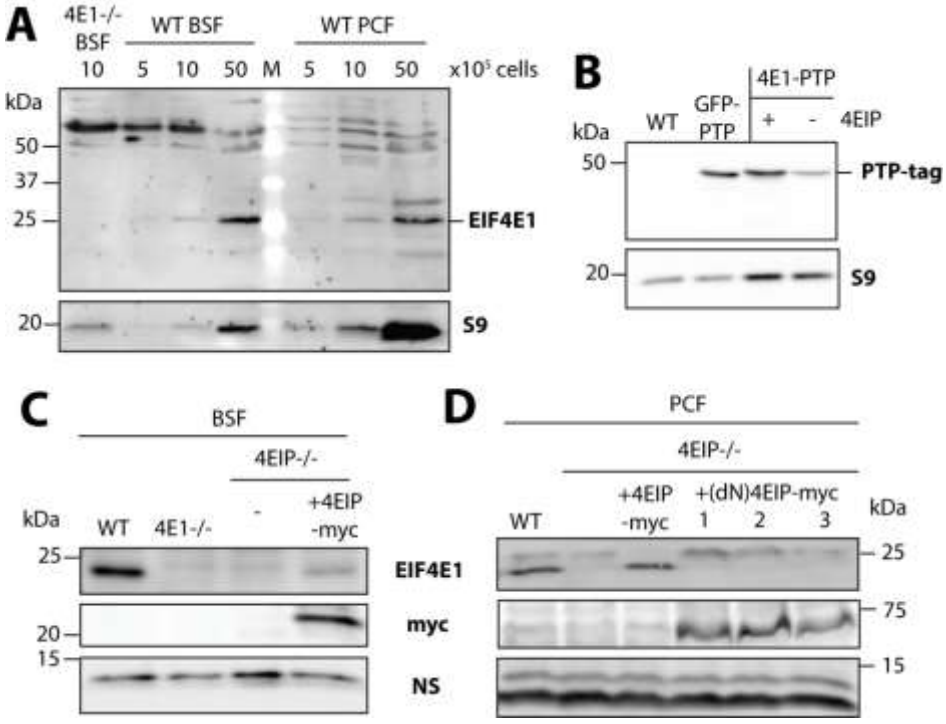

Figure 3.1 EIF4E1 is expressed in bloodstream and procyclic forms (BSFs and PCFs, respectively), where it is more abundant in the presence of 4EIP. (A) Expression of EIF4E1 was analyzed in wildtype (WT) PCFs and BSFs, as well as in BSFs with a homozygous knockout (KO) of *EIF4E1* (4E1-/-). Expression of the 40S ribosomal protein S9 was used as a loading control. The number of cells loaded per lane is indicated at the top. **(B)** Western blot analysis of PTP-tagged versions of EIF4E1 (± 4EIP) and GFP, which were introduced into pleomorphic BSFs of *T. brucei*. WT BSFs that were not expressing any PTP-tagged protein served as a negative control. Expression of the 40S ribosomal protein S9 was used as a loading control. **(C)** Expression of EIF4E1 was analyzed in WT, 4EIP-deficient, and 4EIP-deficient BSFs reconstituted with myc-tagged full-length 4EIP. A non-specific (NS) signal was used as a loading control. Notably, in the case of full-length myc-tagged 4EIP, a degradation product at a smaller size could only be reliably detected, whereas the intact protein was highly unstable. **(D)** Expression of EIF4E1 was analyzed in WT, 4EIP-deficient, and 4EIP-deficient PCFs reconstituted with myc-tagged full-length or N-terminally deleted 4EIP. A non-specific (NS) signal was used as a loading control. Notably, full-length myc-tagged 4EIP was highly unstable, while the deletion mutant was reliably detected at the expected size. The data presented have been published with modifications in Falk et al., 2021 [122]

A sequence encoding a C-terminally PTP-tagged version was introduced into the genomic *EIF4E1* locus of WT and *4EIP* KO BSFs to monitor expression of EIF4E1 and to allow for specific purification (**Figure 3.1B**)**.** The second, untagged version was deleted, which did not compromise cell growth, indicating that the tagged version was functional (data not shown). EIF4E1-PTP-expressing BSFs with a WT background could be differentiated to PCFs using *cis*-aconitate treatment and a temperature reduction from 37 °C to 27 °C. Obtained cells featured a doubling time of 9.5 h, which was similar to that of WT PCFs. As 4EIP expression was required for BSF to PCF differentiation, PCFs with a homozygous KO of *4EIP* and additional expression of EIF4E1-PTP had to be generated the same way as the corresponding BSFs, not by differentiation. To identify unspecific interactions with the PTP-tag in subsequent pulldown experiments, a cell line expressing GFP-PTP was used as a control.
Interestingly, reduced abundance of the EIF4E1-PTP protein was observed in cells lacking both copies of *4EIP* (**Figure 3.1B**). To determine whether this was also true for the untagged, endogenous version of the protein, expression levels of EIF4E1 were analyzed in BSFs and PCFs with a *4EIP* KO background using specific antiserum. In line with the EIF4E1-PTP data, EIF4E1 levels were reduced in the absence of 4EIP, in both BSFs and PCFs (**Figure 3.1C, D**). Ectopic expression of a myc-tagged, full-length version of 4EIP was able to rescue EIF4E1 expression in both BSFs and PCFs, while expression of an N-terminal deletion mutant did not have this effect on EIF4E1 (PCFs tested only), indicating that direct contact between the two proteins was essential for this rescue effect (**Figure 3.1C, D**). However, residual expression of PTP-tagged EIF4E1 in cells lacking 4EIP was still sufficient for subsequent experiments, allowing for targeted purification of EIF4E1 in absence and presence of 4EIP.

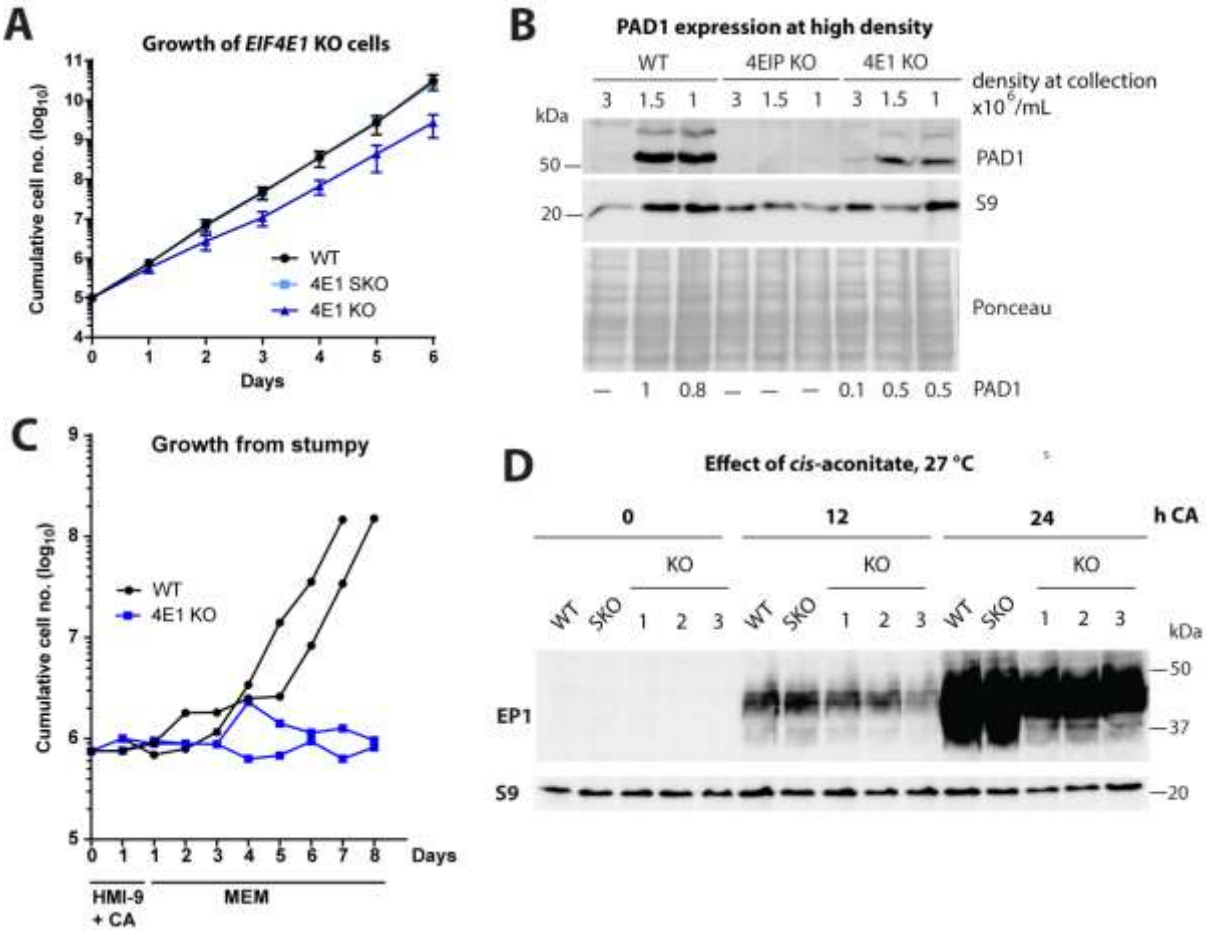

Figure 3.2 EIF4E1 is essential for survival of procyclic cells. (A) Growth of bloodstream forms (BSFs) lacking either a single copy or both copies of *EIF4E1* (4E1 SKO and KO, respectively) was monitored over the course of one week. Parental

wildtype (WT) BSFs served as a reference for normal growth. Mean and standard deviation of three independent experiments are shown. **(B)** Western blot analysis of PAD1 expression in 4EIP-, EIF4E1-deficient and WT BSFs after induction of stumpy formation by growth to high densities in methylcellulose-containing culture medium. Relative PAD1 expression and cell densities at cell harvest are indicated in the bottom and top panels, respectively. **(C)** Growth monitoring after induction of differentiation in WT and EIF4E1-deficient cells. For this, cells were grown to maximum densities of approximately 3×10^6 cells/mL in methylcellulose-containing culture medium. As the cell densities were starting to decline, they were monitored at 1 h intervals. When reaching a density of 1×10^6 cells/mL, the cells were collected, filtered, and transferred to HMI-9 medium with 6 mM *cis*-aconitate (CA) at a starting density of 0.75×10^6 cells/mL. Additionally, the temperature at which the cells were cultured was reduced from 37 °C to 27 °C. After 24 h, the cells were transferred to procyclic form (PCF)-specific culture medium (MEM) and cell growth was followed over the course of one week. Results from two independent experiments are shown side by side. **(D)** Expression of the procyclic surface marker protein EP1 in either WT cells or cells lacking a single copy (SKO) or both copies of *EIF4E1* (KO clones 1, 2, and 3) was analyzed by western blotting after addition of *cis*-aconitate and incubation at 27 °C for the times indicated. Expression of the 40S ribosomal protein S9 was used as a loading control. The data presented have been published with modifications in Terrao et al., 2018 [100]

3.1.2 EIF4E1 is dispensable in the BSF, but essential for survival of PCFs

Differentiation-competent BSFs with a homozygous KO of *EIF4E1* were obtained by replacing the ORFs with blasticidin S deaminase (BSD) and puromycin N-acetyl-transferase (PAC) genes. This was confirmed by both PCR and Southern blotting (**Supplementary Figure S1**). These cells featured only a mild growth defect compared to the WT, highlighting that EIF4E1 is not essential for survival of the BSF (**Figure 3.2A**). Cells lacking only one copy of the gene grew at similar rates as WT cells (**Figure 3.2A**).

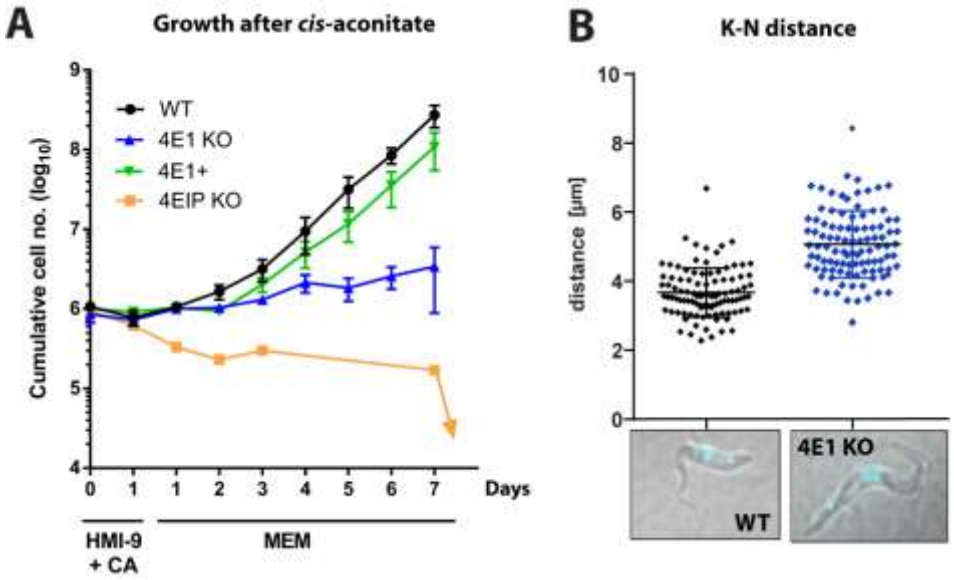

Figure 3.3 EIF4E1-deficient procyclic forms (PCFs) feature a stress-related phenotype. (A) Growth monitoring after induction of differentiation to the PCF by *cis*-aconitate (CA). Cells with a homozygous knockout of *4EIP* (4EIP KO), *EIF4E1* (4E1 KO), or with reconstituted expression of EIF4E1 (4E1+), as well as wildtype (WT) cells at a starting density of 0.75-1 × 10^6 cells/mL were treated with 6 mM *cis*-aconitate and grown at 27 °C for 24 h. On the following day, the medium was exchanged for an equal volume of PCF-specific culture medium (MEM) and cell counts were documented during the following week. For WT, 4E1 KO, and 4E1+ cells, mean and standard deviation of three independent experiments are shown. In the case of 4EIP KO cells, one representative experiment is shown. **(B)** WT and 4E1 KO cells were differentiated to PCFs by *cis*-aconitate treatment and analyzed by fluorescence microscopy after 7 days post transfer to PCF-specific culture medium. Kinetoplast (K) and nuclear (N) DNAs were visualized by DAPI staining and the K-N distance was measured in 100 cells each. Data points represent single cells, and mean and standard deviation are indicated. One representative image of each cell population is shown at the bottom. The data presented in **(A)** have been published with modifications in Terrao et al., 2018 [100]

While 4EIP-deficient cells reportedly fail to differentiate to stumpy BSFs [100], cells lacking EIF4E1 could progress to the stumpy stage, as evidenced by expression of the stumpy marker PAD1 (**Figure 3.2B**), a membrane transporter protein specifically expressed during this particular life cycle stage, as the cells were grown to maximal densities in methylcellulose-containing medium. When these *EIF4E1* KO stumpy forms were further differentiated to the PCF by addition of *cis*-aconitate, early PCF-specific markers were found to be up-regulated with a minor delay (**Figure 3.2D**). Nonetheless, cells lacking EIF4E1 could not grow as proper procyclic cells even after an extended period in culture and eventually died after several days to weeks (**Figure 3.2C**). Moreover, in contrast to WT cells and cells with reconstituted expression of EIF4E1 (addback cell lines), EIF4E1-deficient cells did not resume growth after induction of differentiation to the PCF in late-log phase BSFs by addition of *cis*-aconitate, a "shortcut" differentiation protocol (**Figure 3.3A**). Morphologically, this was accompanied by an elongated shape and a longer kinetoplast-nucleus (K-N) distance, a known stress-related phenotype (**Figure 3.3B**). The cells did not recover, even after several weeks in culture. Furthermore, several attempts to obtain PCFs with homozygous KO of *EIF4E1* by transfecting the constructs used to generate the corresponding BSF cell line did not succeed. Therefore, it was concluded that EIF4E1, unlike its binding partner 4EIP, is not required for differentiation to the growth-arrested stumpy form, but essential for established PCFs, a stage at which 4EIP is no longer essential. Unfortunately, RNAi of EIF4E1 was not effective in both BSFs and PCFs (data not shown).

3.1.3 EIF4E1 does not serve as an activator of translation in the absence of 4EIP

The non-overlapping phenotypes of EIF4E1- and 4EIP-deficient cells raised the hypothesis that EIF4E1 and 4EIP may serve cellular functions independent of each other. In this regard, it had been speculated that EIF4E1 could act as a translational activator that is inhibited by 4EIP. Based on previous studies reporting an association between the translation factor EIF3A and EIF4E1 in *Leishmania*, I pulled down tagged EIF4E1 from *T. brucei* BSFs, but EIF3A-V5 could not be co-purified with it in presence or absence of 4EIP (**Figure 3.4A, B**) [101]. Compared to EIF4E1, the components of the multisubunit EIF3 complex are highly abundant, and were most likely associated with other, translation-promoting complexes.

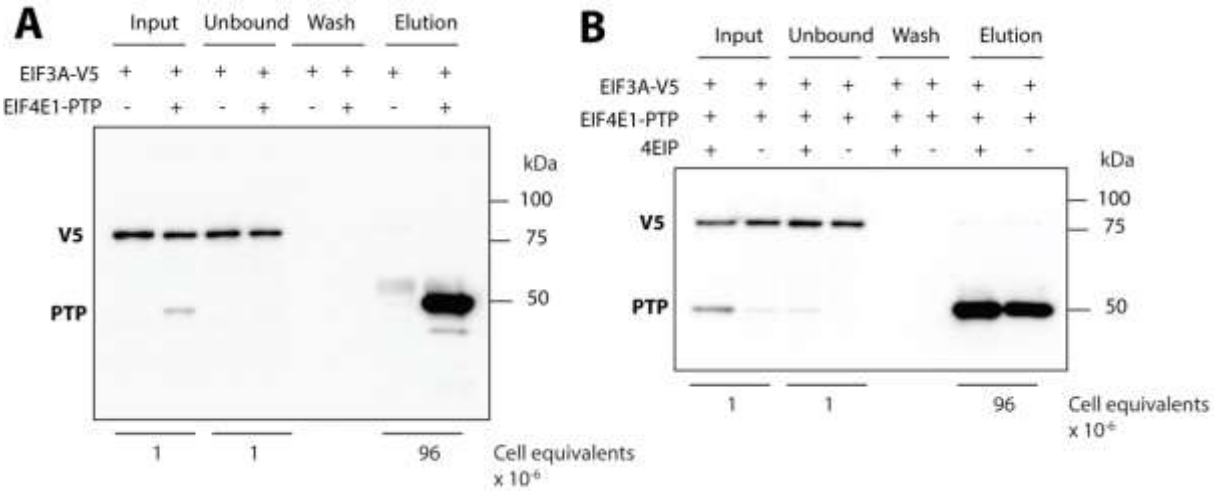

Figure 3.4 EIF4E1 does not interact with the general translation initiation factor EIF3A. (A) C-terminally PTP-tagged EIF4E1 was purified from bloodstream forms (BSFs) co-expressing V5-tagged EIF3A. For this, lysates of 1×10^8 BSFs (input) were incubated with IgG-coupled magnetic beads for 2 h. Proteins bound to the beads were immobilized using a magnet to collect the unbound fractions. The beads were subjected to three sequential washing steps, the first of which was collected

for subsequent analyses. Bound proteins were eluted by addition of Laemmli buffer. The different fractions were analyzed by western blotting using V5-specific antibody. Cells expressing EIF3A-V5 without PTP-tagged EIF4E1 served as a control. **(B)** C-terminally PTP-tagged EIF4E1 was purified from BSFs co-expressing V5-tagged EIF3A with and without 4EIP. For this, lysates of 1 × 10^8 BSFs (input) were incubated with IgG-coupled magnetic beads for 2 h. Proteins bound to the beads were immobilized using a magnet to collect the unbound fractions. The beads were subjected to three sequential washing steps, the first of which was collected for subsequent analyses. Bound proteins were eluted by addition of Laemmli buffer. The different fractions were analyzed by western blotting using V5-specific antibody. The data presented have been published with modifications in Falk et al., 2021 [122]

In order to identify protein-interaction partners of EIF4E1 on a broader scale and dissect its roles with and without 4EIP, I performed quantitative mass spectrometry on EIF4E1-PTP purified from both BSFs and PCFs in presence and absence of 4EIP. Proteins associated with GFP-PTP served as a reference for unspecific binding. Interestingly, no general translational activators were enriched with EIF4E1-PTP, even when 4EIP had been depleted (**Figure 3.5A, B**). Moreover, 4EIP2 (*Tb*927.10.11000) was pulled down along with EIF4E1, both in the absence and presence of 4EIP, which became evident upon comparison to pulldowns of GFP-PTP (**Figure 3.5C, D**). While the quantities of associated 4EIP2 were roughly similar to those of EIF4E1 and 4EIP in BSFs, associated 4EIP2 levels were much lower in PCFs, while 4EIP was pulled down with EIF4E1 at nearly equimolar levels.

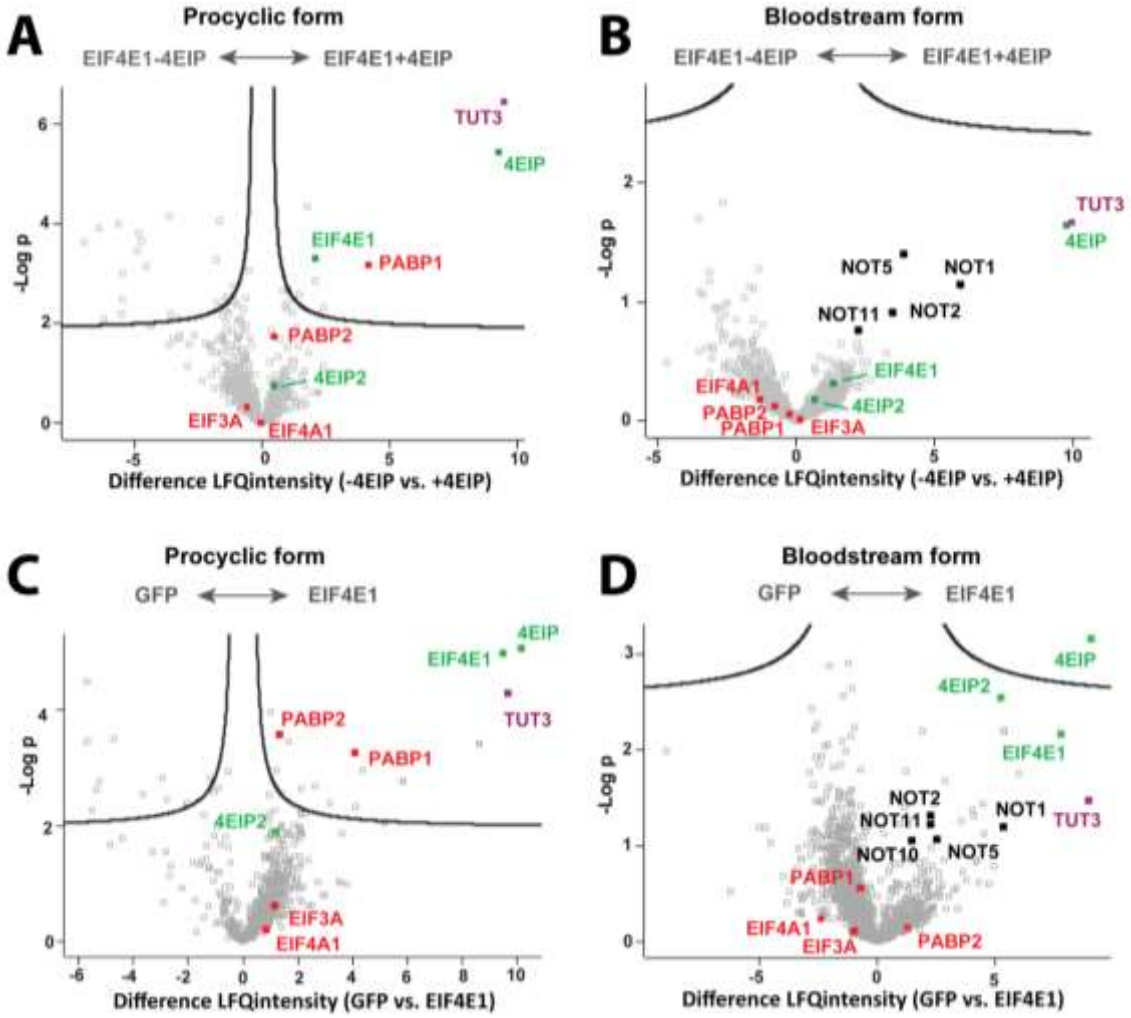

Figure 3.5 EIF4E1-bound proteome in bloodstream and procyclic forms of *Trypanosoma brucei*. (A) PTP-tagged EIF4E1 was pulled down from PCFs with and without 4EIP for comparison of bound proteins using quantitative mass spectrometry. Raw data were analyzed by Sabine Merker from the mass spectrometry core facility using MaxQuant, and interaction partners

were subsequently analyzed in Perseus. In the volcano plot, differences in label-free quantification (LFQ) intensities were plotted against the log10 of the false discovery rate (FDR) calculated by a permutation-based FDR adapted t-test. Data from three independent experiments are shown. Each square represents one protein, and some proteins of interest are highlighted in color. **(B)** PTP-tagged EIF4E1 was pulled down from BSFs with and without 4EIP for comparison of bound proteins using quantitative mass spectrometry. Raw data were analyzed by Sabine Merker from the mass spectrometry core facility using MaxQuant, and interaction partners were subsequently analyzed in Perseus. In the volcano plot, differences in label-free quantification (LFQ) intensities were plotted against the log10 of the false discovery rate (FDR) calculated by a permutation-based FDR adapted t-test. Data from three independent experiments are shown. Each square represents one protein, and some proteins of interest are highlighted in color. **(C)** PTP-tagged GFP or EIF4E1 was pulled down from PCFs for comparison of bound proteins using quantitative mass spectrometry. Raw data were analyzed by Sabine Merker from the mass spectrometry core facility using MaxQuant, and interaction partners were subsequently analyzed in Perseus. In the volcano plot, differences in label-free quantification (LFQ) intensities were plotted against the log10 of the false discovery rate (FDR) calculated by a permutation-based FDR adapted t-test. Abundances of proteins that were not detected in the GFP-PTP purifications were simulated by the program. Data from three independent experiments are shown. Each square represents one protein, and some proteins of interest are highlighted in color. **(D)** PTP-tagged GFP or EIF4E1 was pulled down from BSFs for comparison of bound proteins using quantitative mass spectrometry. Raw data were analyzed by Sabine Merker from the mass spectrometry core facility using MaxQuant, and interaction partners were subsequently analyzed in Perseus. In the volcano plot, differences in label-free quantification (LFQ) intensities were plotted against the log10 of the false discovery rate (FDR) calculated by a permutation-based FDR adapted t-test. Abundances of proteins that were not detected in the GFP-PTP purifications were simulated by the program. Data from three independent experiments are shown. Each square represents one protein and some proteins of interest are highlighted in color. The data presented have been published with modifications in Falk et al., 2021 [122]

A particular cytoplasmic enzyme of the RNA-degradation machinery, the terminal uridylyl transferase 3 (TUT3), was associated with EIF4E1 in the presence of 4EIP only (**Figure 3.5A-D**). This was observed at both life cycle stages and could be confirmed upon precipitation of 4EIP, where TUT3 was reliably detected [122]. In contrast, interactions with different components of the CAF1-NOT deadenylation complex were detected only in samples from BSFs, but at levels that were not significant (**Figure 3.5B, D**). In an attempt to confirm this by co-immunoprecipitation, CAF1-V5 could not be reproducibly pulled down with EIF4E1-PTP (**Figure 3.6A, B**). It was thus speculated that these interactions exist only transiently. Testing the association with other components of the deadenylation complex, i.e. NOT5 and NOT1, were hindered by difficulties in introducing tagged versions of these proteins in cells expressing EIF4E1-PTP. Furthermore, a possible association between EIF4E1 and the RNA helicase DHH1, which is central in removing mRNAs from the pool of translated mRNAs, was analyzed. In two out of three replicates, DHH1 was specifically associated with EIF4E1/4EIP complexes. This was lost upon depletion of 4EIP (**Figure 3.6C-E**). It should be noted that this might have been a consequence of the reduced EIF4E1-PTP levels in 4EIP-deficient cells, rather than the loss of an interaction between DHH1 and EIF4E1.

3.1.4 The terminal uridylyl transferase TUT3 is recruited to EIF4E1 through direct interactions with 4EIP

To test whether the interaction between the terminal uridylyl transferase TUT3 and 4EIP was direct, yeast-2-hybrid assays were conducted. Additionally, the *T. brucei* homolog of Dis3L2, an exonuclease presumed to act on uridylated mRNA targets, was included (**Figure 3.7A, Supplementary Figure S2**). When 4EIP and TUT3 were co-expressed, the yeast cells could survive the selection process on media lacking adenine and histidine. Growth was stronger when TUT3-AD (activation domain) and 4EIP-BD (DNA-binding domain) were combined. However, some growth was observed upon co-expression of 4EIP-AD and 4EIP-BD, which suggested a limited self-interaction. Apart from the positive control, all other combinations could not support growth.

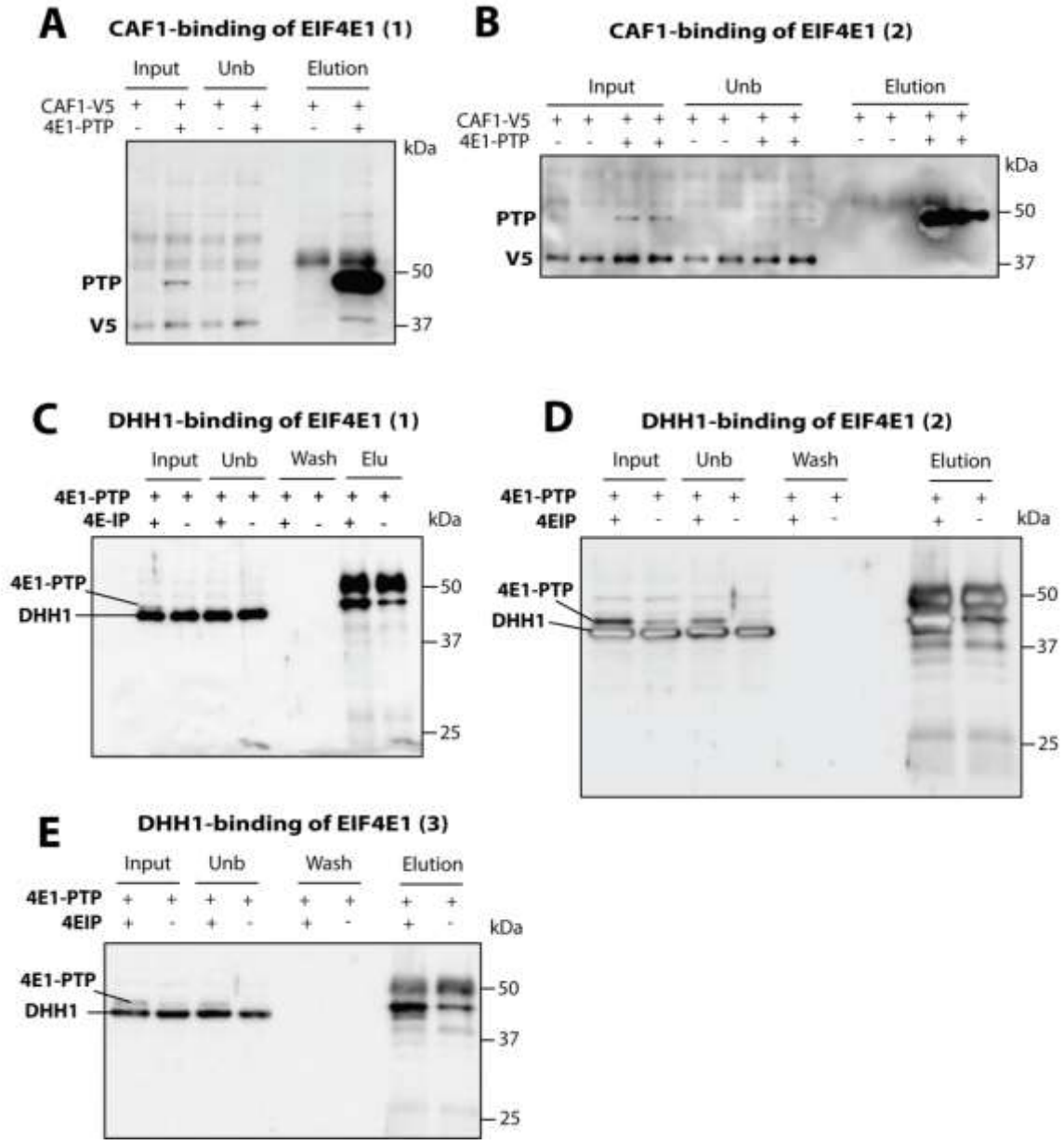

Figure 3.6 Association of EIF4E1 with proteins involved in RNA degradation in bloodstream forms (BSFs). (A) C-terminally PTP-tagged EIF4E1 was purified from BSFs co-expressing V5-tagged CAF1. For this, lysates of 1 × 10^8 BSFs (Input) were incubated with IgG-coupled magnetic beads for 2 h. Proteins bound to the beads were immobilized using a magnet to collect the unbound fractions (Unb). The beads were subjected to three sequential washing steps, the first of which was collected for subsequent analyses. Bound proteins were eluted by addition of Laemmli buffer. The different fractions were analyzed by western blotting using V5-specific antibody. Cells expressing CAF1-V5 without PTP-tagged EIF4E1 served as a control. **(B)** As in **(A)**, with data from two separate experiments shown next to each other. **(C)** C-terminally PTP-tagged EIF4E1 was purified from BSFs with and without 4EIP. For this, lysates of 1 × 10^8 BSFs (Input) were incubated with IgG-coupled magnetic beads for 2 h. Proteins bound to the beads were immobilized using a magnet to collect the unbound fractions (Unb). The beads were subjected to three sequential washing steps, the first of which was collected for subsequent analyses. Bound proteins were eluted by addition of Laemmli buffer. The different fractions were analyzed by western blotting using DHH1-specific antiserum. **(D)** Replicate of the experiment shown in **(C)**. **(E)** Replicate of the experiment shown in **(C)**. The data presented in **(A)** and **(B)** have been published with modifications in Falk et al., 2021 [122]

3.1.5 Expression of GPEET is reduced in PCFs lacking 4EIP

Previous findings suggested that complexes of EIF4E1/4EIP recruit TUT3, potentially resulting in uridylation of the 3' end of bound target mRNAs. These could then serve as targets for degradation by Dis3L2 and/or the exosome, which is schematically depicted in **Figure 3.7B**. With 3'-terminal uridylation likely serving as a signal for targeted RNA-degradation, data on (potentially) uridylated mRNAs are virtually non-existent. Only the highly abundant mRNA encoding the PCF-specific surface protein GPEET has been described as a potential uridylation target in *T. brucei* [33].

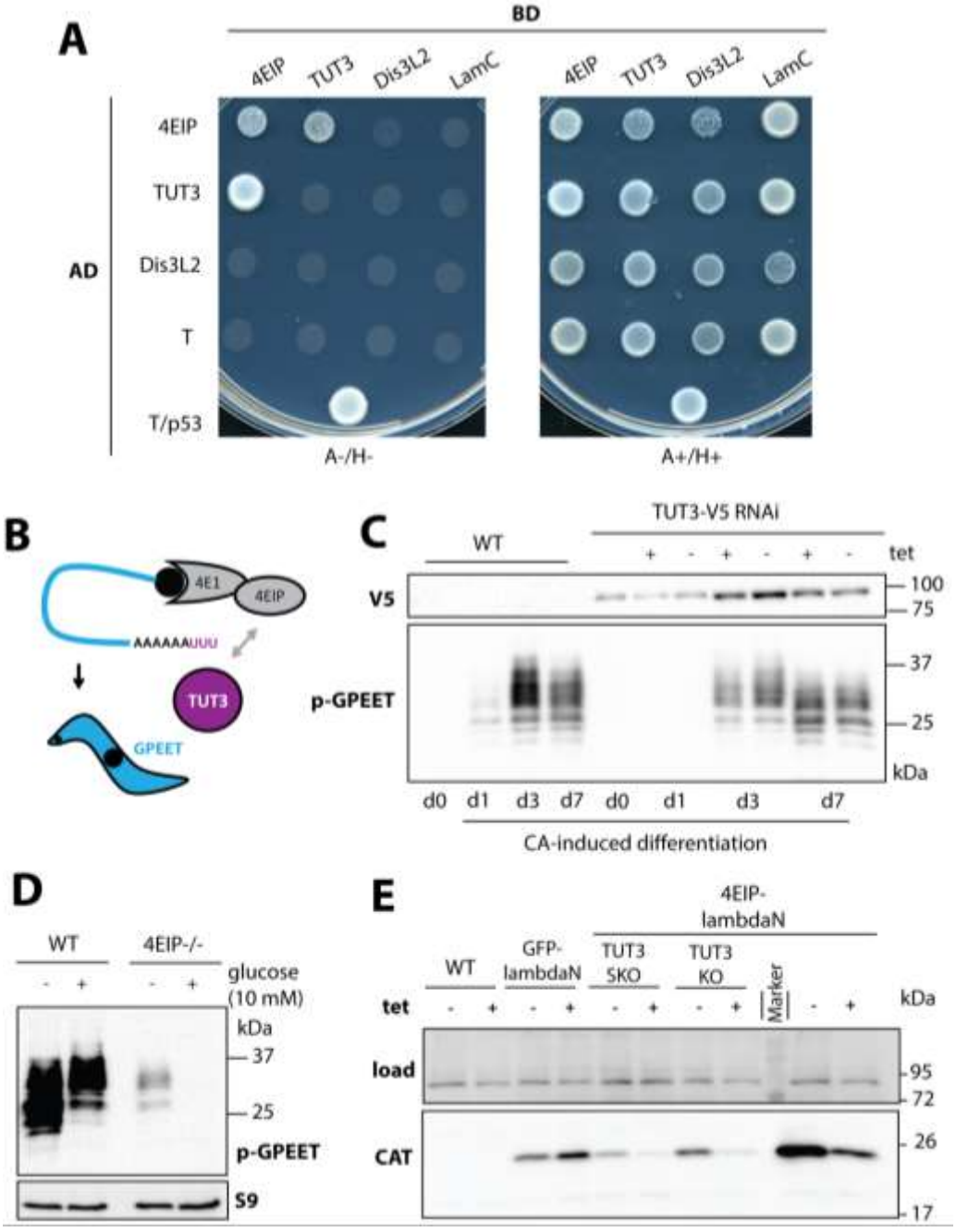

Figure 3.7 Direct interactions between 4EIP and the terminal uridylyl transferase 3 (TUT3) are not required for the suppressive effects of EIF4E1/4EIP complexes. (A) Direct interactions between 4EIP, TUT3, and the exonuclease Dis3L2 were tested by yeast-2-hybrid analysis. Co-expression of large T antigen (T)-AD and lamin C (LamC)-BD served as a negative control, while simultaneous expression of T-AD and p53-BD was used as positive control. Viability of the yeast cells was tested on media supplemented with adenine and histidine (A+/H+), while selection for positive interactions was performed on media lacking adenine and histidine (A-/H-). **(B)** Schematic representation of the proposed regulation of *GPEET* mRNA

expression by uridylation. Direct interactions between EIF4E1/4EIP and TUT3 are hypothesized to result in 3'-terminal uridylation of polyadenylated mRNAs to target them for degradation by the exonuclease Dis3L2. This was to be tested in subsequent experiments. **(C)** Expression of phosphorylated GPEET protein was analyzed by western blotting at different time-points after *cis*-aconitate (CA)-induced differentiation in WT bloodstreams forms (BSFs) and BSFs with *TUT3* RNAi. To monitor TUT3 levels during knockdown experiments, the protein was V5-tagged *in situ*, while the second copy was knocked out. **(D)** Expression levels of p-GPEET were analyzed in WT and 4EIP-deficient procyclic cells grown in the presence of high or low glucose concentrations by western blotting. **(E)** To test the suppressive effects of 4EIP with and without TUT3, tethering assays were performed, including cells lacking a single (SKO) or both copies (KO) of the *TUT3* gene. 4EIP was fused to a λN-peptide and artificially tethered to the box-B element-containing 3'-UTR of a reporter mRNA. Afterwards, reporter expression was analyzed by western blotting using anti-serum directed against the encoded reporter protein, chloramphenicol acetyltransferase (CAT). WT cells expressing neither the reporter mRNA nor a λN-coupled protein, as well as cells with λN-GFP tethered to the reporter mRNA served as negative controls. Expression of the proteins to be tethered was tetracyclin (tet)-inducible. An unspecific signal served as loading control (load). The data presented have been published with modifications in Falk et al., 2021 [122]

GPEET mRNA was followed up as a potential target of uridylation by TUT3. For this, differentiation of BSFs depleted of *TUT3* by RNAi was induced by addition of *cis*-aconitate and a temperature shift from 37 °C to 27 °C. Upon differentiation, GPEET expression was induced in WT cells, as well as in *TUT3* RNAi cells, but with a certain delay (**Figure 3.7C**). Reportedly, induction of EP expression followed similar patterns in both cell lines [100]. Of note, *TUT3* RNAi was inefficient and rapidly lost over the course of only a few days, even if the inducer was added every 24 h, which is evident in **Figure 3.7C**. Therefore, the observations made during differentiation from the BSF to the PCF in the absence of TUT3 are difficult to interpret. KO of the latter was only possible in monomorphic cells, but not in differentiation-competent EATRO1125 cell lines, indicating that TUT3 plays an important role during differentiation. In that regard, 4EIP and TUT3 appear to have overlapping functions. Using this approach, it could further be revealed that overall expression of TUT3 was increased in PCFs compared to BSFs (**Figure 3.7C**).

Reportedly, *GPEET* mRNA is exceptionally stable in early PCFs. The cell lines that were used in this study have been shown to sustain an early PCF phenotype under the standard culturing conditions, even when cultured for an extended period of time. However, adaptation to high-glucose medium for more than three weeks is known to result in the progression to late stage PCFs, as evidenced by the (partial) loss of GPEET protein expression. With low *TUT3* RNAi efficiency over such an extended adaptation period, an indirect approach was chosen. I tested whether down-regulation of GPEET was altered in *4EIP* KO cells, where EIF4E1/4EIP/TUT3 complexes are disrupted. It was presumed that the concerted actions of TUT3 and 4EIP are required to uridylate and thus target *GPEET* mRNA for degradation. Therefore, expression of GPEET was compared between WT and *4EIP* KO cells cultured in standard medium low in glucose and those adapted to high glucose levels in the surrounding medium. Surprisingly, basal levels of GPEET were significantly and reproducibly lower in *4EIP*-deficient cells compared to WT cells already prior to adaptation to high glucose (**Figure 3.7D**). Nonetheless, glucose treatment resulted in further reduction of GPEET protein levels in the case of both WT and *4EIP* KO cells. Together, this strongly argued against my hypothesis.

To look for a connection between reduced GPEET expression and mRNA uridylation, RNA was extracted from cells cultured in an environment high or low in glucose. After removal of the cap, RNAs were circularized by ligation of 5' and 3' ends using T4 RNA ligase and GPEET mRNA sequences were amplified to study poly(A) tails and (potential) oligo-uridylation signals. In the case of cells cultured under low glucose conditions, 8 out of 20 sequences analyzed corresponded to the desired *GPEET* sequence spanning the poly(A) tail (**Supplementary Figure S3**). These did not contain any sequences derived from post-transcriptional, targeted uridylation. Interestingly, as the cells were

grown in medium with high levels of glucose, only 1 out of 20 sequences could be identified as *GPEET* mRNA, indicating that its abundance was reduced. Whether this was the result of uridylation could not be answered using this approach.

Lastly, an *in silico* approach for identification of additional uridylation targets was conducted using pre-existing RNA sequencing data from WT BSFs and PCFs on ArrayExpress (https://www.ebi.ac.uk/arrayexpress/). The criteria were set as a sequence of >15 As followed by >5 Us at the 3'-terminal end, leading to identification of additional potential targets of uridylation, which are listed in **Figure 3.8A**. Using WT and *TUT3* KO cells, relative expression of three mRNAs that were identified in at least three out of the four data sets analyzed was determined using RT-qPCR. However, relative expression was unaffected in both PCFs and BSFs in the absence of TUT3 (**Figure 3.8B**).

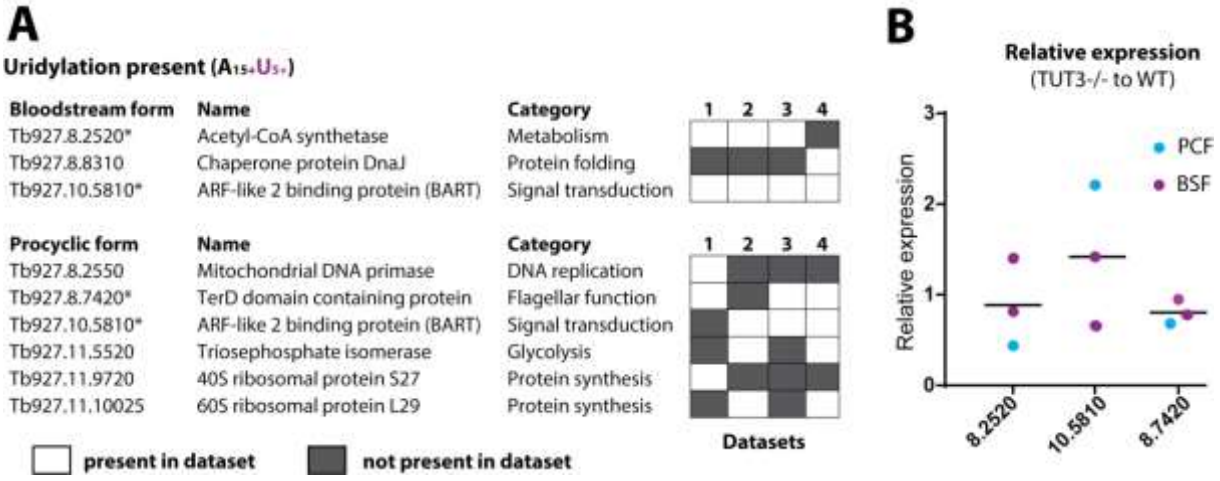

Figure 3.8 *In silico* approach for identification of uridylation targets. (A) RNA sequencing data from wildtype (WT) bloodstream and procyclic forms (BSFs and PCFs, respectively) were downloaded from ArrayExpress (https://www.ebi.ac.uk/arrayexpress/; four datasets each). Search criteria were set as a sequence of >15 As followed by >5 Us at the 3'-terminal end. The number of datasets containing RNA sequences that were in conformance with the search criteria is indicated on the right. The asterisk indicates transcripts that were found in both forms. **(B)** Relative expression levels of three individual RNAs identified by the *in silico* approach described in **(A)** were analyzed by reverse-transcription quantitative (RT-qPCR) in monomorphic BSFs and PCFs with no or both copies of the *TUT3* gene. The data presented have been published in Falk et al., 2021 [122]

3.1.6 TUT3 is dispensable for the suppressive effects of EIF4E1/4EIP complexes

Tethering of 4EIP or EIF4E1 to a reporter mRNA is known to result in repression of reporter expression [100]. It is further known that the presence of 4EIP is essential for the repressive effects observed upon EIF4E1 tethering. In contrast, tethering of 4EIP in cells lacking EIF4E1 is sufficient to induce reduced reporter expression. This inhibitory effect was shown to result from reduced mRNA translation and increased mRNA degradation [100].

Here, 4EIP fused to a λN-peptide was artificially tethered to the 3'-UTR of chloramphenicol acetyltransferase (*CAT*) mRNA through a box-B sequence in *TUT3*-deficient, monomorphic cells to test whether the activity of TUT3 was required for the repressive effects of the EIF4E1/4EIP complex. As shown in **Figure 3.7E**, it was confirmed that tethering of 4EIP in the presence of TUT3 resulted in reduced reporter expression. Moreover, deleting either a single copy or both copies of *TUT3* led to repression of CAT expression, highlighting that the activity of TUT3 is dispensable for the repressive

effects of the EIF4E1/4EIP complex (**Figure 3.7E**). Tethering of TUT3, on the other hand, was not sufficient for repressing reporter mRNA expression in a previous study [109].

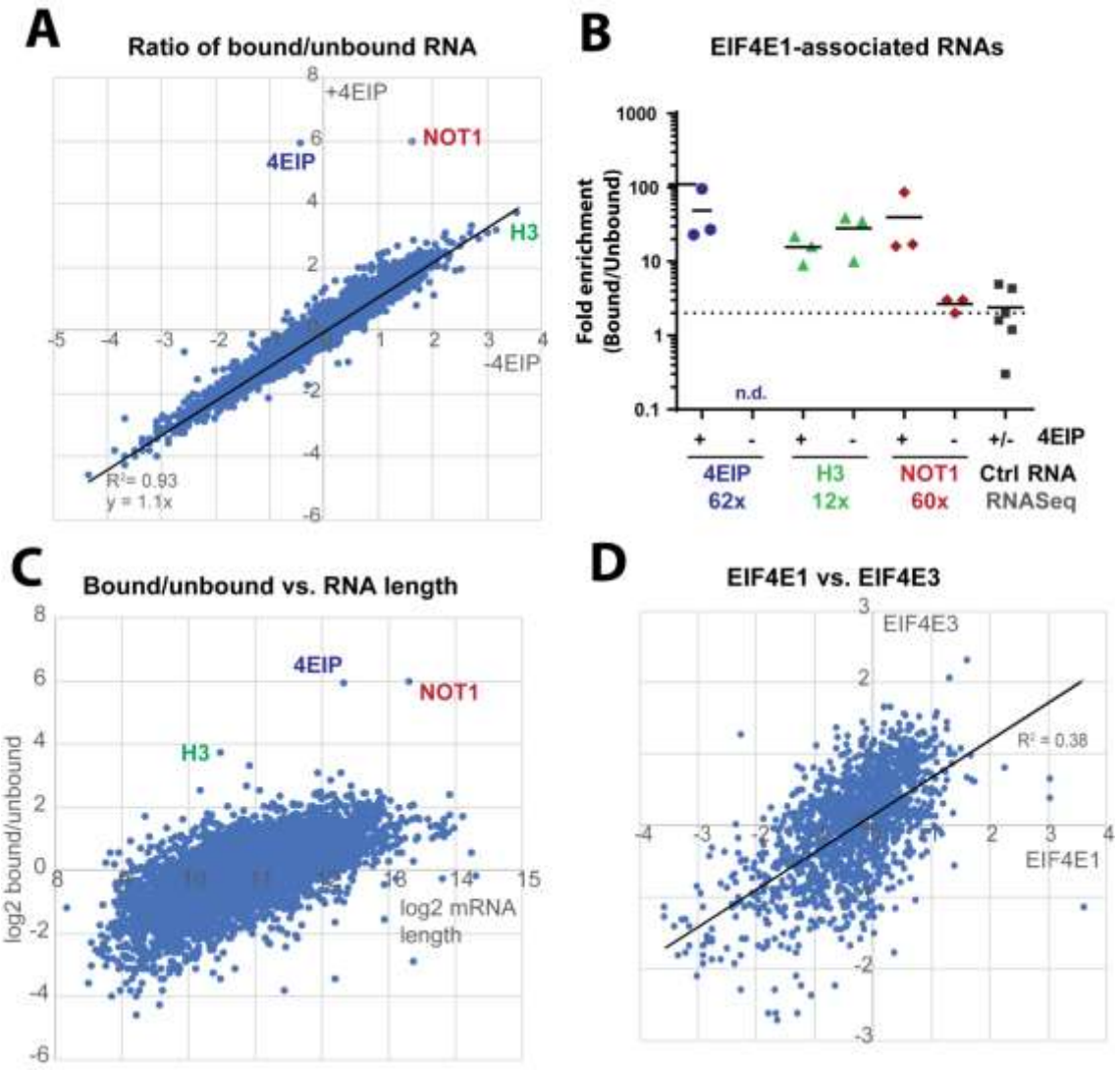

Figure 3.9 Strong overlap between mRNAs bound to EIF4E1 with and without 4EIP in procyclic forms (PCFs). (A) PTP-tagged EIF4E1 (± 4EIP) was purified from 1 × 10^9 PCFs and associated RNAs were analyzed by RNA sequencing. Those mRNAs that were most strongly enriched are indicated. Data from a single experiment are shown. **(B)** EIF4E1-PTP was pulled down from 1 × 10^8 PCFs, after which bound and unbound fractions were analyzed for EIF4E1-associated mRNAs previously identified by RNA sequencing using quantitative reverse transcription PCR (qRT-PCR) with specific primers. Data from three independent pulldowns are shown. **(C)** Ratios of mRNAs present in bound and unbound fractions after EIF4E1 pulldowns from PCFs were compared to the length of the mRNAs. Data from a single experiment are shown. **(D)** Comparisons of the mRNAs bound to EIF4E1 in PCFs with those associating with EIF4E3 in bloodstream forms (BSFs). These were restricted to transcripts that are not developmentally regulated. Data from a single experiment (EIF4E1) and average values of three independent pulldowns (EIF4E3) were plotted against each other. Data were analyzed by Franziska Falk and the plots in **(A)**, **(C)**, and **(D)** were generated by Christine Clayton based on the data provided. The data presented have been published with modifications in Falk et al., 2021 [122]

3.1.7 Selection of mRNA targets by EIF4E1 is not influenced by association with 4EIP/TUT3

In vitro studies have suggested that binding of 4EIP elicits conformational changes in EIF4E1, thus resulting in EIF4E1 falling off the cap structure [102]. In the case that this also holds true *in vivo*, the transcriptome associated with EIF4E1 in absence and presence and 4EIP should be markedly

different. More specifically, a much larger subset of mRNAs should be bound by EIF4E1 in cells lacking *4EIP*. To test this hypothesis, PTP-tagged EIF4E1 was purified from WT and *4EIP* KO PCFs, as EIF4E1 is essential at this life cycle stage. Therefore, a stronger effect was expected in PCFs than in BSFs. RNAs were extracted from bound and unbound fractions and subjected to RNA sequencing. To determine the mRNAs specifically bound to EIF4E1 with and without 4EIP, mRNA abundances were compared between bound and unbound fractions. Surprisingly, the repertoires of RNAs purified in the absence and presence of 4EIP was largely overlapping (**Figure 3.9A**).

Exceptions to this were those mRNAs encoding 4EIP and NOT1 (**Figure 3.9A**), which were enriched about 60-fold in the presence of 4EIP. As this experiment was performed only once, three additional independent pulldowns served to confirm the association with these mRNAs using RT-qPCR (**Figure 3.9B**). Furthermore, a particular, short RNA encoding the histone protein H3 was strongly enriched with EIF4E1-PTP protein, whether 4EIP was present or not. The strong correlation between the two data sets raised the question whether the interactions were specific. Indeed, a clear preference for long mRNAs was observed, which pointed towards non-specific interactions between the protein of interest and the mRNAs identified (**Figure 3.9C**). In line with this preference for long RNAs, a bias towards binding of mRNAs encoding RNA-binding proteins and protein kinases could be observed (**Supplementary Figure S4A**). Those mRNAs associated with EIF4E1 in the PCF were further shown not to overlap with mRNAs pulled down with 4EIP from BSFs (**Supplementary Figure S4B-D**).

Furthermore, a suspiciously strong overlap with RNA sequencing data obtained by pulldowns of EIF4E3 from BSFs supported the hypothesis of unspecific binding (**Figure 3.9D, Supplementary Figure S4E, F**). Therefore, the strong preference for binding of long RNAs may have obscured all specific hits except for those that were exceptionally strong, as exemplified by binding of *4EIP* and *NOT1* mRNAs.

Overall, the results did not support the hypothesis that 4EIP serves as a negative regulator that prevents binding of EIF4E1 to mRNAs.

3.2 *Tb927.10.16070* - Eukaryotic translation initiation factor 4E2 (EIF4E2)

3.2.1 BSFs lacking EIF4E2 have a strong growth defect and differentiate to the stumpy form at low densities

EIF4E2 is a 28 kDa protein, which, like EIF4E1, is not assumed to form classical EIF4F complexes [97, 103]. Neither a growth defect nor an effect on global translation could be observed upon knockdown of *EIF4E2* in PCFs or BSFs in previous studies [97]. In the course of this project, BSFs with a homozygous KO of *EIF4E2* could be obtained, which featured a strong growth defect (**Figure 3.10A, B**). This was accompanied by a maximum density of 0.8×10^6 cells/mL in methylcellulose-containing medium, while WT cells could reach 2-3 $\times 10^6$ cells/mL under these conditions. Similarly, the maximum densities reached in normal HMI-9 medium were also significantly different; 0.3×10^6 cells/mL and 1×10^6 cells/mL for *EIF4E2* KO and WT BSFs, respectively. Reconstitution of *EIF4E2* expression could rescue these effects. Total protein expression profiles were also similar between WT and *EIF4E2* KO and reconstituted cell lines (**Figure 3.10C**). With the aim to uncover the mechanisms underlying this growth impairment, total RNA was isolated and separated on a polyacrylamide gel to analyze small RNA species by methylene blue staining. However, there were no notable differences in small rRNAs or tRNAs compared to WT or cells with reconstituted EIF4E2 expression. Other RNA species, such as snoRNAs or sRNAs, could not be detected using this approach (**Figure 3.10D**).

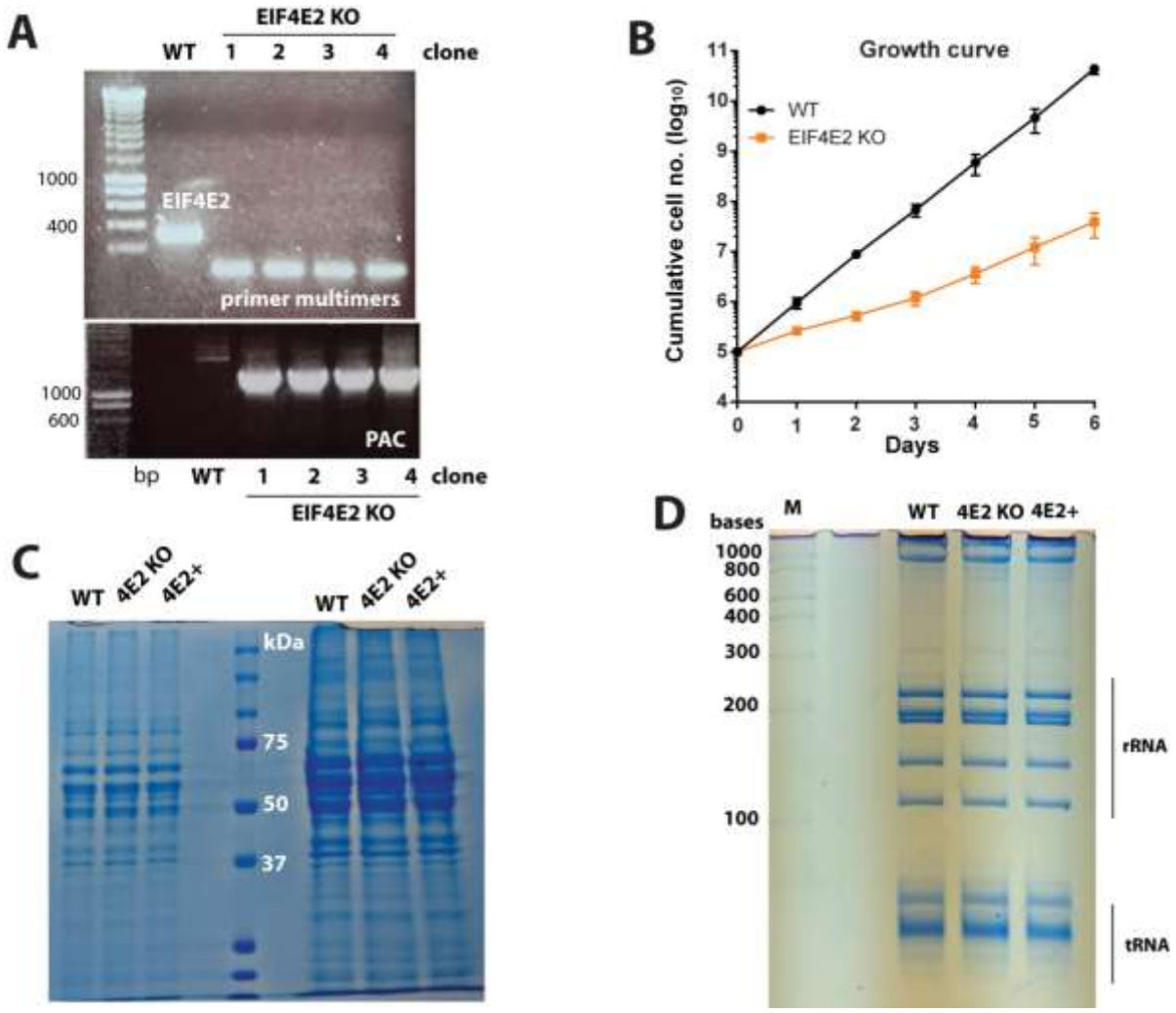

Figure 3.10 Loss of EIF4E2 results in major growth impairment in bloodstream forms (BSFs). (A) PCR reactions with primers specifically detecting the *EIF4E2* ORF were used to verify knockout of the target gene in differentiation-competent BSF *Trypanosoma brucei* parasites. A combination of primers binding to the *EIF4E2* UTR and the puromycin N-acetyltransferase were selected to confirm the incorporation of the gene sequence into the *EIF4E2* locus. **(B)** The growth of BSFs with a homozygous knockout of *EIF4E2* was monitored over the course of one week and compared to WT cells. **(C)** Total protein extracts were obtained from WT BSFs, as well as from BSFs with a homozygous knockout of *EIF4E2* (4E2 KO) or KO cells with reconstituted expression of EIF4E2 (4E2+). Proteins were separated by sodium dodecyl sulfate polyacrylamide gel electrophoresis and analyzed by Coomassie staining. **(D)** Total RNA was extracted from WT BSFs, BSFs with a homozygous KO of *EIF4E2* (4E2 KO), and *EIF4E2* KO cells with reconstituted EIF4E2 expression (4E2+). Small RNA species were separated by polyacrylamide gel electrophoresis and analyzed by methylene blue staining.

Interestingly, however, upon addition of *cis*-aconitate and a reduction in temperature from 37 °C to 27 °C, the cells were capable of differentiation to PCFs, which resumed growth at normal kinetics (**Figure 3.11A**). Furthermore, stumpy formation could be initiated by growth in HMI-9 containing methylcellulose, as evidenced by expression of PAD1. As stumpy formation was induced at the same starting density, expression of PAD1 was initiated even earlier in *EIF4E2* KO cells than in WT and *EIF4E2* addback cells, despite reduced growth rates (**Figure 3.11B**).

In accordance with previous reports identifying a homolog of the histone mRNA stem-loop-binding protein (SLBP2) as major binding partner of EIF4E2 in PCFs, SLBP2 was strongly enriched in pulldowns of tagged EIF4E2 from BSFs upon performing quantitative mass spectrometry (**Supplementary Figure S5**). There were no indications that EIF4E2 associated with any translational initiation factors other than EF-2α and PABP2 in comparison to GFP (**Supplementary Figure S5A**). It should be noted that the

two replicates performed showed a strong variation in non-specific binding of proteins, impeding the identification of binding partners that were not as prominent as SLBP2.

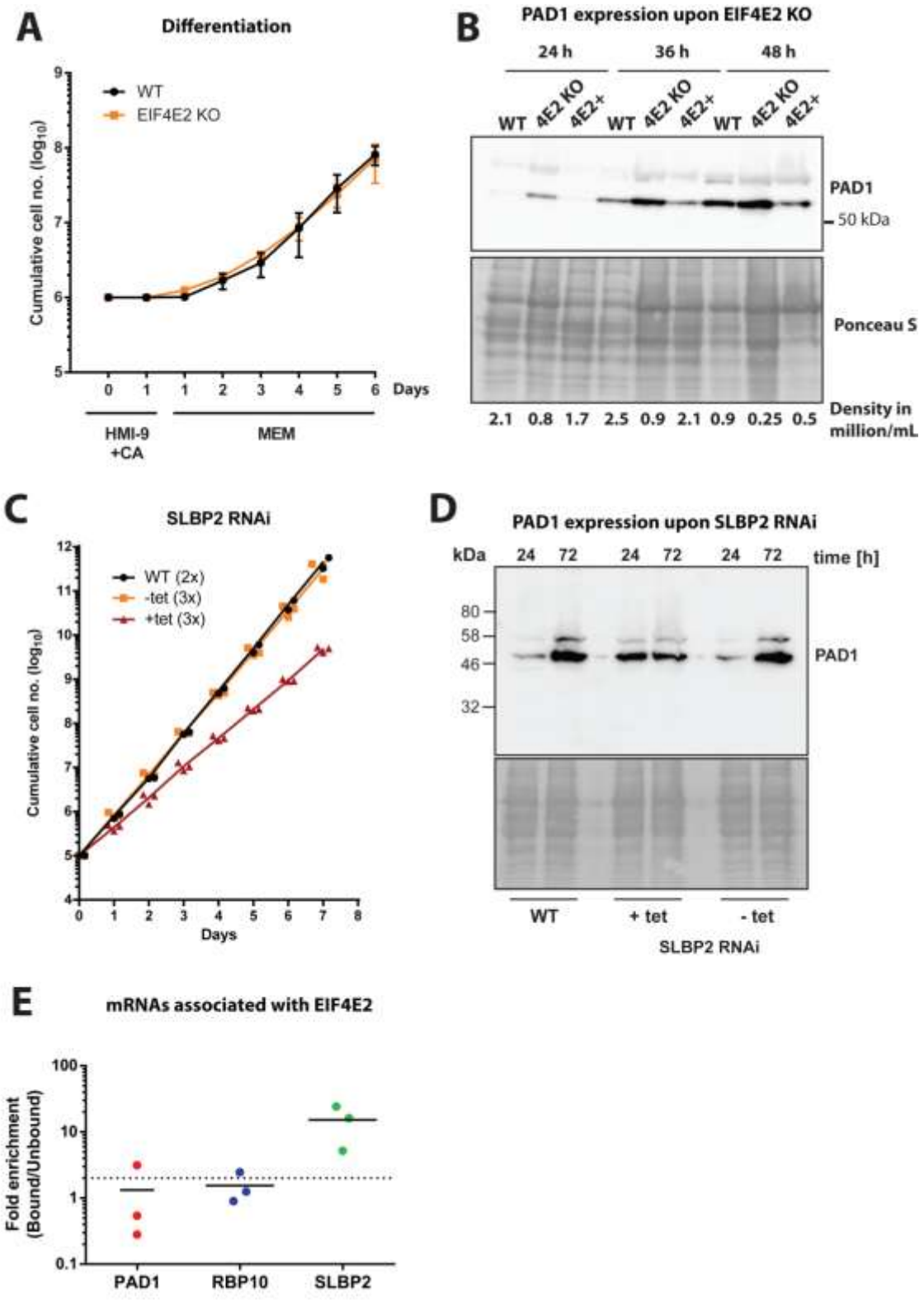

Figure 3.11 Stumpy formation and differentiation to the procyclic form (PCF) proceed normally in EIF4E2-deficient cells.
(A) Wild type (WT) and *EIF4E2* knockout (KO) bloodstream forms (BSFs) were differentiated to PCFs by *cis*-aconitate (CA) treatment and a temperature shift from 37 °C to 27 °C. On the following day, the cells were transferred to PCF-specific culture medium (MEM) and continuously cultured at 27 °C. Growth was monitored over the course of one week. Mean and

standard deviation from three independent experiments are shown. **(B)** BSFs with WT genetic background, BSFs depleted of both *EIF4E2* alleles (4E2 KO), and *EIF4E2* KO cells with reconstituted EIF4E2 expression (4E2+) were grown to high densities in HMI-9 medium with methylcellulose for the times indicated to induce stumpy formation. Expression of the stumpy-specific marker PAD1 was analyzed by western blotting. Cell densities at harvest are indicated at the bottom. **(C)** A homolog of the histone mRNA stem-loop-binding protein, SLBP2, was depleted by tetracyclin (tet)-inducible RNAi in BSFs. WT BSFs and *SLBP2* RNAi BSFs grown without tetracyclin were used as controls. Data from three independent experiments are shown. **(D)** BSFs with tet-inducible RNAi for depletion of *SLBP2* were grown to high densities in HMI-9 medium with methylcellulose (±tet) for the times indicated to induce stumpy formation. Expression of the stumpy-specific marker PAD1 was analyzed by western blotting. WT BSFs were used as a positive control. **(E)** PTP-tagged EIF4E2 was purified from BSFs at log-phase. The levels of mRNAs encoding the stumpy marker PAD1, the BSF-specific protein RBP10, as well as SLBP2 were analyzed by quantitative real-time PCR (qRT-PCR). Data from three independent experiments are shown, as well as the mean.

In accordance with these results, cells with *SLBP2* knockdown displayed a differentiation phenotype that was reminiscent of that of *EIF4E2* KO cells (**Figure 3.11C**). Reduced levels of *SLBP2* mRNA were confirmed by qPCR. To test the hypothesis whether EIF4E2 was involved in mediating regulation of PAD1 expression throughout different life cycle stages, PTP-tagged EIF4E2 was pulled down from BSFs and associated mRNAs were isolated and analyzed by qPCR with primers specifically detecting *PAD1*, *RBP10* (a BSF marker), and *SLBP2*. However, developmentally regulated mRNAs enconding PAD1 or RBP10 were not specifically enriched in pulldowns of EIF4E2, but *SLBP2* mRNA was enriched by more than 10-fold in bound compared to unbound fractions, suggesting a co-translational association of EIF4E2 and SLBP2 proteins (**Figure 3.11D**).

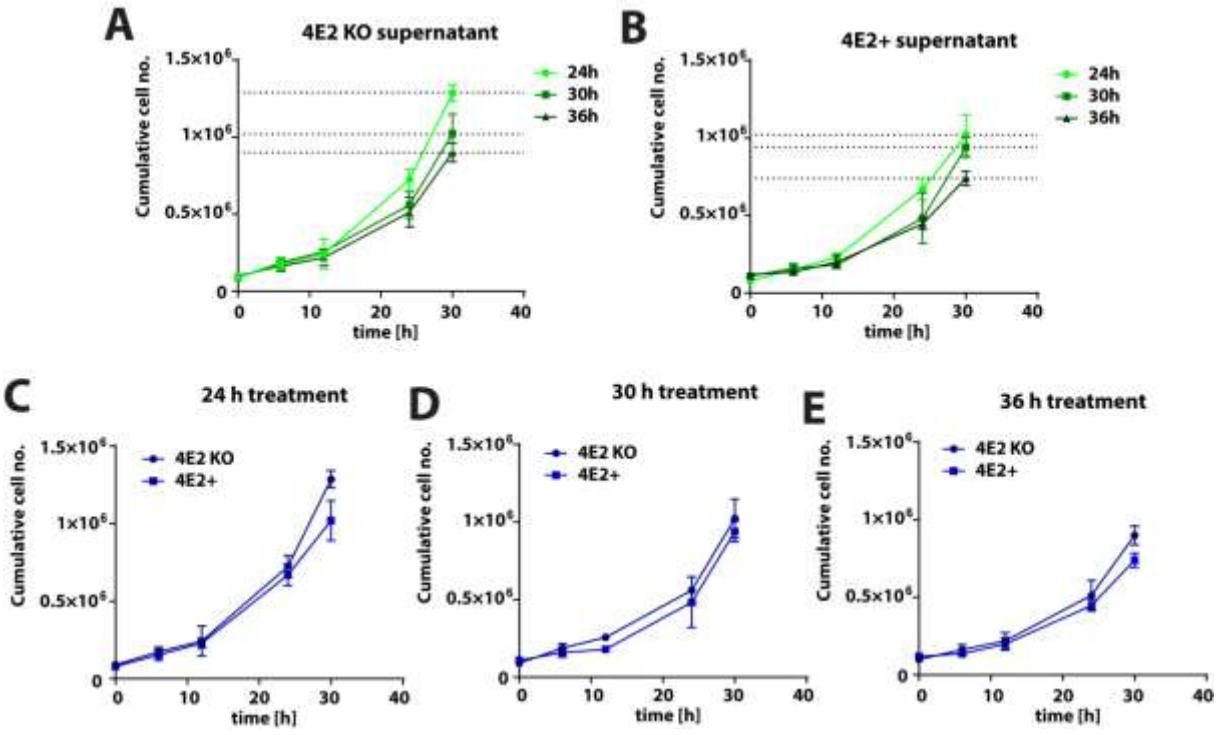

Figure 3.12 Secretion of stumpy induction factor (SIF) by *EIF4E2* knockout (KO) cells is normal. (A) The medium of cultured *EIF4E2* knockout bloodstream forms (4E2 KO BSFs) was collected after 24, 30, and 36 h in culture and used to culture wildtype (WT) BSFs. Growth of WT cells was followed over the course of 32 h. Mean and standard deviation of three independent experiments are shown. **(B)** The medium of cultured *EIF4E2* KO BSFs forms with reconstituted *EIF4E2* expression (4E2+) was collected after 24, 30, and 36 h in culture and used to culture WT cells. Growth of WT cells was followed over the course of 32 h. Mean and standard deviation of three independent experiments are shown. **(C)** The medium of cultured *EIF4E2* KO BSFs or *EIF4E2* KO BSFs with reconstituted EIF4E2 expression (4E2+) was collected after 24 h

in culture and used to culture WT cells. Growth of WT cells was followed over the course of 32 h. Mean and standard deviation of three independent experiments are shown. **(D)** The medium of cultured *EIF4E2* KO BSFs or *EIF4E2* KO BSFs with reconstituted EIF4E2 expression (4E2+) was collected after 30 h in culture and used to culture WT cells. Growth of WT cells was followed over the course of 32 h. Mean and standard deviation of three independent experiments are shown. **(E)** The medium of cultured *EIF4E2* KO BSFs or *EIF4E2* KO BSFs with reconstituted *EIF4E2* expression (4E2+) was collected after 36 h in culture and used to culture wild type (WT) cells. Growth of WT cells was followed over the course of 32 h. Mean and standard deviation of three independent experiments are shown.

To ultimately test whether the differentiation-competence observed at low densities was related to increased secretion or more efficient uptake of SIF, exchange of supernatants from different cells lines were performed. Firstly, treatment of WT cells with *EIF4E2* KO/addback-derived supernatants did not affect growth to high densities (**Figure 3.12**), arguing against increased secretion rates from *EIF4E2* KO cells.

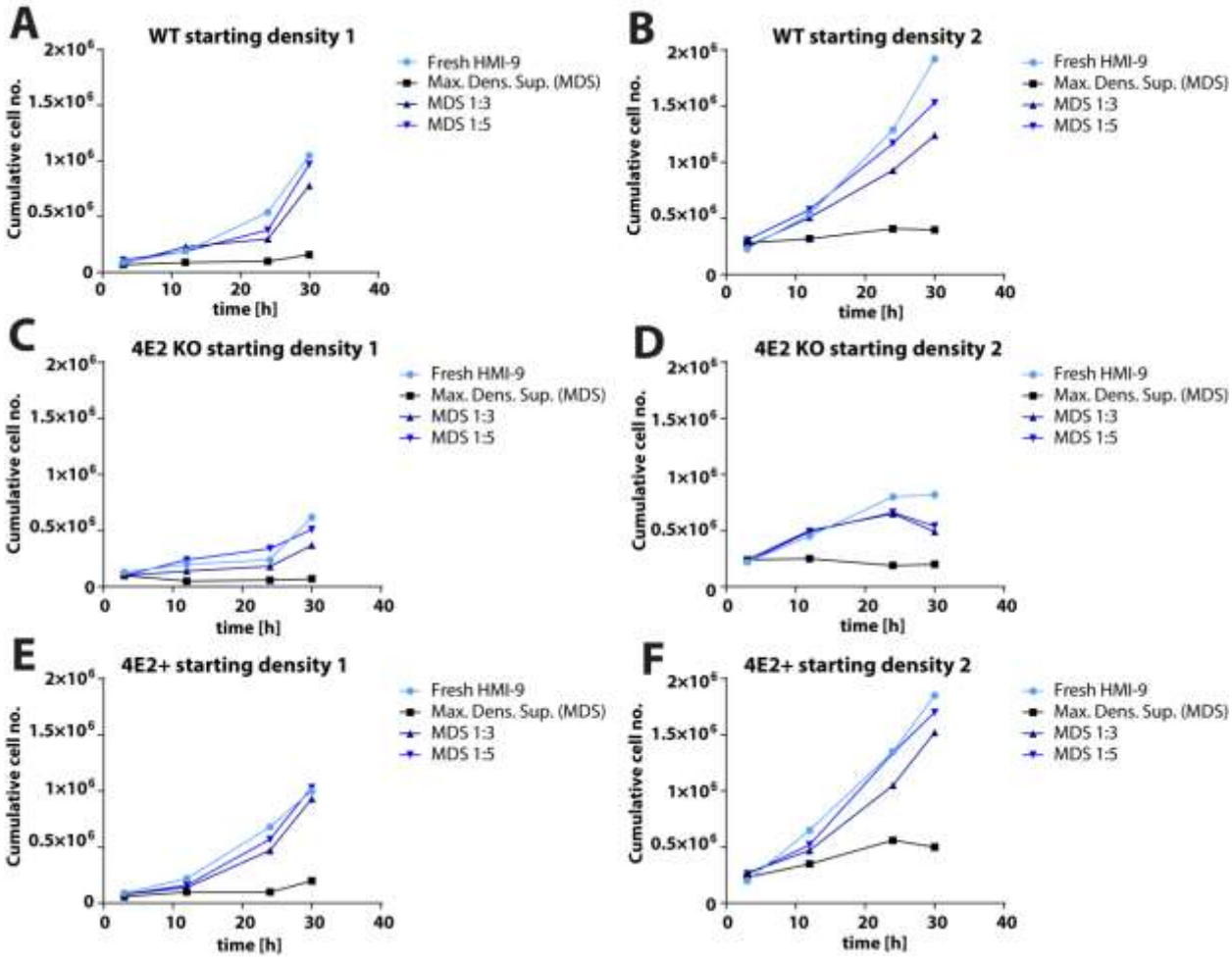

Figure 3.13 Growth impairment of *EIF4E2*-deficient bloodstream forms (BSFs) is independent of factors in the surrounding medium. (A) Wildtype (WT) BSFs at a starting density of 1 × 10^5 cells/mL were grown in either fresh HMI-9 medium or medium collected from WT cells at maximal density (maximum density supernatant, MDS), as well as in 1:3 and 1:5 dilutions of the MDS. Growth was monitored at 4, 12, 24, and 30 h of incubation. Data from a single experiment are shown. **(B)** WT BSFs at a starting density of 2.5 × 10^5 cells/mL were grown in either fresh HMI-9 medium or MDS from WT cells, as well as in 1:3 and 1:5 dilutions of the MDS. Growth was monitored at 4, 12, 24, and 30 h of incubation. Data from a single experiment are shown. **(C)** BSFs with a homozygous knockout of *EIF4E2* (4E2 KO) at a starting density of 1 × 10^5 cells/mL were grown in either fresh HMI-9 medium or MDS from WT cells, as well as in 1:3 and 1:5 dilutions of the MDS. Growth was monitored at 4, 12, 24, and 30 h of incubation. Data from a single experiment are shown. **(D)** BSFs with a homozygous knockout of *EIF4E2* (4E2 KO) at a starting density of 2.5 × 10^5 cells/mL were grown in either fresh HMI-9 medium or MDS from WT cells, as well as in 1:3 and 1:5 dilutions of the MDS. Growth was monitored at 4, 12, 24, and 30 h

of incubation. Data from a single experiment are shown. **(E)** *EIF4E2* KO BSFs with reconstituted expression of *EIF4E2* (4E2+) at a starting density of 1×10^5 cells/mL were grown in either fresh HMI-9 medium or MDS from WT cells, as well as in 1:3 and 1:5 dilutions of the MDS. Growth was monitored at 4, 12, 24, and 30 h after incubation. Data from a single experiment are shown. **(F)** *EIF4E2* KO BSFs with reconstituted expression of *EIF4E2* (4E2+) at a starting density of 2.5×10^5 cells/mL were grown in either fresh HMI-9 medium or MDS from WT cells, as well as in 1:3 and 1:5 dilutions of the MDS. Growth was monitored at 4, 12, 24, and 30 h of incubation. Data from a single experiment are shown.

Secondly, WT, *EIF4E2* KO, and *EIF4E2* KO cells with reconstituted EIF4E2 expression, were grown in either fresh medium or WT-derived medium that was collected at maximal density, here referred to as maximum density supernatant or MDS (**Figure 3.13 and Supplementary Figure S6**). Additionally, 1:3 and 1:5 dilutions of the latter were tested on the different cell lines, whereas fresh culture medium served as a control. While WT and EIF4E2 addback cells grew at similar kinetics in the presence of the different types of media, *EIF4E2* KO cells were characterized by reduced growth already early after exchange of the medium. Furthermore, as the growth of the *EIF4E2* KO cells was similarly compromised in fresh medium and dilutions of the MDS, more efficient uptake and metabolism of the stumpy induction factor is rather unlikely to account for the observed phenotype.

3.2.2 EIF4E2 as a potential regulator of S-phase mRNAs and chromatin dynamics

The mechanisms of action of non-canonical translation factors not only include changes in the rates at which the proteins encoded by the bound mRNAs are synthesized, but further comprise destabilization or stabilization of the targets, either directly or indirectly by recruitment of additional RBPs. Therefore, for potentially identifying the pathways affected, I performed RNA sequencing of total transcriptomes derived from *EIF4E2* KO cells and those with reconstituted expression of *EIF4E2*. In doing so, it was revealed that mRNAs encoding the cell cycle regulator PUF9 target 1 (PNT1) were decreased by more than 3-fold in the absence of EIF4E2, likely contributing to the observed growth defects (**Figure 3.14A and Table 48**). In addition, *Tb927.11.14840* (CPC2, chromosomal passenger complex) and *Tb927.7.610* (mitochondrial DNA ligase homolog) mRNAs, the protein products of which act during S-phase, were down-regulated in cells lacking EIF4E2. It is known that the levels of these transcripts are regulated in a cell-cycle dependent manner, and are highest during mid to late S-phase. Furthermore, their 3'-UTRs carry the sequence 5'-*UUGUACC*-3', which is overrepresented in targets of the pumilio/Fem-3 RNA-binding domain-containing protein PUF9. Accordingly, it has been described that *EIF4E2* mRNA is highest in late G1, so the protein is likely highest in S-phase.

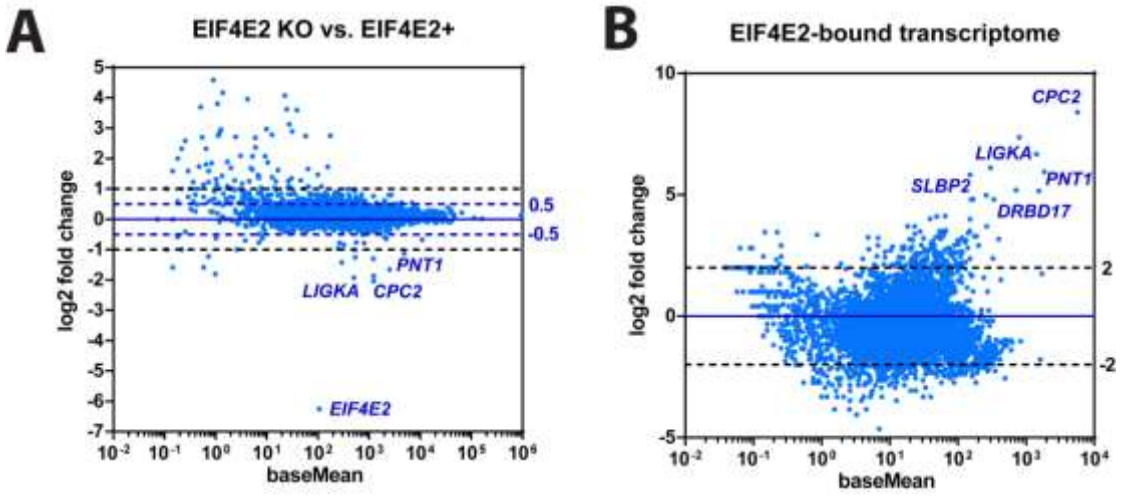

Figure 3.14 EIF4E2 is involved in the regulation of S-phase-specific mRNAs in bloodstream forms (BSFs). (A) Total transcriptomes of BSFs lacking both *EIF4E2* alleles (EIF4E2 KO) or with reconstituted expression of EIF4E2 (EIF4E2+) were

analyzed by RNA sequencing. Four mRNAs that were strongly down-regulated in the absence of EIF4E2 are indicated. Data from three independent experiments were analyzed. **(B)** PTP-tagged EIF4E2 was pulled down from BSFs and mRNAs present in bound and unbound fractions were analyzed by RNA sequencing. Five of the most strongly enriched mRNAs are indicated. Data from three independent experiments were analyzed.

To determine whether the observed effect on the transcriptome resulted from direct interactions between the presumed target mRNAs and EIF4E2 protein and to identify additional targets, pulldowns of PTP-tagged EIF4E2 were performed and subjected to analysis by RNA sequencing. Interestingly, the mRNAs that were associated with EIF4E2-PTP largely corresponded to those downregulated in the absence of EIF4E2. Apart from mRNAs encoding CPC2, PNT1, and *Tb*927.7.610 proteins, EIF4E2 specifically bound to *SLBP2*, *DRBD12*, and *DRBD17* mRNAs (**Figure 3.14B and Table 49**). Based on these results, it could not be determined whether the association with *SLBP2* mRNA occurred indirectly through binding of EIF4E2 to the nascent SLBP2 chain or because it binds the mRNA directly.

Because of these results pointing towards an effect on cell cycle progression, WT and *EIF4E2* KO cells were examined by microscopy to analyze the DNA content by DAPI staining (**Table 50**), with the aim to unravel defects in cell cycle regulation. Although messages encoding S-phase proteins were affected by the loss of EIF4E2, cell cycle progression did not appear to be significantly affected, as the nuclear content was comparable between WT and *EIF4E2* KO cells. There were slightly more *EIF4E2* KO cells with two nuclei and two kinetoplasts than WT cells with similar nuclear contents. This is indicative of cells in G2-phase, as both the nucleus and kinetoplast are doubled during S-phase.

Apart from the effects on S-phase mRNAs, expression of over 20 *VSG* variants, pseudogenes, and expression-site associated genes was upregulated between 1.5- to 18-fold at the mRNA level, while expression of the major *VSG* was not affected by *EIF4E2* KO. This suggested that EIF4E2 was required for regulating allelic exclusion (**Table 51**). Accordingly, mRNA sequencing results further revealed that mRNAs encoding proteins required for maintaining chromosomal organization, such as CPC, were downregulated in the absence of EIF4E2. This promiscuous expression of *VSG* genes may thus have been a secondary effect to changes in chromatin structure in cells lacking *EIF4E2*. Damaged DNA in cells lacking both *EIF4E2* alleles could have further contributed to this effect.

3.2.3 SLBP2 associates with PUF9

As several targets are shared between EIF4E2 complexes and PUF9, a potential association between EIF4E2/SLBP2 and PUF9 proteins was tested by yeast-2-hybrid analysis. Although this was not supported by the mass spectrometry data (**Supplementary Figure S5**), transient interactions or bridging of different proteins by an additional factor may have been missed using this approach.

EIF4E2, *SLBP2*, and *PUF9* ORFS were cloned into yeast-2-hybrid vectors and tested for direct interactions with one another. Expectedly, interactions between EIF4E2 and SLBP2 could be confirmed using this approach (**Supplementary Figure S7**). Furthermore, SLBP2 appeared to interact with PUF9 and consequently supported strong growth under selection. One of the three replicates also provided evidence that combinations of PUF9-AD and EIF4E2-BD were able to promote growth of yeast cells, while EIF4E2-AD and PUF9-BD did not appear to interact with one another (**Supplementary Figure S7**). Furthermore, combinations of PUF9-AD/PUF9-BD and SLBP2-AD/SLBP2-BD resulted in growth, pointing towards self-interaction.

GeneID	Annotation	Category	Cell cycle	KO1	KO2	KO3	AB1	AB2	AB3	mean KO	mean AB	FC AB/KO
Tb927.8.710	DRBD17	RNA binding	S	37131	40937	38313	66261	63253	56379	38794	61964	1.6
Tb927.11.6550	PUF nine target 1 (PNT1)	Cell cycle	S	5294	5949	5520	19204	17008	16572	5587.7	17595	3.1
Tb927.9.2800	hypothetical protein, conserved, DNA_binding_1 6-O-methylguanine DNA methyltransferase domain	ZUnknown	(S)	2900	2741	2468	4972	4482	4595	2703	4683	1.7
Tb927.11.14840	CPC2, chromosomal passenger complex	Chromatin	S	2209	2285	2164	9362	9187	8901	2219.3	9150	4.1
Tb927.6.3180	hypothetical protein, conserved	ZUnknown	S	2869	3480	3312	8453	7578	7760	3220.3	7930.3	2.5
Tb927.11.890	hypothetical protein, conserved	ZUnknown	S	14208	14685	12956	33762	30009	27852	13950	30541	2.2
Tb927.7.610	LIGKA, putative mitochondrial DNA ligase homolog, putative	DNA	S	2466	2539	2294	9314	9230	8161	2433	8901.7	3.7
Tb927.10.9730	hypothetical protein, conserved	ZUnknown	S	1640	1692	1508	3430	3237	3065	1613.3	3244	2.0
Tb927.7.2290	hypothetical protein, conserved	Cytoskeleton	S	1851	2041	1809	3465	3032	3188	1900.3	3228.3	1.7

dstream forms lacking *EIF4E2*. Data from three independent experiments are shown. KO, knockout;

GeneID	Annotation	Class	EL1/U1	EL2/U2	EL3/U3	mean EL/U
Tb927.11.14840	CPC2, chromosomal passenger complex	Chromatin	272.3	184.4	338.3	265.0
Tb927.7.610	LIGKA, putative,mitochondrial DNA ligase homolog, putative	DNA	76.4	53.0	101.9	77.1
Tb927.9.2800	hypothetical protein, conserved	ZUnknown	105.8	52.6	164.9	107.7
Tb927.11.6550	PUF nine target 1 (PNT1)	Cell.cycle	43.6	45.0	61.4	50.0
Tb927.8.710	DRBD17	RNA.binding	26.7	13.6	35.9	25.4
Tb927.11.890	hypothetical protein, conserved	ZUnknown	23.1	13.5	36.6	24.4
Tb927.7.2290	hypothetical protein, conserved	Cytoskeleton	19.7	11.1	28.0	19.6
Tb927.10.9730	hypothetical protein, conserved	ZUnknown	18.3	10.9	28.3	19.2
Tb927.6.3180	hypothetical protein, conserved	ZUnknown	7.0	5.1	9.8	7.3
Tb927.2.2670	histone H4 variant	Chromatin	16.4	10.1	28.0	18.1
Tb927.11.7580	hypothetical protein, conserved	Mito.DNA	8.7	5.4	13.0	9.0
Tb927.7.5380	DRBD12	RNA.binding	11.8	5.1	11.2	9.4
Tb927.11.14930	hypothetical protein, conserved	ZUnknown	21.0	7.2	31.6	19.9
Tb927.8.4200	hypothetical protein, conserved, no domains, no yeast.humanmatch	ZUnknown	9.0	5.5	10.7	8.4
Tb927.3.870	**SLBP2, like histone RNA hairpin binding proteins, binds to EIF4E2**	**RNA.binding**	46.5	9.2	69.5	41.7
Tb927.10.16070	**EIF4E2**	**Translation**	1.7	1.0	2.6	1.7

Table 50. DNA content of wild type and EIF4E2-deficient bloodstream forms. N, nucleus; K, kinetoplast

Data from three independent experiments are shown. EL, elution fraction; U, unbound fraction

WT	1N1K	1N2K	2N 1-2K	zoid
Image 1	46	5	5	1
Image 2	64	6	9	1
Image 3	60	7	8	0
Image 4	47	7	5	0
Image 5	74	5	8	0
Percent	**83**	**7**	**9**	**1**
EIF4E2 KO	**1N1K**	**1N2K**	**2N 1-2K**	**zoid**
Image 1	39	8	0	0
Image 2	48	12	4	2
Image 3	48	12	5	0
Image 4	70	19	9	2
Image 5	84	11	9	3
Percent	**77**	**15**	**6**	**2**

coprotein (*VSG*) genes upon loss of EIF4E2 in bloodstream forms. KO, knockout; AB, addback; ESAG, expression site-associated

GeneID	Annotation	Class	KO1	KO2	KO3	AB1	AB2	AB3	mean KO	mean AB	FC KO/AB
Tb927.1.3670	expression site-associated gene 8 (ESAG8)	ESAG	1705	1708	1521	1050	999	936	1711.3	995	1.72
Tb927.7.3250	expression site-associated gene 6 (ESAG6)	ESAG	16034	17590	14162	9470	8805	9069	15928.7	9114.7	1.75
Tb927.7.3260	expression site-associated gene 7 (ESAG7)	ESAG	14734	15903	12824	8789	7929	8255	14487	8324.3	1.74
Tb927.9.7340	expression site-associated gene 9 (ESAG9)	ESAG	3094	3385	2896	2060	1816	1849	3175	1908.3	1.66
Tb927.11.17850	expression site-associated gene 9 (ESAG9)	ESAG.pseudo	698	730	667	458	410	389	715	419	1.71
Tb927.5.4720	expression site-associated gene 3 (ESAG3)	ESAG.pseudo	20	21	18	2	4	3	19.7	3	6.56
Tb927.5.4760	expression site-associated gene 3 (ESAG3)	ESAG.pseudo	14	21	11	0	0	2	12	0.7	18.00
EATRO1125_MVSG5	EATRO1125_MVSG5	VSG	84	83	80	13	29	20	75.7	20.7	3.66
EATRO1125_VSG1654	EATRO1125_VSG1654	VSG	90	92	99	49	37	41	87	42.3	2.06
EATRO1125_VSG224	EATRO1125_VSG224	VSG	112	94	97	15	11	18	101	14.7	6.89
EATRO1125_VSG2523	EATRO1125_VSG2523	VSG	209	196	184	13	12	10	196.3	11.7	16.83
EATRO1125_VSG276	EATRO1125_VSG276	VSG	233	226	211	33	14	31	226.7	26	8.72
EATRO1125_VSG313	EATRO1125_VSG313	VSG	497	400	414	79	64	65	463.7	69.3	6.69
EATRO1125_VSG383	EATRO1125_VSG383	VSG	38	32	33	11	11	10	34.3	10.7	3.22
EATRO1125_VSG385	EATRO1125_VSG385	VSG	40	33	36	1	4	2	36.3	2.3	15.57
EATRO1125_VSG4040	EATRO1125_VSG4040	VSG	1229	1008	1067	361	315	325	1101.3	333.7	3.30
EATRO1125_VSG421	EATRO1125_VSG421	VSG	315	255	258	128	115	127	299.3	123.3	2.43
EATRO1125_VSG4710	EATRO1125_VSG4710	VSG	214	228	195	16	22	13	209	17	12.29
EATRO1125_VSG4862	EATRO1125_VSG4862	VSG	1388	1509	1395	217	188	217	1397.3	207.3	6.74
EATRO1125_VSG4959	EATRO1125_VSG4959	VSG	370	327	307	31	25	26	331.3	27.3	12.12
EATRO1125_VSG514	EATRO1125_VSG514	VSG	486	404	416	157	144	125	448.7	142	3.16
EATRO1125_VSG84	EATRO1125_VSG84	VSG	57	43	49	8	8	11	46.3	9	5.15
Tb927.9.16010	expression site-associated gene 4 (ESAG4, pseudogene)	ESAG.pseudo	396	373	292	249	229	220	353.7	232.7	1.52
Tb927.9.680	expression site-associated gene 9 (ESAG9), pseudogene	ESAG.pseudo	202	274	233	161	161	154	236.3	158.7	1.49
Tb927.5.291b	variant surface glycoprotein (VSG)-related, putative	Vesicular.transport	1427	1100	1544	1074	961	1072	1590.3	1035.7	1.54
EATRO1125_VSG2564	EATRO1125_VSG2564	VSG	247	227	287	138	152	152	237	147.3	1.61

3.3 *Tb927.10.5020* - Eukaryotic translation initiation factor 4E5 (EIF4E5)

3.3.1 EIF4E5 is dispensable in the BSF, but essential for survival of PCFs

EIF4E5 is smaller than the canonical cap-binding proteins EIF4E3 and EIF4E4, but is known to form EIF4F-like complexes with EIF4G1 and EIF4G2 [98]. It is unknown whether it mediates translational activation of a selected subset of mRNAs or operates on the same targets as EIF4E3/4. A balance of these two mechanisms is also possible. As a first indication of non-overlapping functions, BSFs lacking *EIF4E5* featured only a slight growth defect (**Figure 3.15A, B**), whereas depletion of EIF4E3/4 severely compromised cell growth or even led to cell death [85, 97, 98].

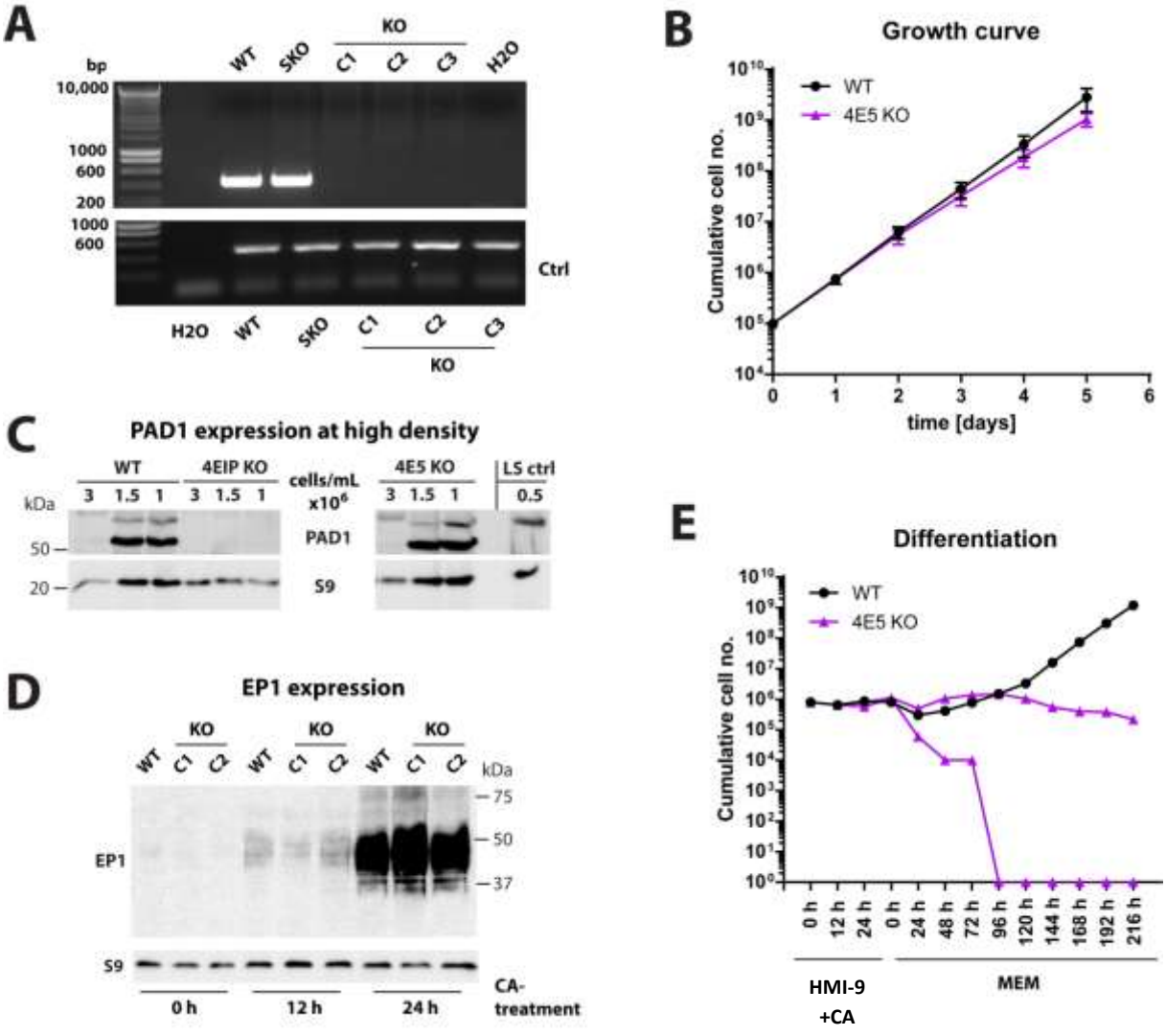

Figure 3.15 EIF4E5 is required for survival of procyclic forms (PCFs), but dispensable in bloodstream forms (BSFs). (A) Homozygous knockout (KO) of *EIF4E5* in BSFs was confirmed by PCR using primers specific for the *EIF4E5* open reading frame (ORF, upper panel). Wildtype (WT) BSFs and BSFs lacking only a single *EIF4E5* allele (SKO) were included as controls. Genomic tubulin sequences were detected using specific primers (lower panel) to confirm the presence of DNA in all of the samples analyzed. **(B)** Growth of WT and *EIF4E5* KO BSFs was monitored over the course of one week. **(C)** *EIF4E5* KO cells were grown to maximal densities in HMI-9 medium containing methylcellulose to induce stumpy formation. The cells were harvested at the indicated densities. Expression of the stumpy form marker PAD1 was analyzed by western blotting, with the 40S ribosomal protein S9 serving as a loading control. WT and *4EIP* KO BSFs were used as positive and negative controls of stumpy formation, respectively. **(D)** Differentiation to the PCF was induced in WT and *EIF4E5* KO BSFs by treatment with *cis*-aconitate (CA) for the times indicated and a temperature shift from 37 °C to 27 °C. Expression of the PCF-specific marker EP1 was analyzed by western blotting, with the 40S ribosomal protein S9 serving as a loading control. **(E)** Differentiation to

the PCF was induced in WT and *EIF4E5* KO BSFs by treatment with *cis*-aconitate for the times indicated and a temperature shift from 37 °C to 27 °C. On the following day, the cells were transferred to PCF-specific medium (MEM) and continuously cultured at 27 °C. Growth of the cells was then followed for another 9 days. One (WT) or two (*EIF4E5* KO) representative experiments are shown.

Furthermore, differentiation of *EIF4E5* KO BSFs to the PCF proceeded similarly to that of WT cells, as evidenced by PAD1 and EP1 expression kinetics, which serve as markers of stumpy and procyclic forms, respectively (**Figure 3.15C, D**).

Similar to *EIF4E1* KO cells, which failed to grow as proper procyclic cells, cells without *EIF4E5* exhibited a stress phenotype, including an elongated shape and little movement, which was followed by cell death after several days (**Figure 3.15E**). The differential KO phenotype observed between the BSF and PCF suggested different roles during these life cycle stages.

To test whether this was reflected at the level of protein binding partners, quantitative mass spectrometry was performed on BSFs expressing PTP-tagged EIF4E5 and bound proteins were compared to those co-purified with EIF4E3-PTP or GFP-PTP (**Figure 3.16A, B**). The data obtained were very reminiscent of those reported for PCFs. EIF4G1 and EIF4G2 could be identified as proteins present in EIF4E5-containing complexes, as well as 14-3-3(I) proteins. It is thus very likely that EIF4E5 forms similar complexes in both forms, despite EIF4E5 being essential in the PCF only.

Furthermore, EIF4E5 was shown to interact with RBP3 and *Tb*927.8.4560 in PCFs, which were present in only 2 of the 3 replicates in purifications done in the BSF in the course if this project. While homologs of DHH1, PUF1, and *Tb*927.5.4270 were associated with EIF4E5 in *Leishmania*, similar interactions were not observed in *T. brucei* (**Figure 3.16A, B**).

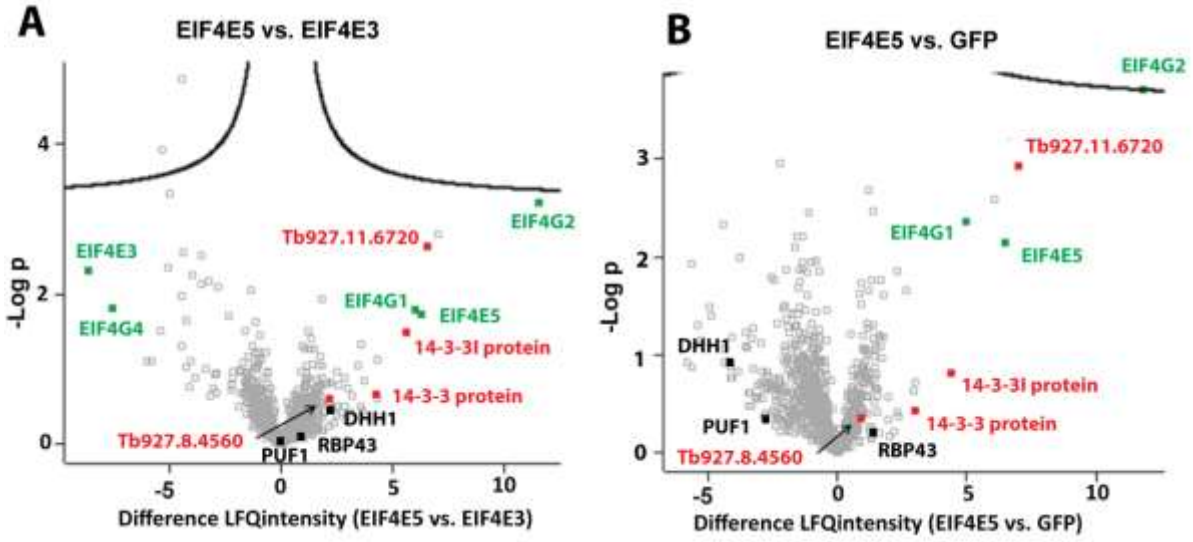

Figure 3.16 EIF4E5-bound proteome in bloodstream forms (BSFs). (A) PTP-tagged EIF4E5 and EIF4E3 cap-binding proteins were purified from 1 × 10^9 BSFs and bound proteins were analyzed by quantitative mass spectrometry. Raw data were analyzed by Sabine Merker from the mass spectrometry core facility using MaxQuant, and interaction partners were subsequently analyzed in Perseus. In the volcano plot, differences in label-free quantification (LFQ) intensities were plotted against the log10 of the false discovery rate (FDR) calculated by a permutation-based FDR adapted t-test. Data from three independent experiments are shown. Each square represents one protein and some proteins of interest are highlighted in color. **(B)** PTP-tagged EIF4E5 and GFP proteins were purified from 1 × 10^9 BSFs and bound proteins were analyzed by quantitative mass spectrometry. Raw data were analyzed by Sabine Merker from the mass spectrometry core facility using MaxQuant, and interaction partners were subsequently analyzed in Perseus. In the volcano plot, differences in label-free quantification (LFQ) intensities were plotted against the log10 of the false discovery rate (FDR) calculated by a permutation-based FDR adapted t-test. Data from three independent experiments are shown. Each square represents one protein and some proteins of interest are highlighted in color.

Two EIF4E5 partners were already known to increase expression in the tethering assay. Unpublished data obtained by Larissa Melo do Nascimento indicate that full-length EIF4E5 can also modestly enhance expression (not shown).

3.4 *Tb927.7.1670* - Eukaryotic translation initiation factor 4E6 (EIF4E6)

3.4.1 EIF4E6 is essential in BSFs and PCFs

EIF4E proteins in trypanosomatids were originally classified into two groups, but the discovery of EIF4E6 and EIF4E5 led to the introduction of a third group with little EIF4E homology. Despite their small size, group 3 EIF4E proteins are able to form EIF4F-like complexes. Previous studies identified EIF4G5 as the binding partner of EIF4E6 [99]. Furthermore, EIF4G5 is known to recruit another protein component to the complex, which is called G5-interacting protein (G5-IP) [99].

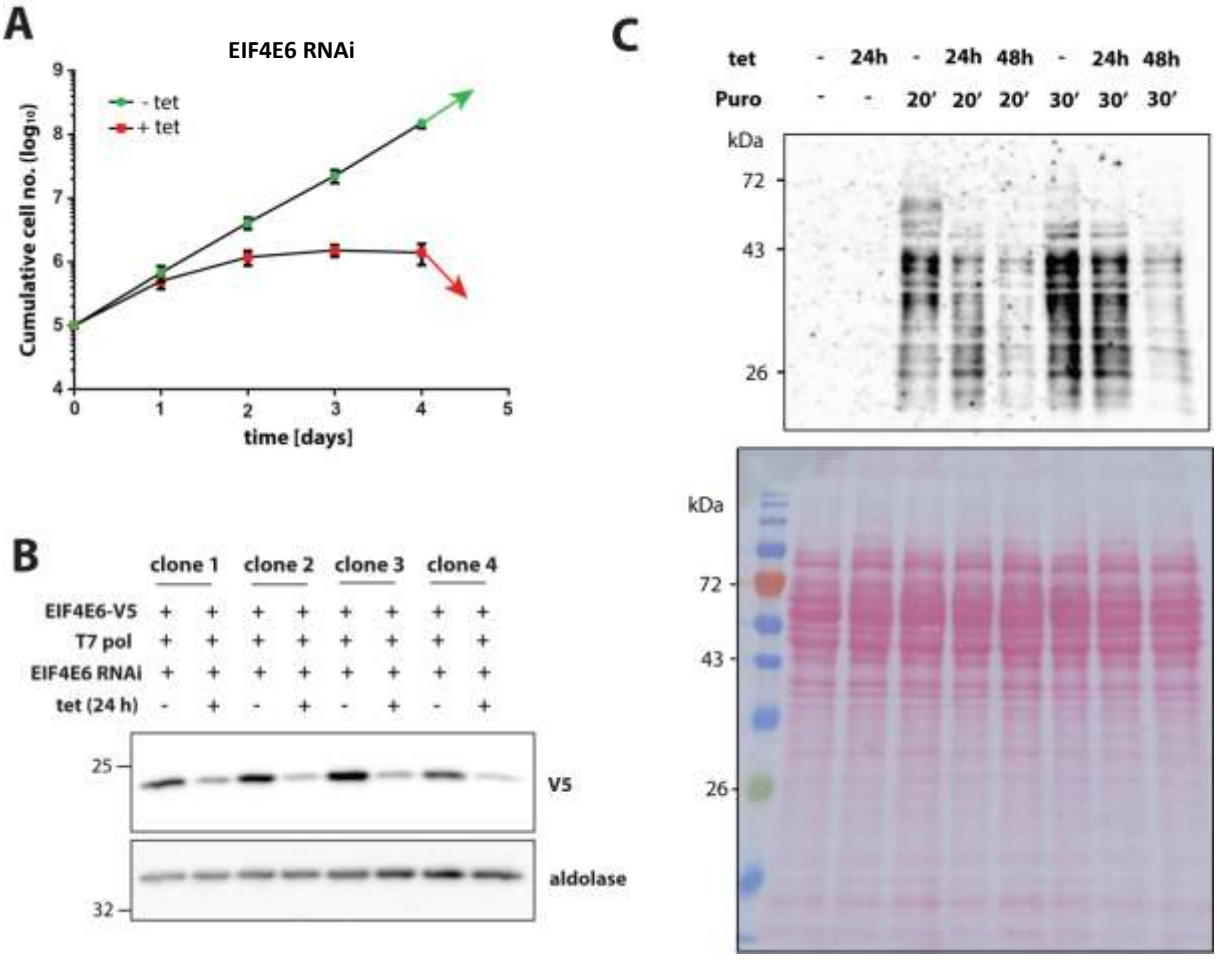

Figure 3.17 Depletion of *EIF4E6* results in cell death and translation suppression in bloodstream forms (BSFs). (A) *EIF4E6* was depleted in BSFs by tetracyclin (tet)-inducible RNAi. Growth was followed over the course of five days. Cells cultured in the absence of tet were used as a control. Mean and standard deviation from three independent experiments are shown. **(B)** Knockdown efficiency of *EIF4E6* RNAi was tested in four different clones by western blotting at 24 h after induction. In the case of one *EIF4E6* allele, a sequence encoding a V5-tag was introduced to follow expression; the second copy was deleted from the genome. Expression of aldolase was used as a loading control. **(C)** BSFs depleted of *EIF4E6* by tet-inducible RNAi for the times indicated were subjected to 20 or 30 min of puromycin (Puro) labeling. Proteins were then separated by polyacrylamide gel electrophoresis and incorporated puromycin was detected by western blotting using specific antibodies. Staining with Ponceau S red was used as a loading control.

In accordance with previous reports, neither BSFs nor PCFs with a homozygous KO of *EIF4E6* could be obtained, suggesting that it is essential in both forms. Accordingly, knockdown of *EIF4E6* in BSFs expressing V5-tagged EIF4E6 resulted in a growth arrest, which was followed by cell death within five to six days, in spite of detectable, residual expression of V5-tagged EIF4E6 (**Figure 3.17A, B**). The second allele was deleted in those cells. To unravel global effects on protein synthesis, incorporation of puromycin within 20 min and 30 min was analyzed. Subsequent detection of puromycin with specific antibodies revealed significantly reduced incorporation efficiencies after 24 h of RNAi induction. This effect was even more pronounced after 48 h of *EIF4E6* knockdown (**Figure 3.17C**). In accordance with these observations, depletion of *EIF4E6* led to removal of mRNAs from polysomes (**Supplementary Figure S8**).
BSFs with *EIF4E6* RNAi could be differentiated to the PCF. However, knockdown efficiency was very poor in PCFs compared to BSFs, and subsequent analyses were largely restricted to BSFs.

3.4.2 EIF4E6 is found in activating MKT1 complexes

There is evidence that a multicomponent complex consisting of MKT1, PBP1, XAC1, and LSM12 is recruited to target mRNAs by specific RNA-binding proteins, such as ZC23H11, ZC3H20, and ZC3H21, or the F-box protein CFB2. Data on protein-protein interactions obtained by mass spectrometry and yeast-2-hybrid assays revealed a direct interaction between MKT1 and EIF4G5 [113]. It was therefore speculated that cap-binding complexes of EIF4E6/EIF4G5 serve as initiators of translation of mRNAs specifically bound by MKT1 complexes.
Association of EIF4E6 with components of the MKT1 complex was therefore tested by purification of EIF4E6-PTP and subsequent detection of V5-tagged MKT1 or MKT1-Like (MKT1L) proteins. As shown in **Figure 3.18A** and **3.18B**, MKT1-V5 could be co-purified with EIF4E6, while MKT1L was absent from bound fractions. The latter resembles MKT1 at the C-terminus, but has an N-terminal extension. Functionally, MKT1L protein appears not to interact with RNA-binding proteins or mRNAs, but with the protein components present in MKT1 complexes, such as PBP1, LSM12, and XAC1 [113]. This could result in competition for protein binding partners, possibly regulating the activity of MKT1 complexes.
I also identified interaction partners of EIF4E6 on a broader scale using mass spectrometry. In line with my expectations, other proteins present in MKT1 complexes were identified as binding partners of EIF4E6, including PBP1, PABPs, and MKT1. However, upon comparison with pulldowns of GFP-PTP, MKT1L protein was absent from the EIF4E6-associated protein pool (**Figure 3.18C**). Notably, CFB2 was co-purified with EIF4E6 (**Figure 3.18C, D**) [124].

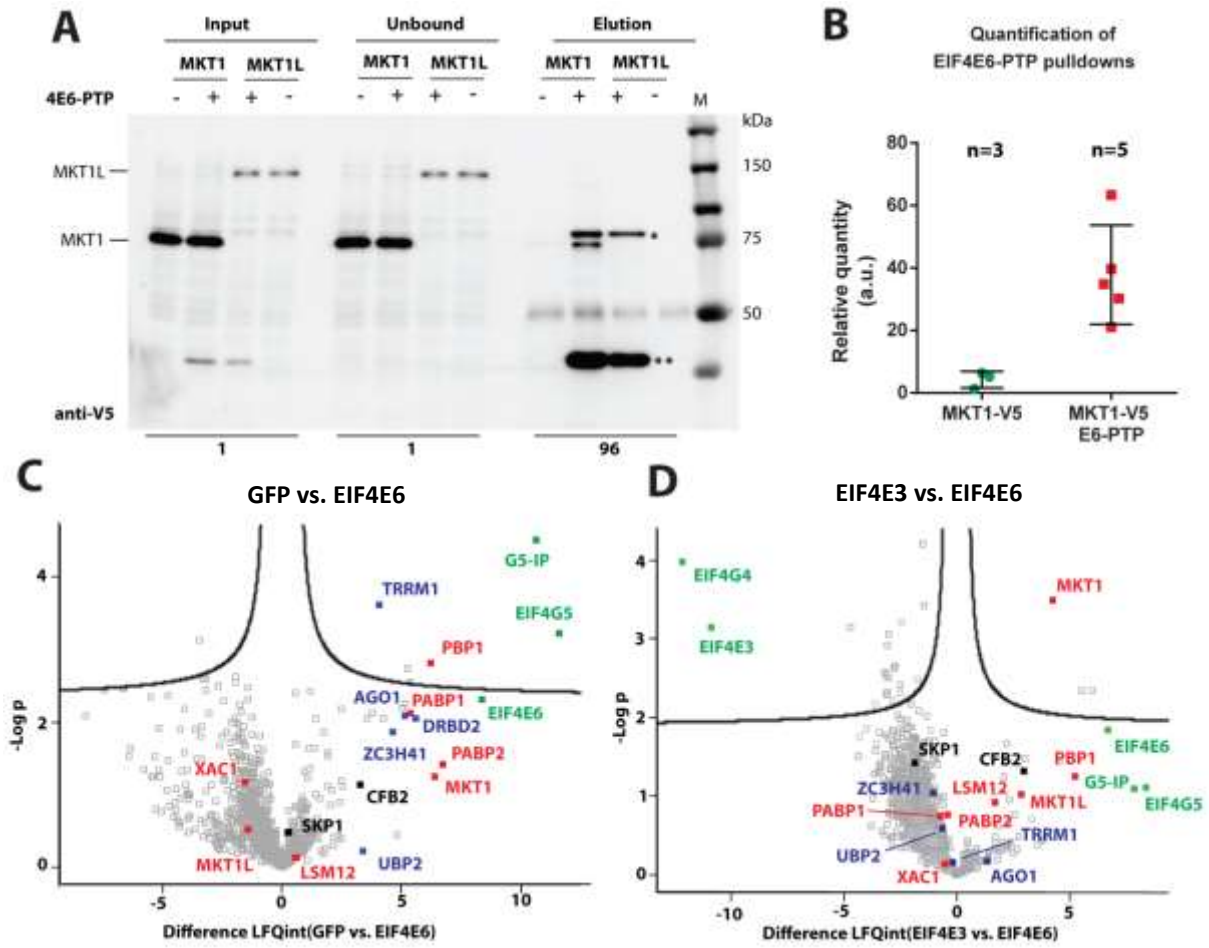

Figure 3.18 EIF4E6 is present in activating MKT1 complexes. (A) EIF4E6-PTP was purified from bloodstream forms (BSFs) expressing V5-tagged MKT1 or MKT1-Like (MKT1L) protein. The presence of MKT1-V5 and MKT1L-V5 in input, unbound, and elution fractions was analyzed by western blotting. Cells expressing MKT1-V5 or MKT1L-V5 without EIF4E6-PTP were used as controls to monitor unspecific binding. *, additional band that is reproducibly seen in the EIF4E6-PTP line, unknown; **, EIF4E6-PTP-derived signal (PTP binds to IgG). **(B)** The presence of MKT1-V5 in pulldowns of EIF4E6-PTP was compared to unspecific binding of MKT1-V5 to the IgG beads that were used to purify EIF5E6-PTP. Data from at least three independent experiments were included. **(C)** PTP-tagged EIF4E6 and GFP proteins were expressed in BSFs and purified using IgG beads. The proteins bound to the proteins of interest were analyzed by quantitative mass spectrometry. Raw data were analyzed by Sabine Merker from the mass spectrometry core facility using MaxQuant, and interaction partners were subsequently analyzed in Perseus. In the volcano plot, differences in label-free quantification (LFQ) intensities were plotted against the log10 of the false discovery rate (FDR) calculated by a permutation-based FDR adapted t-test. Data from three independent experiments are shown. Each square represents one protein and some proteins of interest are highlighted in color. **(D)** PTP-tagged EIF4E6 and EIF4E3 cap-binding proteins were expressed in BSFs and purified using IgG beads. The proteins bound to the proteins of interest were analyzed by quantitative mass spectrometry. Raw data were analyzed by Sabine Merker from the mass spectrometry core facility using MaxQuant, and interaction partners were subsequently analyzed in Perseus. In the volcano plot, differences in label-free quantification (LFQ) intensities were plotted against the log10 of the false discovery rate (FDR) calculated by a permutation-based FDR adapted t-test. Data from three independent experiments are shown. Each square represents one protein and some proteins of interest are highlighted in color. The data presented in **(A)** have been published in Nascimento et al., 2020 [113]

3.4.3 Does EIF4E6 mediate translation of the BSF-specific major surface protein VSG?

CFB2 is an RNA-binding F-box protein known to promote translation and stability of *VSG* mRNAs through MKT1 complex recruitment. I therefore tested whether EIF4E6 was involved in MKT1-complex/CFB2-dependent translation of *VSG* mRNAs. For this, tagged versions of different EIF4E proteins were pulled down from total lysates and both unbound and bound fractions analyzed and compared by PCR (**Figure 3.19A, B**) or qPCR (**Figure 3.19C**) using *VSG*-specific primers. Interestingly, the presence of a *VSG*-specific signal was not restricted to bound fractions from EIF4E6 pulldowns, but an association with EIF4E3 was also observed, indicating that the stringency of the pulldowns was either not high enough or that both proteins could bind to *VSG* mRNA. The fact that *VSG* mRNAs were not detected in pulldowns of EIF4E4 (**Figure 3.19B, C**) and the massive amounts of VSG proteins required argue for the latter hypothesis. In accordance with these results, *VSG* mRNA has previously been shown to associate with EIF4G5, which was absent from purifications of tubulin mRNA [124].
Whether knockdown of *EIF4E6* would also lead to reduced *VSG* mRNA stability was tested by PCR (**Figure 3.19D**). However, there was no indication that this was the case.

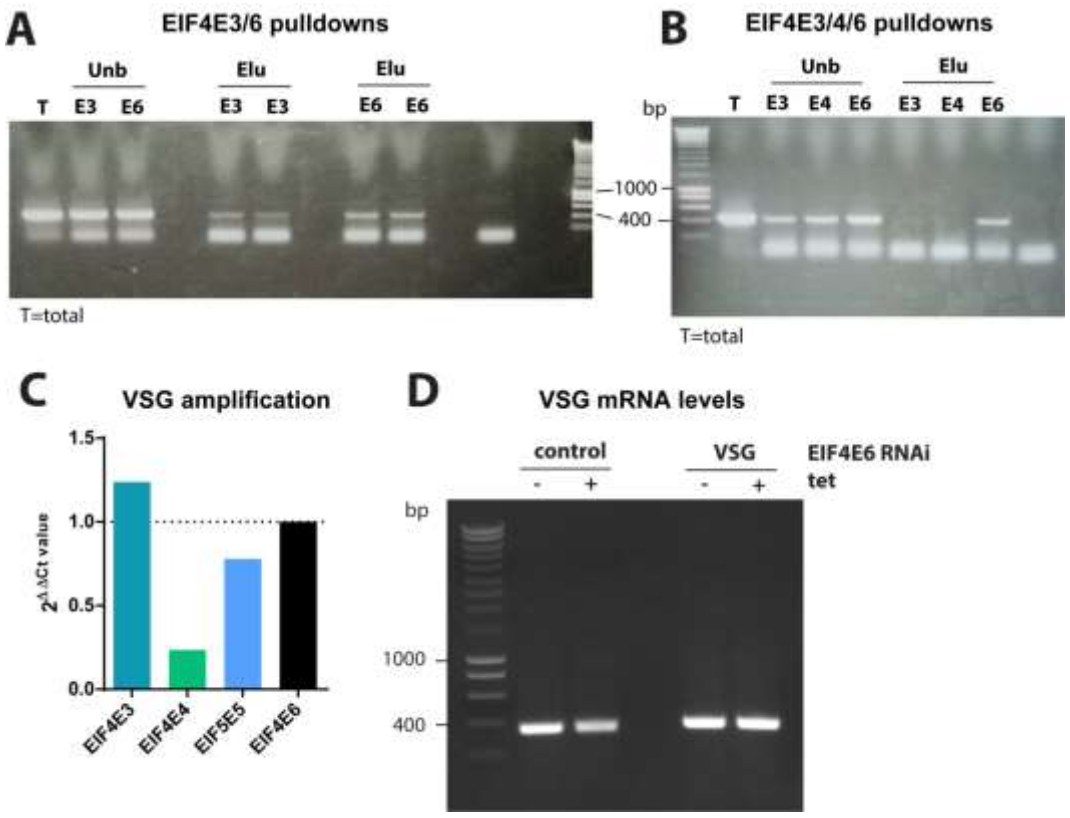

Figure 3.19 Associations of EIF4E proteins with variant surface glycoprotein (*VSG*) mRNAs. (A) Immunoprecepitations were performed to pull down PTP-tagged EIF4E3 and EIF4E6 from bloodstream forms (BSFs). Unbound and bound fractions were then analyzed by reverse transcription PCR (RT-PCR) for the presence of *VSG* mRNAs using primers binding to the spliced leader and a sequence within the *VSG* ORF. T, total RNA from WT cells**. (B)** Immunoprecepitations were performed to pull down PTP-tagged EIF4E3, EIF4E4, and EIF4E6 from BSFs. Unbound and bound fractions were then analyzed by RT-PCR for the presence of *VSG* mRNAs using primers binding to the spliced leader and a sequence within the *VSG* ORF. T, total RNA from WT cells. **(C)** Immunoprecepitations were performed to pull down PTP-tagged EIF4E3, EIF4E4, EIF4E5, and EIF4E6 from BSFs. Unbound and bound fractions were then analyzed by quantitative (q)RT-PCR for the presence of *VSG* mRNAs using primers binding to the spliced leader and a sequence within the *VSG* ORF. Means of triplicates from one experiment are shown. **(D)** *VSG* and *tubulin* (control) mRNA levels in total RNA from *EIF4E6* RNAi cells cultured with and without tetracycline were analyzed by RT-PCR using primers binding to the spliced leader and a sequence within the *VSG* ORF.

Binding of mRNAs by EIF4E6 and EIF4E3 in BSFs was then analyzed using RNAseq, but obtained data revealed a suspiciously strong correlation between the mRNAs associated with the two proteins (**Figure 3.20A**). Furthermore, there was a large overlap between those mRNAs reportedly binding to EIF4E1 in PCFs and EIF4E3 in BSFs (**Figure 3.9D**). Based on this, it was assumed that most of the presumed associations were rather due to unspecific binding.
Contrary to my expectations, a correlation between those mRNA subsets bound to EIF4E6 and MKT1 was not observed (**Figure 3.20C**). Instead, a stronger correlation with EIF4E2-associated mRNAs again pointed towards largely unspecific interactions (**Figure 3.20D**).
Nonetheless, EIF4E6 pulled down the mRNA encoding EIF4G5, to which it binds. Thus, complex formation presumably occurs with nascent polypeptides and is independent of the association with the cap. The same was true for EIF4E3 and its binding partner EIF4G4. Additionally, there was a stronger association between EIF4E6 protein and *VSG* mRNA than with the message encoding tubulin (**Figure 3.20B**). This bias was also seen for EIF4E3, but it was much less pronounced (**Figure 3.20B**).
With the aim to strengthen the link between EIF4E6 and regulation of *VSG* mRNA translation, an indirect approach was additionally chosen. For specific co-purification of the EIF4E6/EIF4G5 complex with CFB2 protein, specific antibodies were produced against recombinant CFB2. To that end, a fusion protein of CFB2 and a carrier protein was expressed in and purified from BL21 recombinant *E. coli* cells (**Supplementary Figure S9A**). Polyclonal antiserum was produced in rabbit at David's Biotechnology (https://www.davids-bio.de/). The antibodies generated were shown to detect recombinant CFB2 protein when employed for western blotting (**Supplementary Figure S9B**). Nonetheless, the endogenous protein was not recognized in lysates of BSFs, where CFB2 is known to be expressed (**Supplementary Figure S9B**). Therefore, the antiserum was subjected to an additional purification step, after which it could successfully recognize CFB2 protein in lysates of BSF *T. brucei* parasites, which was shown by Nascimento et al. [124]. Upon coupling to magnetic beads, anti-CFB2 antibody was used to pull down CFB2 protein from BSFs, and potential binding partners were analyzed by western blotting (**Supplementary Figure S9C**). However, V5-tagged EIF4E6 could not be specifically enriched using this approach. MKT1L, which served as a negative control not presumed to bind CFB2, was present at similar quantities, arguing for unspecific binding to the beads. In line with this, specific enrichment of EIF4E6-PTP using IgG-coupled beads did not result in co-purification of detectable levels of CFB2, which was contrasted by the data obtained by mass spectrometry, where CFB2 was present in the EIF4E6-associated proteome.

3.4.4 A ribosome profiling protocol from *Leishmania* is not applicable to *T. brucei*

Ribosome occupancy of the cytoplasmic mRNA pool can be analyzed by digesting those parts of the mRNA that are not protected by ribosomal proteins, followed by sequencing of the protected mRNA fragments. Here, a ribosome profiling protocol established and tested in *Leishmania* parasites was used with the aim to analyze ribosome occupancy in EIF4E6-depleted cells compared to cells with normal EIF4E6 levels [125]. For this purpose, the cells were treated with cycloheximide, lysed, and mRNAs were digested using RNAse I. Ribosome fragment isolation was performed using S400 columns, after which the RNA was isolated and subjected to PAGE purification to obtain 28-30 nt fragments by cutting the corresponding parts of the gel. A sequencing library was prepared using the NEXTFLEX® Small RNA-Seq Kit v3 for Illumina® Platforms, which was then sequenced at the RNA Sequencing Core Facility Heidelberg. Against my expectations, the data revealed primarily ribosomal sequences and a lack of mRNA sequences, indicating that the wrong RNA species had been extracted using this protocol previously used for analyzing ribosome-protected fragments in *Leishmania*.

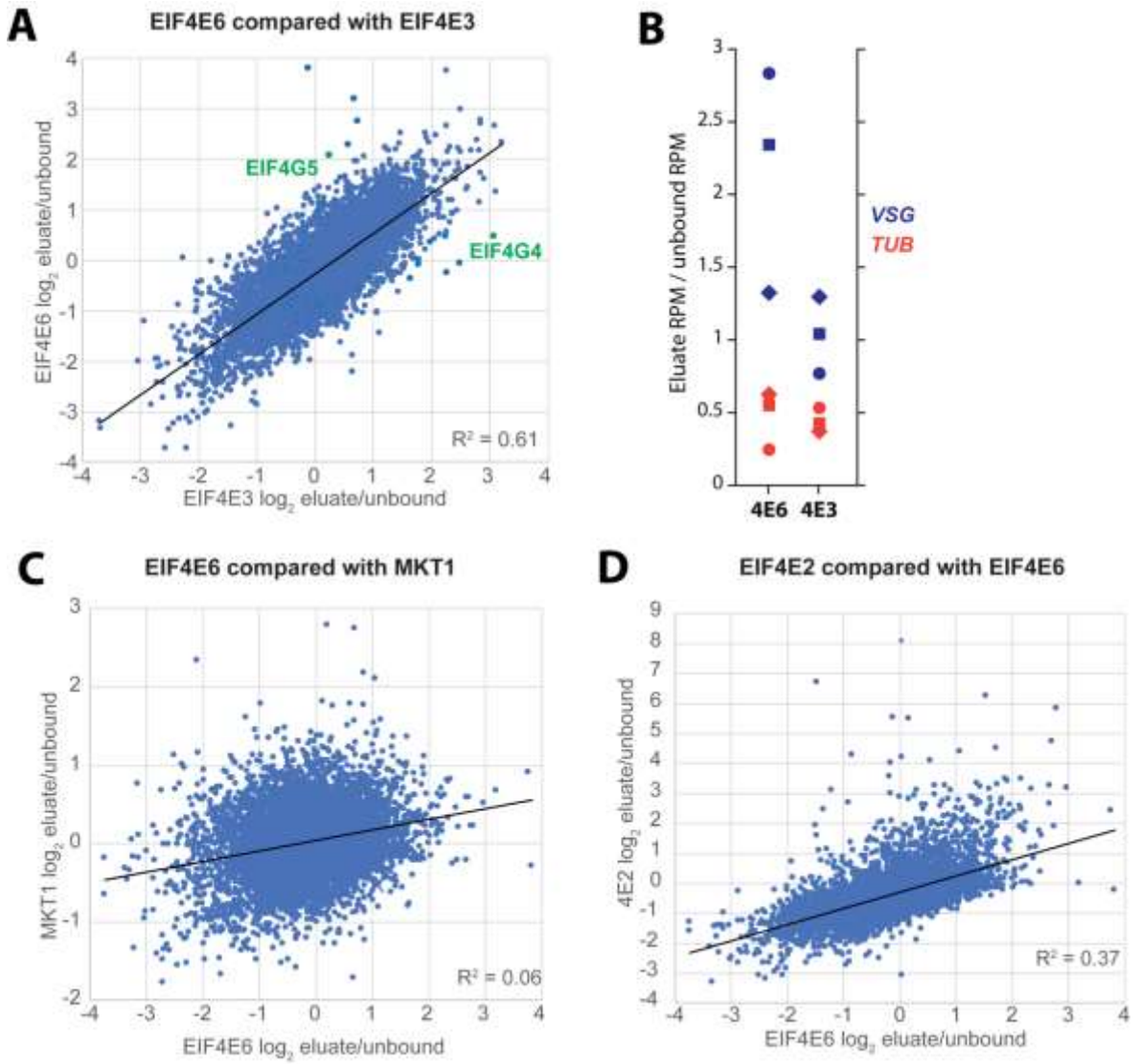

Figure 3.20 Variant surface glycoprotein (*VSG*) mRNA sequences are overrepresented in pulldowns of EIF4E6. (A) The mRNAs associated with EIF4E6 and EIF4E3 in bloodstream forms (BSFs) were pulled down and analyzed by RNA sequencing. Selected mRNAs encoding the EIF4G5 and EIF4G4 binding partners EIF4E6 and EIF4E3, respectively, are highlighted. Data from three independent pulldowns are shown. **(B)** Bound and unbound fractions of EIF4E6- and EIF4E3-PTP pulldowns from BSFs were analyzed for the presence of *VSG* and *tubulin* transcripts. Data from three independent experiments are shown. **(C)** The mRNAs associated with EIF4E6-PTP were pulled down from BSFs, analyzed by RNA sequencing, and compared to those specifically enriched with MKT1 protein in the BSF. Data from three independent experiments are shown. **(D)** The mRNAs associated with EIF4E6 and EIF4E2 were pulled down from BSFs, analyzed by RNA sequencing and compared to each other. Data from three independent experiments are shown, analyzed by Franziska Falk and plotted by Christine Clayton.

4. Discussion

4.1 EIF4E1 supports translational repression by 4EIP

The aim of this part of the project was to dissect the roles of EIF4E1 during translation in the absence and presence of its binding partner 4EIP. Based on previous reports from *Leishmania*, the working hypothesis was that an *in vivo* translation activity of EIF4E1 is blocked by binding of 4EIP. In support of this, EIF4E1 from *Leishmania* has been reported to bind to the C-terminus of EIF3A and could be pulled down with EIF3A *in vitro* [101]. Structural data from *Leishmania* further provided evidence that the affinity of EIF4E1 for the cap was strongly reduced upon binding of 4EIP [102]. An EIF4G-independent translation-promoting activity of EIF4E1 outside the complex with 4EIP was thus proposed. To confirm this in *T. brucei brucei*, EIF4E1 with and without 4EIP was purified from BSFs. Contrary to expectations and previous data obtained in *Leishmania* parasites, the translational activator EIF3A was not enriched in pulldowns of EIF4E1-PTP, irrespective of whether 4EIP was present or not.

To identify all proteins bound to EIF4E1 in complex and without 4EIP, pulldowns of EIF4E1-PTP were analyzed by quantitative mass spectrometry. Indeed, EIF4E1 and 4EIP were enriched at roughly equimolar levels when 4EIP was expressed. In accordance with the results obtained by co-immunoprecipitation, there was no evidence that EIF4E1 associates with general translation factors in BSFs or PCFs when released from 4EIP. Accordingly, upon tethering to a reporter mRNA, EIF4E1 was unable to activate translation of the reporter, even when 4EIP was depleted [100]. EIF4E3, EIF4E4, EIF4E5, and EIF4E6, on the other hand, could stimulate reporter expression when tethered [109]. However, it is still possible that EIF4E1 acts as a translational activator during other life cycle stages that were not analyzed in the course of this study.

Moreover, it was revealed that loss of 4EIP results in reduced levels of EIF4E1 protein, assigning a stabilizing role to 4EIP. The results obtained by mass spectrometry provided additional insights into 4EIP function, as the terminal uridylyl transferase TUT3 was associated with EIF4E1/4EIP at approximately similar quantities. This interaction was lost once cap-binding complexes around EIF4E1 were depleted of 4EIP. This was observed in samples from both BSFs and PCFs. Additionally, 4EIP2 was found to associate with EIF4E1 independently of 4EIP. 4EIP2 is a cytoplasmic protein that was included in a previous high-throughput RNAi screening approach, where knockdown had no apparent effect on cell viability [126, 127]. Associated 4EIP2 levels could be estimated to be roughly 10% of those of EIF4E1 and 4EIP. In accordance with this, about one tenth of the EIF4E1 in *Leishmania* was found to be associated with 4EIP2 [128].

Interestingly, 4EIP2 was absent from protein interactomes of 4EIP, raising the possibility that 4EIP and 4EIP2 may compete for binding to EIF4E1 [100]. In support of this, the two proteins presumably bind to EIF4E1 via the $Y(X)_4L\Phi$ motif, which is shared between both proteins, as well as with EIF4Gs. Whether these two proteins also have overlapping functions is yet to be determined. However, the observation that loss of 4EIP results in cell death during stumpy differentiation argues against this hypothesis. It is also possible that a certain quantity is needed, which cannot be compensated for by 4EIP2 during this transition stage. Furthermore, the drastically reduced abundance of EIF4E1 molecules upon depletion of 4EIP could not be rescued by 4EIP2. It may, on the other hand, be the case that the fraction of EIF4E1 that was bound by 4EIP2 was stable, while free EIF4E1 was rapidly degraded, leading to the strong reduction in EIF4E1 protein in the absence of 4EIP. Studies in *Leishmania* reported an interaction between 4EIP2 and several EIF4E proteins, including EIF4E1, raising the hypothesis that 4EIP2 may act as a broad-range repressor, as 4EIP is specifically binding to EIF4E1 [129]. In this study, however, a specific enrichment of 4EIP2 with EIF4E proteins other than

EIF4E1 was not observed in comparison to pulldowns of GFP. Nevertheless, it cannot be excluded that these interactions occur only under specific conditions, such as stress, or during translationally repressed stages, such as the stumpy form. It was further shown that overexpression of 4EIP2 in *Leishmania* resulted in an inhibition of the translation-promoting activities of EIF4E1, EIF4E3, and EIF4E4 by reducing the cap-binding affinities of these proteins. However, it cannot be excluded that this was an artifact, as overexpression often results in cellular disturbances and off-target effects. Therefore, expression patters of 4EIP2 at different *T. brucei* life cycle stages could provide an insight into the *in vivo* functions of 4EIP2.

The Drosophila cap-binding protein 4EHP associates with GIGYF2 to exert its repressive functions [130]. This is achieved, at least in part, through additional recruitment of components of the NOT deadenylation complex [131]. Deadenylation typically constitutes the initial step of RNA decay. In line with this, small amounts of the NOT complex were co-purified with complexes of EIF4E1/4EIP in BSFs. Co-immunoprecipitations were employed to confirm this interaction, but the results were inconclusive. It is possible that these interactions exist only transiently and were therefore hard to catch. Collectively, these results led to the conclusion that EIF4E1 presumably acts as a supporter of translational repression, at least during the life cycle stages analyzed. In contrast, the previous working hypothesis that 4EIP could suppress a translation-promoting activity of EIF4E1 could not be confirmed.

To investigate this in more detail, mRNAs associated with EIF4E1 with and without 4EIP were analyzed by RNA sequencing. Differences in the subsets of mRNAs bound by EIF4E1 under these conditions should provide additional insights into the roles of EIF4E1 in PCFs, where it is essential. Translation-promoting activities in the absence of 4EIP were expected to result in a larger repertoire of mRNAs bound to EIF4E1 in *4EIP* KO cells. However, this was not the case; the subsets of mRNAs bound to EIF4E1 with and without 4EIP were overlapping to a great extent. However, there was also a strong correlation with mRNAs bound to EIF4E3 in the BSF, arguing that binding was (largely) unspecific. This was supported by the preference for long RNAs.

Despite these limitations, RNA sequencing results after pulldown of PTP-tagged EIF4E1 revealed that *4EIP* mRNA was strongly enriched in bound fractions. This could be the result of an association with the nascent polypeptide chain, as EIF4E1 interacts with the 4EIP N-terminus.

Additionally, *NOT1* mRNA was strongly associated with EIF4E1 in PCFs, but only when 4EIP was present. The approach did not allow for determining whether this interaction occurred indirectly through the nascent polypeptide chain or an actual interaction with the mRNA. In contrast, EIF4E1/4EIP from PCFs did not associate with components of the NOT complex. Furthermore, previous pulldowns of 4EIP did not result in an enrichment of *NOT1* mRNA [100].

The observation that complexes of EIF4E1/4EIP associate with TUT3 led to the conclusion that 4EIP-dependent translational suppression could result from targeted 3’-uridylation by TUT3 since in mammalian cells, uridylated mRNAs have been shown to serve as targets for degradation by the exonuclease Dis3L2 [121]. The *T. brucei* genome encodes five proteins resembling terminal uridylytransferases, three of which are present in the mitochondrion to catalyze 3’-end-directed uridylation of guide RNAs (gRNAs) and to insert and/or delete U-residues at RNA editing sites. TUT3 and TUT4, as well as a homolog of the 3’-exonuclease Dis3L2, were shown to be present in the cytoplasm where RNA decay occurs [120].

However, identifying uridylated mRNAs is hindered by their (presumed) unstable nature. It is thus not surprising that up to this point, only the highly abundant *GPEET* mRNA has been reported to be subjected to cytoplasmic uridylation. An *in silico* approach aimed at identifying additional targets was employed in the course of this study. The potential targets identified were then analyzed in WT and

TUT3 KO backgrounds, but expression was unchanged, suggesting that these were not direct targets of TUT3. It cannot be excluded, however, that TUT4 compensated for the loss of TUT3.
Consequently, *GPEET* mRNA was further investigated as a potential target of terminal uridylation. To that end, RNAs were extracted from WT PCFs cultured in the presence of low or high glucose concentrations. High levels of glucose in the culture medium are known to induce downregulation of GPEET expression in PCFs, which I suspected to depend on 3'-uridylation. Subsequently, mRNAs were then specifically amplified, circularized by ligation, and subjected to amplification by PCR with *GPEET*-specific primers. The sequences obtained were then cloned into a plasmid and sent for sequencing. In accordance with my expectations, the ratio of unspecific amplicons to *GPEET* amplicons was much higher after incubation with high levels of glucose, arguing for a reduced abundance of *GPEET* mRNAs. However, this approach could not help identify 3'-targeted uridylation of these mRNAs. Non-templated insertions or deletions of uridines were also not observed.
In addition, I tested whether the activity of TUT3 as part of EIF4E1/4EIP complexes was required for the suppressive effects observed upon tethering of 4EIP to the 3'-UTR of a reporter mRNA. Against my expectations, 4EIP could suppress expression of the reporter in the absence of TUT3, showing that TUT3 was not essential in this context. Again, it cannot be excluded that TUT4 compensated for the loss of TUT3, and additional experiments in cells lacking both isoforms could help clarify this. Furthermore, the kinetics of the degradation process has not been studied. It is possible that binding of 4EIP activates several degradation machineries and that degradation is only slowed down in the absence of TUT3.
In sum, EIF4E1 acts in concert with 4EIP to suppress translation in *T. brucei*, but the dependence on terminal uridylation for these suppressive functions needs to be explored in more detail. It does appear that EIF4E1 does not serve additional functions independent of 4EIP. In that regard, EIF4E1/4EIP complexes are reminiscent of 4EHP/GIGYF2 in mammals. It is being hypothesized that this cap-binding complex assists ribosome associated quality control by inhibiting translation of defective mRNAs. Moreover, the GIGYF2 component of the repressor complex was shown to have three independent domains displaying repressive activities. Some of the repressive functions of GIGYF2 are 4EHP-independent, but require the CCR4/NOT complex. Based on the observation that 4EIP features an intrinsic RNA-binding activity, similar mechanisms might underlie the differences observed in loss-of-function phenotypes of cells lacking EIF4E1 or 4EIP. Interestingly, 4EIP has been identified as a novel target for nucleoside analogues, the inhibitory effects of which were shown to act independently of EIF4E1 [126]. Additionally, associations between EIF4E1 and 4EIP2 might also account for these differences. At present, the expression patterns and roles of 4EIP2 have not been dissected in detail, and should thus be addressed in future studies.

4.2 EIF4E2 is a regulator of S-phase mRNAs

Like EIF4E1, EIF4E2 has not been found in association with an EIF4G homolog at the life cycle stages analyzed to this point. Instead, it is known to bind a histone mRNA stem-loop-binding protein, SLBP2 [103]. The interaction with SLBP2 was first identified upon pulldown of EIF4E2 in PCFs, and could be verified for the BSF as well in the course of this work. Of the two SLBP proteins in *T. brucei*, only SLBP2 contains a central region that is missing in other SLBP homologs, which mediates EIF4E2 binding. Previous studies reported differential expression of both EIF4E2 and SLBP2 during different growth phases [103]. Both are more abundant during the early log phase and expression is lower during late log and stationary phases. However, only SLBP2 displays a cell-cycle dependent expression pattern, while SLBP1 expression is independent of growth and cell cycle stages. Based on its association with SLBP2, it is assumed that EIF4E2 target selection likely occurs through the recognition of specific stem-loop structures [103].

In line with previous reports that knockdown of *EIF4E2* had no effect on the growth of PCFs, PCFs with a homozygous KO of *EIF4E2* grew with similar kinetics to WT cells. In contrast, BSFs lacking *EIF4E2* featured a major growth defect that was accompanied by the inability to grow to densities higher than 0.3×10^6 in normal HMI-9 medium. Despite this strong growth impairment, the cells could still undergo differentiation processes. The transition to the growth-arrested stumpy form was evidenced by PAD1 expression, which occurred already at much lower densities than in a WT or *EIF4E2* addback context. This differentiation competence did not result from a higher sensitivity to the stumpy induction factor, SIF, or faster generation of SIF in the surrounding medium, based on supernatant exchange experiments between the different cell types. Growth of *EIF4E2* KO cells was already impaired directly after fresh medium had been added.

Based on the phenotype displayed by *EIF4E2* KO cells, total transcriptomes of *EIF4E2* KO and addback cells were analyzed by RNA sequencing. It was revealed that loss of EIF4E2 expression resulted in downregulation of mRNAs that are known to be involved in replicative processes over the cell cycle. These included messages encoding PNT1, CPC2, and a mitochondrial DNA ligase homolog. These transcripts are stabilized during S-phase by PUF9 binding to the 5'-*UUGUACC*-3' sequence, which is present in their 3'-UTRs and serves as a cell-cycle regulatory element (CCRE). Therefore, encoded proteins are highest during S-phase. This is a common regulatory mechanism. Certain mRNAs are stabilized during specific phases of the cell cycle, but once complete, these mRNAs need to be removed for the next stage to be reached. While binding of most PUF proteins leads to destabilization of target mRNAs, PUF9 increases the stability of its targets. Accordingly, point mutations in the PUF9-specific CCRE reportedly resulted in transcript destabilization [75]. In line with these observations, EIF4E2 targets identified by pulldowns were destabilized in cells lacking EIF4E2, suggesting that EIF4E2 acts as a stabilizer for bound targets.

Previously, RNAi targeting *PUF9* has been shown to result in an accumulation of cells in G2/M-phase. However, KO of *EIF4E2* led only to a very slight increase in cells in G2/M-phase, with a non-significant reduction in the proportion of 1N1K *EIF4E2* KO cells. There were also less 1N1K cells upon knockdown of *PUF9* [75]. Furthermore, organelle copy number defects were observed in cells with *PUF9* RNAi, which has not been examined in *EIF4E2* KO cells to this point. To test this, electron microscopy could help identify similar phenotypes in *EIF4E2* KO cells. Interestingly, the phenotype described after depletion of *PUF9* was specific for BSFs, while similar experiments in PCFs had no detectable effects. In line with this, loss of EIF4E2 expression was shown to elicit a strong growth defect in BSFs, while PCFs grew normally.

Yeast-2-hybrid experiments should help clarify whether SLBP2 or EIF4E2 and PUF9 interacted directly. Expectedly, interactions between EIF4E2 and SLBP2 were detected. Both SLBP2 and PUF9

appeared to feature self-interactions, as combinations of SLBP2-AD/SLBP2-BD and PUF9-AD/PUF9-BD supported growth. Moreover, there was evidence that PUF9 interacted with both SLBP2 and EIF4E2. Previously, studies by Freire et al. identified SLBP2 as a potential auto-activator. However, it was not stated whether this was the case for SLBP2-AD or SLBP2-BD protein [103]. In contrast, similar analyses presented in this work could not confirm this. Truncated versions of the different proteins could help identify the domains involved in establishing direct interactions between these proteins.

In the course of the studies by Freire and colleagues, it was further revealed that expression of SLBP2 and EIF4E2 was highest during early log phase and coincided with exponential growth in PCFs [103]. Additionally, it was shown that mRNAs encoding EIF4E2 and SLBP2 were highest during the G1-phase of the cell cycle and rapidly disappeared during S-phase. Consequently, it is assumed that the proteins encoded by these mRNAs are highest during S-phase. This is in good agreement with the observation that EIF4E2/SLBP2 complexes serve as regulators of S-phase transcripts in BSFs.

Apart from that, KO of *EIF4E2* did not affect expression of the main VSG variant expressed by the BSFs, but led to a significant increase in the expression of various *VSG* genes, which are otherwise silenced in WT cells. The fact that mRNAs encoding proteins involved in regulating chromatin packaging and dynamics were bound by EIF4E2 pointed towards an indirect mechanism by which silenced *VSG* genes were rendered more accessible for RNA pol I in the absence of EIF4E2. Furthermore, other expression site-associated genes were upregulated in these cells. Since mixed VSG coats are not assumed to result in growth defects, this unlikely contributed to the observed phenotype.

In contrast to the results obtained in *T. brucei*, hemizygous deletion of *EIF4E2* in *Leishmania mexicana* using CRISPR/Cas9 technology did not affect translation or growth of the parasites. However, reduced EIF4E2 levels resulted in morphological changes and impaired the ability to infect cultured macrophages. Proteome profiles revealed that cytoskeletal and flagellar rod proteins, as well as proteins required for virulence were down-regulated. It was thus hypothesized that EIF4E2 might serve to activate translation of a particular set of transcripts. Nevertheless, the effects on the transcriptomes might have been secondary, as specific binding to the transcripts was not studied in that context. Presence of *Leishmania* EIF4E2 in polysomes further argues in favor of a translation-promoting role [132]. This should also be tested for *T. brucei* in future studies to determine whether EIF4E2 only stabilizes bound transcripts until other, translation-promoting cap-binding proteins take over, or whether it can serve to initiate translation at bound targets. In some metazoans, SLBP2 is expressed exclusively at the oocyte stage, where it represses translation of bound histone mRNAs. This is achieved by preventing SLBP1, a translational activator, from binding [105, 133].

Further studies are needed to determine as to why EIF4E2 has an essential role in BSFs, but not in PCFs, despite similar interaction partners. Furthermore, how the effects on the transcriptomes are reflected at the protein level could be analyzed by quantitative mass spectrometry. This could also help gather information on whether EIF4E2 indeed acts as a translational activator.

To address whether EIF4E2 merely acts as a stabilizer of bound transcripts or actually mediates translation of bound mRNAs, polysomes could be analyzed for the presence of EIF4E2 protein. Moreover, *in vitro* translation studies on EIF4E2 and selected target mRNAs may help clarify this in the future. Additionally, the potential connection between EIF4E2- and PUF9-mediated functions could be addressed by introducing mutations in the CCRE that is bound by PUF9 to subsequently test associations of EIF4E2 with the target mRNAs. This could help determine whether PUF9 binds first and then recruits the EIF4E2 cap-binding protein to either stabilize the transcripts or induce EIF4E2-dependent translation.

4.3 EIF4E5 is required for survival of PCFs, but dispensable in BSFs

EIF4E5 is a small, cytosolic cap-binding protein that is known to form two types of EIF4F-like complexes by association with either EIF4G1 or EIF4G2. In PCFs, the composition of the two types of complexes was further dissected and it was revealed that EIF4E5/EIF4G1 complexes bind to one of the two 14-3-3 isoforms, one protein with two RNA-binding domains, and another with both guanylyltransferase and methyltransferase motifs (*Tb*927.11.6720), suggesting that it may be involved in the modification of the caps of target mRNAs. In contrast, complexes of EIF4E5/EIF4G2 were characterized by the presence of both 14-3-3 isoforms [98]. In accordance with the data obtained in PCFs, EIF4E5 from BSFs pulled down EIF4G1, EIF4G2, the two 14-3-3 protein isoforms, as well as *Tb*927.11.6720, along with *Tb*927.8.4560, another protein enriched with EIF4E5 in PCFs. However, with the approach used in this work, it was not possible to distinguish between the composition of EIF4E5/EIF4G1 and EIF4E5/EIF4G2 complexes, but rather gave an overall impression of EIF4E5 complexes.

Despite the similarities in binding partners of EIF4E5 in PCFs and BSFs, the KO phenotypes were significantly different. Lack of EIF4E5 in BSFs neither had drastic effects on cell viability, nor did it impair the differentiation process to the PCF through the stumpy stage, as evidenced by expression of PAD1 and, later, EP1 proteins. However, PCFs lacking both *EIF4E5* alleles were not viable. Subsequent to the differentiation process, the cells did not resume growth as established procyclic cells, but lingered for a few more days and eventually died. Furthermore, PCFs were resistant to direct *EIF4E5* knockout, supporting the hypothesis that EIF4E5 is essential in the PCF.

Interestingly, knockdown of *EIF4E5* did not result in a pronounced growth defect in PCFs, leading to the assumption that residual levels of EIF4E5 were sufficient for promoting normal cell growth. More strikingly, however, was the effect that loss of *EIF4E5* expression had in previous studies. It resulted in a loss of social motility and productive cell movement, along with a so-called “settling” phenotype. Unfortunately, BSFs do not display social motility, which could therefore not be addressed in *EIF4E5* KO cells. Furthermore, BSFs lacking EIF4E5 did not display a settling phenotype or impairments of cellular movement. Together, the results obtained in this study indicate that EIF4E5 is dispensable in the BSF, but essential for survival of PCFs. As the binding partners are largely overlapping between the two life cycle stages studied, target selection may be achieved through mutual exclusion between EIF4E5 and another cap-binding protein with higher levels in the BSF.

Based on the observation that two EIF4E5 binding partners, as well as EIF4E5 itself, have translation-promoting abilities in the tethering assay it is assumed that EIF4E5 exerts its roles by promoting rather than inhibiting translation of bound targets [109]. Examining the presence of EIF4E5 in polysomes from BSFs and PCF may help clarify its role in translation.

4.4 EIF4E6 cooperates with MKT1 complexes to activate translation of target mRNAs

Depending on the binding partners, cap-binding proteins may act as translational activators or repressor. Previously, EIF4E6 was shown to form EIF4F-like complexes with EIF4G5. The latter was described to act as a translational activator upon artificial tethering to the 3' UTR of a reporter RNA, supporting a translation-promoting function of EIF4E6/EIF4G5 complexes [109].

According to previous studies on PCFs, knockdown of *EIF4E6* resulted only in minor growth impairment [99]. To study the effects on translation, S^{35}-methionine labeling was employed, which revealed no significant reduction in incorporation, suggesting that general translation was not affected [99]. It was thus concluded that EIF4E6 serves rather specific functions. In this context, it should be noted that residual expression in PCFs after RNAi was shown to be 12% of that in WT cells, thus not authentically reflecting cells lacking EIF4E6. Moreover, despite almost normal growth, morphological examination identified an increased frequency of abnormal flagellar phenotypes, such as flagellar detachment, which was particularly pronounced after centrifugation, affecting up to 30% of induced cells. In accordance with the results obtained in *EIF4E5*-depleted cells, knockdown of *EIF4E6* could abolish social motility behavior. In contrast to the results obtained using EIF4E5-depleted cells, loss of EIF4E6 did not result in a "settling" phenotype [98, 99].

To follow up on this, I attempted homozygous knockout of *EIF4E6* in both BSFs and PCFs; it proved impossible in both cases. This suggested that EIF4E6 serves important functions during both life cycle stages analyzed. These functions were probably not revealed in previous work in PCFs because of residual expression. An indication that global translation was indeed affected was provided by puromycin incorporation assays, as well as by preliminary data from polysome profiling experiments using BSFs. More specifically, polysomes were strongly reduced after 24 h of *EIF4E6* RNAi induction. However, whether this was a consequence of a global translation defect remains to be determined. It has further been shown that RNAi of *EIF4E6* resulted in cell death after 2-3 days, thus the global impairment might have resulted from the cells being stressed or undergoing apoptosis. To further investigate this, the RNAs present in polysomal and monosomal fractions, as well as free RNAs are to be compared by RNA sequencing between *EIF4E6* RNAi cells grown with or without the inducer. Alternatively, northern blotting could be performed to specifically look for (presumed) targets of EIF4E6, such as *VSG* mRNA, in polysomal and monosomal fractions of cells with normal and strongly reduced expression levels of EIF4E6.

To perform similar experiments in PCFs, BSFs with *EIF4E6* RNAi were differentiated using *cis*-aconitate. Curiously, knockdown efficiency in PCFs was very poor, which were thus not further examined.

In PCFs, EIF4E6 has been described to associate with EIF4G5, G5-IP, EF1b, as well as the RNA-binding protein ALBA3. To test whether these binding partners could also be found in association with EIF4E6/EIF4E5 in BSFs, PTP-tagged EIF4E6 was pulled down from differentiation-competent BFSs and bound proteins were analyzed by mass spectrometry. In doing so, EIF4G5 and G5-IP were detected, which was in good agreement with previous reports. However, neither ALBA3 nor EF1b co-purified with EIF4E6. Interestingly, components of activating MKT1 complexes were present, including PBP1, MKT1, and PABPs. In line with the assumption that MKT1L protein regulates MKT1 complexes, but is not actively promoting translation of bound messages, it was not significantly enriched in pulldowns of EIF4E6. Accordingly, co-immunoprecipitaions confirmed this association with MKT1, but not MKT1L protein. Additionally, CFB2, an RNA-binding F-box protein known to direct MKT1 complexes to target mRNAs, co-purified with EIF4E6. Therefore, I suggest that CFB2 is involved in targeting EIF4E6 to selected targets to be translated.

A previous study aimed at identifying proteins bound to *VSG* mRNAs. An association between *VSG* mRNA and EIF4G5 protein was revealed, establishing a link to EIF4E6/EIF4G5 complexes [124]. In addition, other components of MKT1 complexes, such as CFB2, PBP1, and MKT1, as well as PABP2 were identified as part of the *VSG* mRNA-bound proteome, providing further evidence for EIF4E6-dependent translation of *VSG* mRNAs. Anti-CFB2 serum was obtained to provide an additional tool for studying these complexes and bound target mRNAs. However, despite an additional purification step, which eventually allowed for specific detection of CFB2 protein [124], the serum could not be used to successfully co-purify EIF4E6 with CFBs from lysates of BSFs. Nevertheless, the CFB2 antiserum did prove useful in those studies in order to examine protein expression levels [124].

To test the hypothesis of EIF4E6 mediating *VSG* mRNA translation by a direct approach, EIF4E6 was pulled down from BSFs, where *VSG* mRNAs are highly expressed, and bound mRNAs were analyzed by PCR, qPCR, and RNA sequencing. In line with previous results, EIF4E6 could be employed to purify *VSG* mRNA from BSFs. However, obtained data also pointed towards an association between EIF4E3 and *VSG* mRNAs, but to a lesser extent. Furthermore, EIF4G4, which associates with EIF4E3, was bound to *VSG* mRNA [124]. This was not surprising, as VSG protein, which covers the surface of the BSF, is highly expressed, comprising nearly 10% of total cellular protein. As a general translation factor mediating translation of numerous mRNAs, EIF4E3 alone might not be sufficient to meet the cell's high demand. Therefore, another cap-binding protein, EIF4E6, appears to be specialized in this task. In line with this, loss of EIF4E6 is lethal in BSFs, which is also true for loss of VSG expression.

It has been shown previously that a block in VSG synthesis results in cell division cycle arrest at the onset of cytokinesis, when the demand for new VSG-containing membranes is highest [134, 135]. Mechanisms ensuring the production of sufficient amounts of VSG proteins have been proposed. In the light of previous findings that CFB2 protein associates with a conserved 16-mer sequence in the 3'-UTR of the *VSG* mRNA, it is possible that CFB2 is involved in the regulation of *VSG* mRNA and protein levels by stabilizing the transcripts and promoting their translation by recruitment of EIF4E6- and EIF4E3-containing initiation complexes. Accordingly, expression of another VSG variant from a transgene reduces endogenous *VSG* mRNA levels. This suggests that the different VSG variants might compete for CFB2 binding. Levels of CFB2 comprise less than 1000 molecules per cell [124]. This is further supported by the observation that *VSG* mRNAs constitute 4-11% of the 20,000 mRNA molecules per trypanosome, resulting in roughly equimolar levels of CFB2 protein and *VSG* mRNA [54]. Correspondingly, ectopically expressed *VSG2* mRNAs with premature termination codons resulted in reduced levels of membrane-anchored VSG protein. This in turn elicited a feedback response to up-regulate the mRNA levels of the endogenous VSG variant [136].

Interestingly, the identity of the expressed VSG can affect cellular growth rates, while some VSG variants can effectively constrain proliferation [137]. Whether this is linked to differences in CFB2 binding, for example through point mutations in the conserved 16-mer sequence or at additional contact sites between CFB2 protein and *VSG* mRNAs, could be worth investigating in future studies.

In PCFs, where EIF4E6 is also essential, EIF4E6 may accommodate different functions that render it indispensable at this life cycle stage, which remain to be determined.

5. Conclusions

T. brucei possesses a surprisingly large repertoire of cap-binding proteins comprising six EIF4Es and five EIF4Gs. The aim of this work was to dissect the individual roles of these proteins to determine whether they were redundant or varying in their functions. It was suspected that the reality lies somewhere in between these extremes. Indeed, evidence supporting both scenarios could be provided in this work. On the one hand, EIF4E3 and EIF4E6 are assumed to have overlapping functions in promoting translation of *VSG* mRNAs to deal with the high demand for VSG protein copy numbers. On the other hand, EIF4E2 appears to be highly specialized in mediating the translation of S-phase mRNAs, while EIF4E1 is suspected to act solely as a translational repressor without translation-promoting functions, at least during the life cycle stages analyzed.

6. Supplementary material

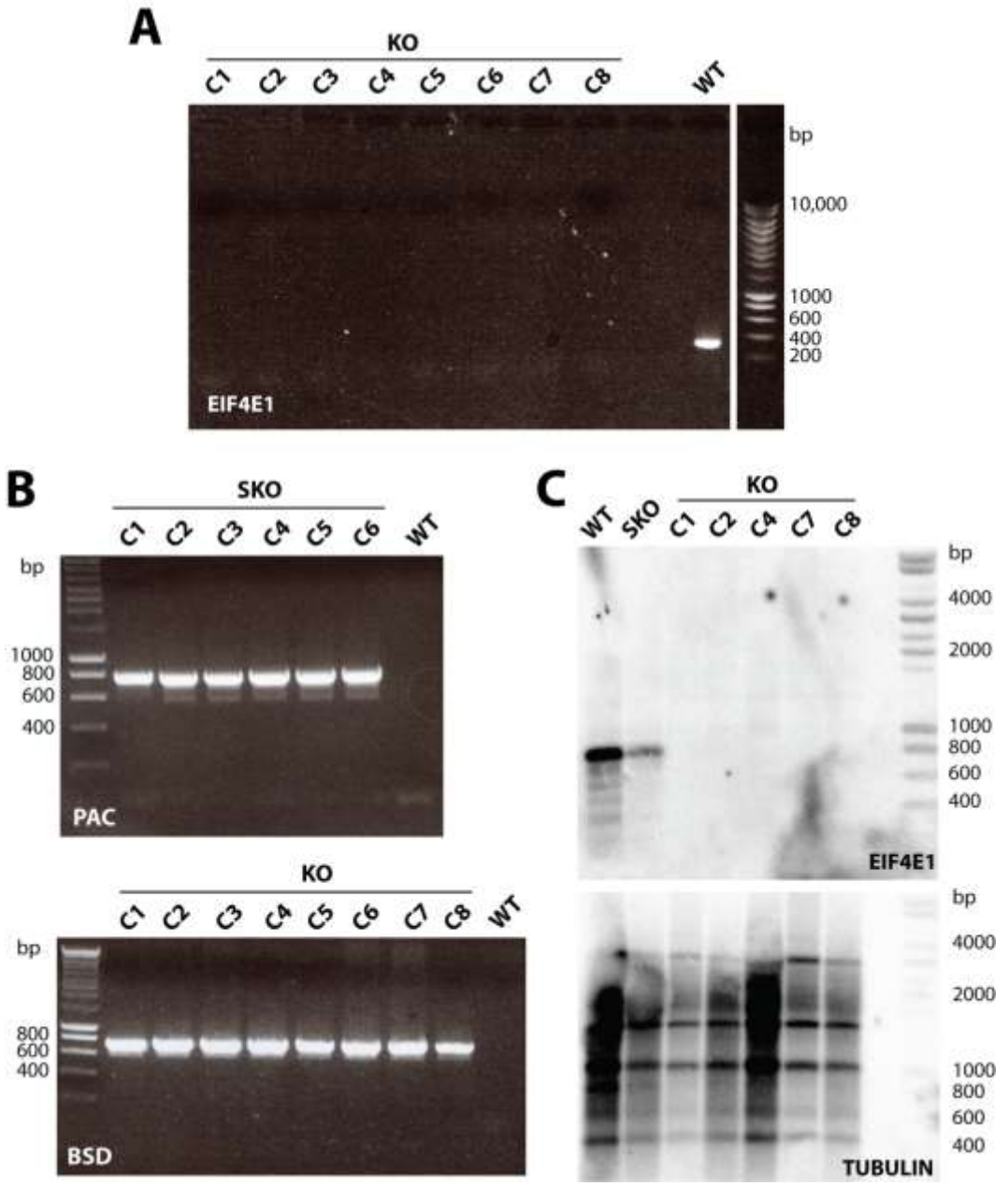

Supplementary Figure S1 Homozygous deletion of *EIF4E1* in bloodstream forms (BSFs) of *Trypanosoma brucei.* (A) PCR for detection of the *EIF4E1* open reading frame (ORF) in DNA samples from eight individual *EIF4E1* knockout (KO) clones (C1-8), with DNA isolated from wildtype (WT) BSFs serving as a positive control. **(B)** PCR for detection of puromycin N-acetyl-transferase (*PAC*) and blasticidin S deaminase (*BSD*) gene integration into *EIF4E1* loci. In each case, one of the primers was binding in the *EIF4E1* UTR, while the other one was complementary to a region inside the ORF of the resistance gene. DNA isolated from WT BSFs served as a positive control. **(C)** EIF4E1 transcript levels were examined in cells with a single or homozygous KO of *EIF4E1* (SKO and KO clones C1, C2, C4, C7, and C8, respectively) by Southern blotting with probes complementary to the *EIF4E1* ORF. A probe recognizing the *tubulin* ORF was used as a loading control. The data presented have been published with modifications in Terrao et al., 2018 [100]

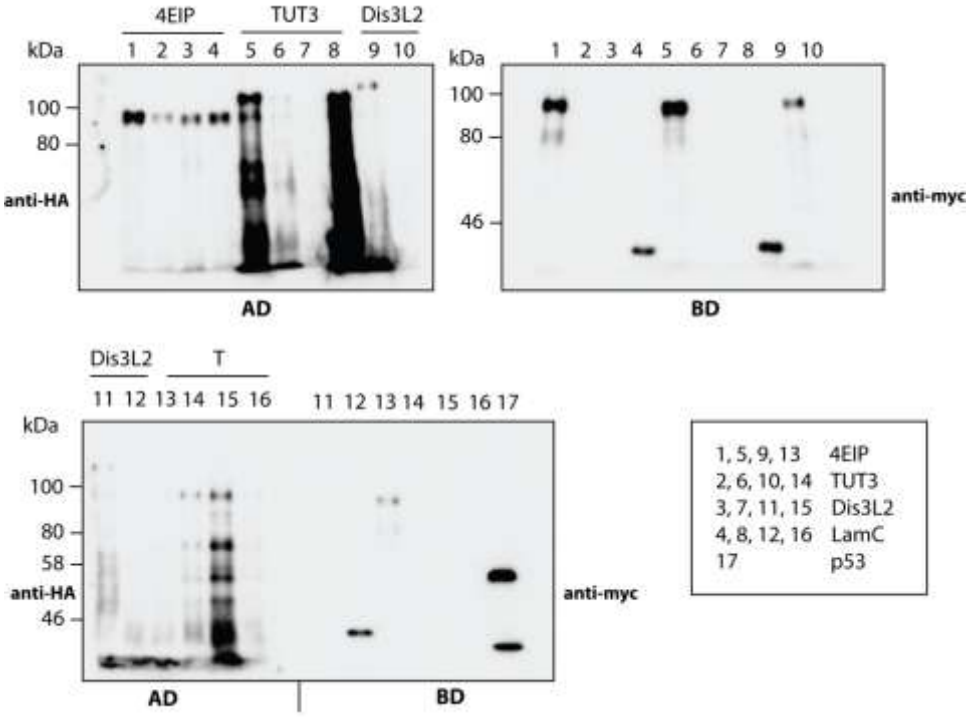

Supplementary Figure S2 Expression analysis of trypanosomal proteins in *S. cerevisiae.* Detection of AD- and BD-domain containing proteins expressed in *S. cerevisiae* via HA- and myc-tags using western blotting. The data presented have been published with modifications in Falk et al., 2021 [122]

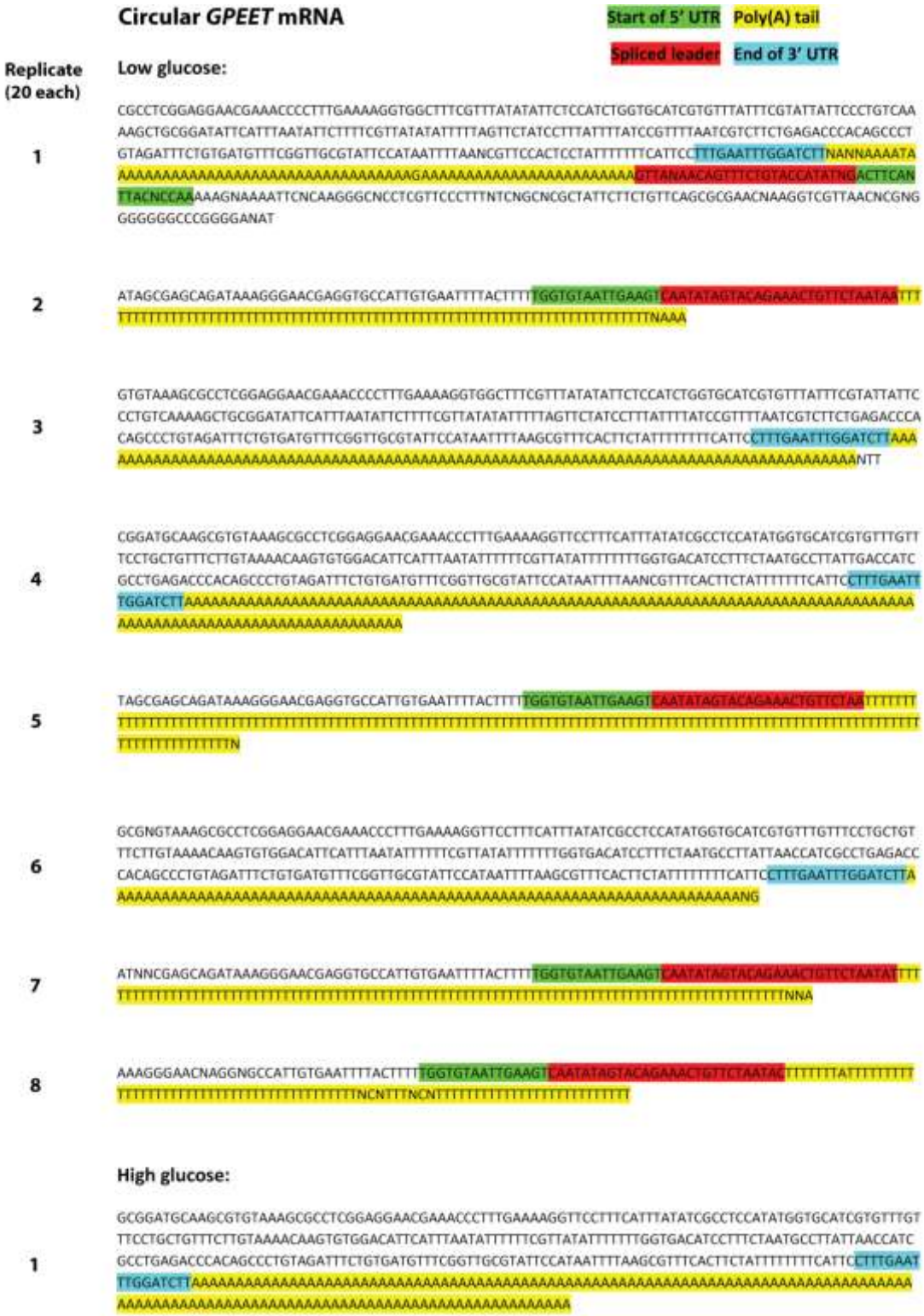

Supplementary Figure S3 Analysis of circular RNA sequences reveals *GPEET* mRNAs without terminally uridylated 3'-ends. Total RNA was extracted from cells cultured in an environment high or low in glucose. After removal of the cap, the RNAs were circularized by ligation of 5' (green) and 3' (blue) ends using T4 RNA ligase, and *GPEET* mRNA sequences were amplified to study poly(A) tails (yellow) and (potential) uridylation signals. After cloning into the p2T7 vector, 20 clones were randomly collected for both conditions and sent for sequencing. Sequences corresponding to *GPEET* transcripts are shown, while nonspecifically amplified sequences were excluded. The data presented have been published with modifications in Falk et al., 2021 [122]

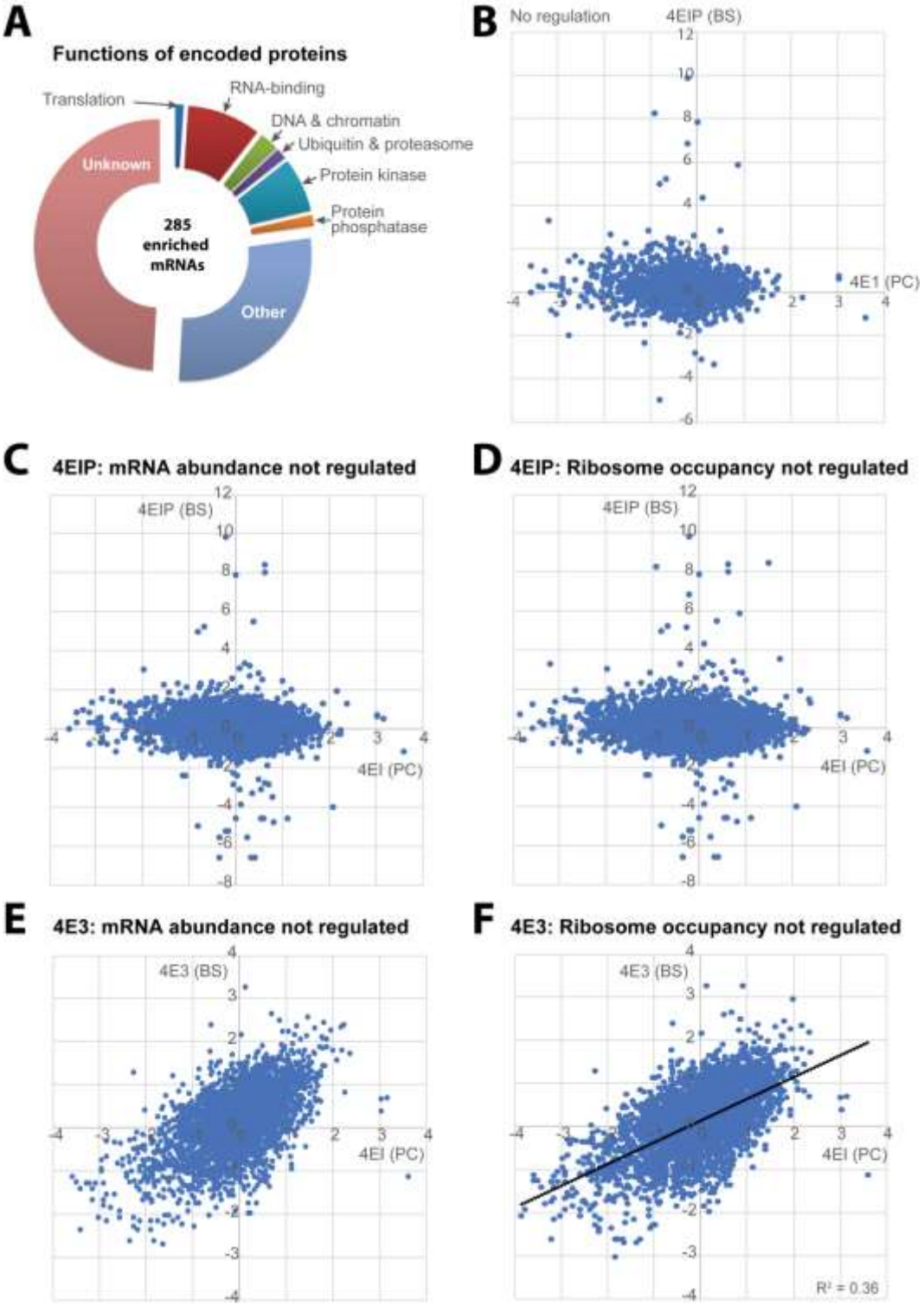

Supplementary Figure S4 Correlations between EIF4E1-/4EIP-/EIF4E3-bound mRNAs. (A) Functions of the proteins encoded by the 285 most strongly enriched mRNAs in EIF4E1 pulldowns from procyclic forms (PCFs). Data from a single experiment are shown. **(B)** Comparisons of the mRNAs bound to EIF4E1 in PCFs with those associating with 4EIP in bloodstream forms (BSFs), which were restricted to mRNAs showing less than 1.5-fold differences between BSFs and PCFs in both mRNA abundance and ribosome occupancy. Data from one experiment (EIF4E1) and three independent experiments (4EIP) are shown. **(C)** As **(B)**, but restricted to mRNAs that show less than 1.5-fold differences in mRNA abundance between BSFs and PCFs. Data from one experiment (EIF4E1) and three independent experiments (4EIP) are shown. **(D)** As **(B)**, but restricted to mRNAs that show less than 1.5-fold differences in ribosome occupancy between BSFs and PCFs. Data from one experiment (EIF4E1) and three independent experiments (4EIP) are shown. **(E)** Comparisons of the

mRNAs bound to EIF4E1 in PCFs with those associating with EIF4E3 in BSFs, which were restricted to mRNAs showing less than 1.5-fold differences between BSFs and PCFs in mRNA abundance. Data from one experiment (EIF4E1) and three independent experiments (EIF4E3) are shown. **(F)** Comparisons of the mRNAs bound to EIF4E1 in PCFs with those associating with EIF4E3 in BSFs, which were restricted to mRNAs showing less than 1.5-fold differences between BSFs and PCFs in ribosome occupancy. Data from one experiment (EIF4E1) and three independent experiments (EIF4E3) are shown. Data were analyzed by Franziska Falk and the plots in **(B)-(F)** were generated by Christine Clayton based on the data provided.

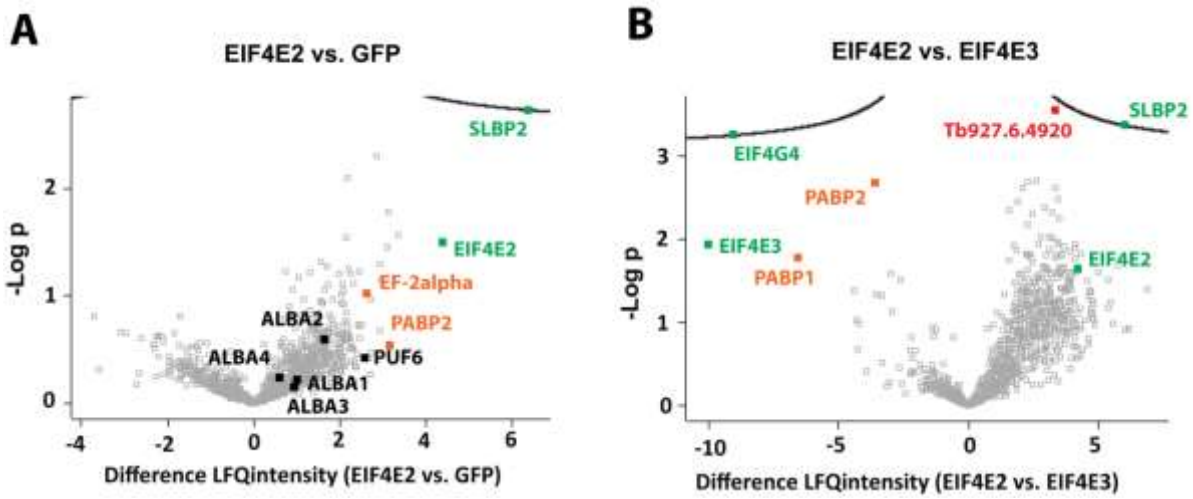

Supplementary Figure S5 EIF4E2-bound proteome in bloodstream forms (BSFs). (A) PTP-tagged EIF4E2 and GFP proteins were expressed in and pulled down from BSFs, and bound proteins were analyzed by quantitative mass spectrometry. Raw data were analyzed by Sabine Merker from the mass spectrometry core facility using MaxQuant, and interaction partners were subsequently analyzed in Perseus. In the volcano plot, differences in label-free quantification (LFQ) intensities were plotted against the log10 of the false discovery rate (FDR) calculated by a permutation-based FDR adapted t-test. Data from two (EIF4E2) and three (GFP) independent experiments are shown. Each square represents one protein and some proteins of interest are highlighted in color. **(B)** PTP-tagged EIF4E2 and EIF4E3 proteins were expressed in and pulled down from BSFs, and bound proteins were analyzed by quantitative mass spectrometry. Raw data were analyzed by Sabine Merker from the mass spectrometry core facility using MaxQuant, and interaction partners were subsequently analyzed in Perseus. In the volcano plot, differences in label-free quantification (LFQ) intensities were plotted against the log10 of the false discovery rate (FDR) calculated by a permutation-based FDR adapted t-test. Data from two (EIF4E2) and three (EIF4E3) independent experiments are shown. Each square represents one protein and some proteins of interest are highlighted in color.

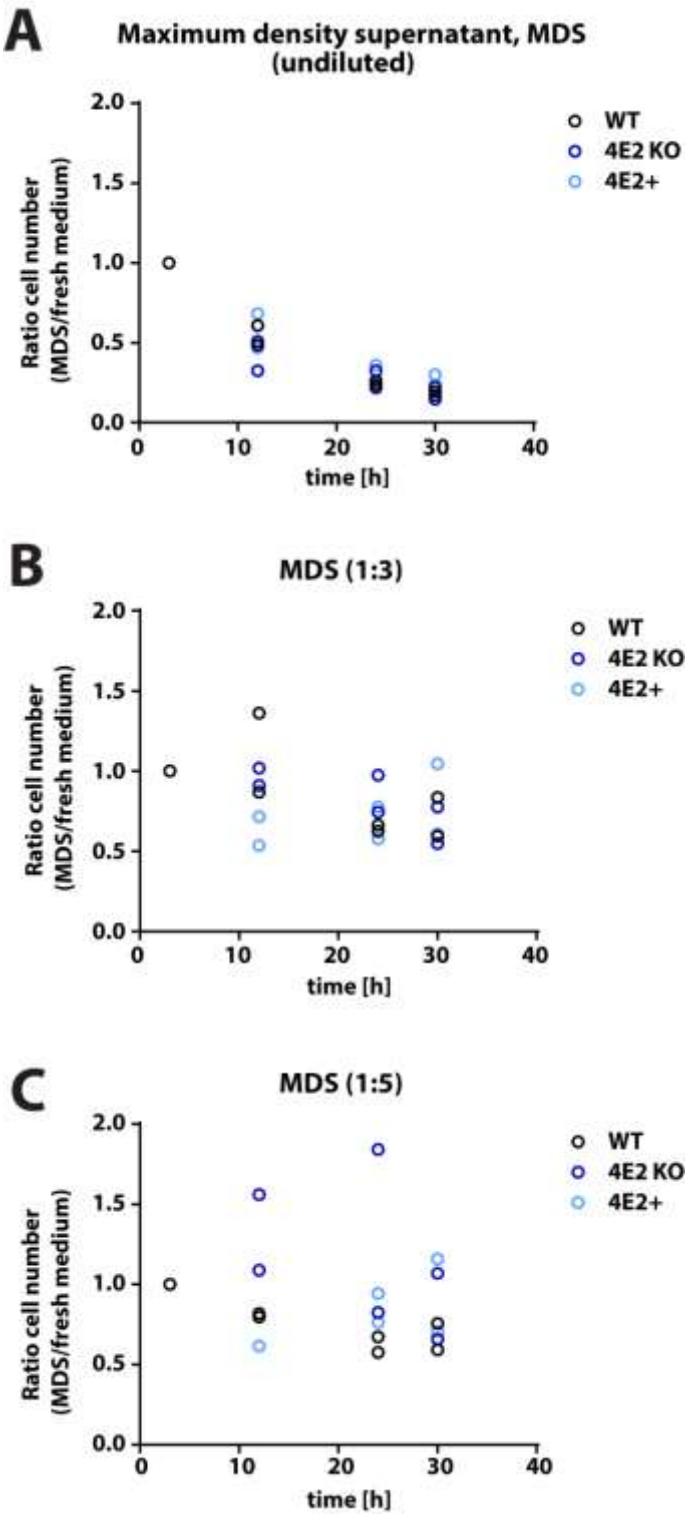

Supplementary Figure S6 Ratios of cells grown in maximum density supernatant versus fresh medium. (A) Wild type (WT) bloodstream forms (BSFs), BSFs with a homozygous knockout (KO) of *EIF4E2*, and *EIF4E2* KO BSFs with reconstituted expression of EIF4E2 (4E2+) at a starting density of 1×10^5 cells/mL were grown in either fresh HMI-9 medium or medium collected from WT cells at maximal density (MDS). Growth was monitored at 4, 12, 24, and 30 h. Ratios of cell numbers from two independent experiments are shown. **(B)** As in **(A)**, but cells were grown in either fresh HMI-9 medium or 1:3-diluted MDS. **(C)** As in **(A)**, but cells were grown in either fresh HMI-9 medium or 1:5-diluted MDS.

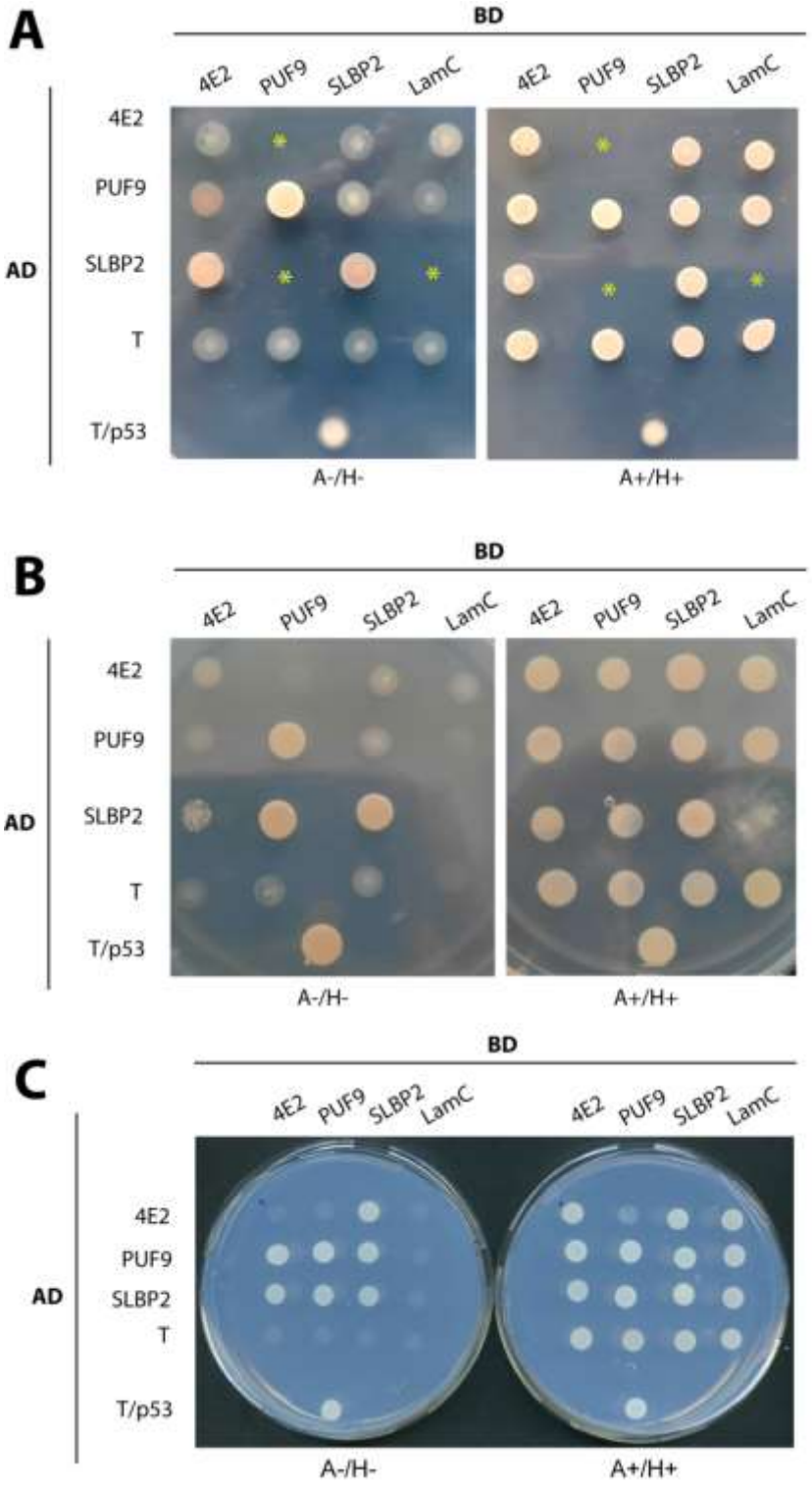

Supplementary Figure S7 Yeast-2-hybrid analysis of interactions between EIF4E2, SLBP2, and PUF9. (A) Direct interactions between EIF4E2, PUF9, and SLBP2, as well as LamC and large T antigen controls were tested by yeast-2-hybrid analysis. Co-expression of large T antigen (T)-AD and lamin C (LamC)-BD served as a negative control, while simultaneous expression of T-AD and p53-BD were used as positive control. Viability of the yeast cells was tested on media supplemented with adenine and histidine (A+/H+), while selection for positive interactions was performed on media lacking adenine and histidine (A-/H-). *, combinations that did not yield any transformants. **(B)** Repetition of the experiment described in **(A)**. **(C)** Repetition of the experiment described in **(A).** The third replicate, which is shown in **(C)**, was conducted by Rafael Melo Pelhares.

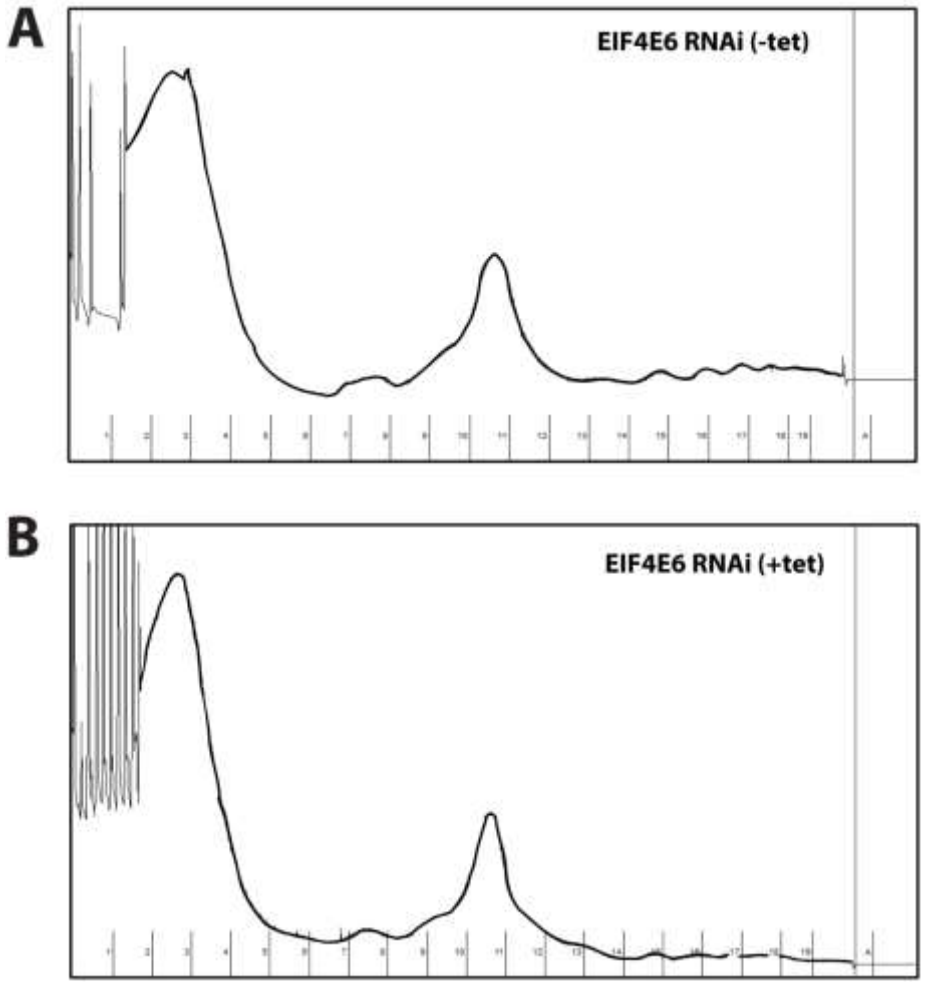

Supplementary Figure S8 Knockdown of *EIF4E6* in bloodstream forms (BSFs) leads to fewer mRNAs in polysomes. (A) Extracts from BSFs with tetracyclin (tet-)inducible *EIF4E6* RNAi grown in the absence of tet were separated using sucrose gradients. RNA in polysomal gradients was analyzed by UV light absorption. Data from one experiment are shown. The experiment was conducted by Rafael Melo Pelhares. **(B)** Extracts from BSFs with tetracyclin (tet-)inducible *EIF4E6* RNAi grown with tet for 24 h were separated using sucrose gradients and RNA in polysomal gradients was analyzed by UV light absorption. The method was established by Franziska Falk and Rafael Melo Pelhares. The experiment shown was conducted by Rafael Melo Pelhares.

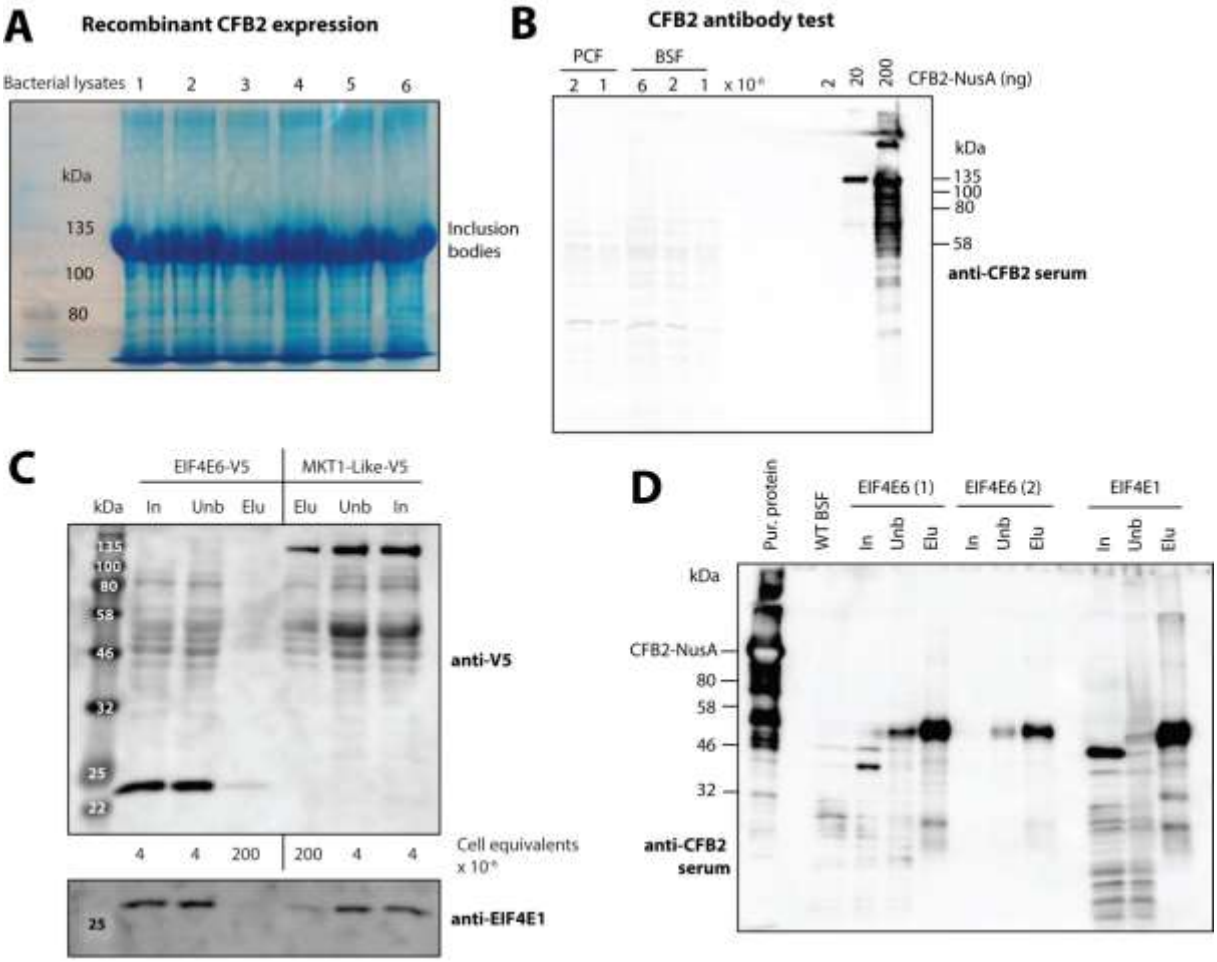

Supplementary Figure S9 Production of anti-CFB2 antiserum. (A) CFB2 was recombinantly expressed in BL21 *E. coli* cells. Proteins present in inclusion bodies were then separated by sodium dodecyl sulfate polyacrylamide gel electrophoresis and stained with Coomassie blue. **(B)** Polyclonal anti-CFB2 antiserum produced in rabbit was tested by western blotting with lysates from bloodstream and procyclic forms (BSFs and PCFs, respectively), while the recombinant protein served as a control. **(C)** Anti-CFB2 antibody coupled to magnetic beads was used to purify CFB2 from 1×10^8 BSFs expressing V5-tagged EIF4E6 or MKT1-Like protein. Input (In), unbound (Unb) and elution (Elu) fractions were analyzed by western blotting using anti-V5 antibody. The amount of EIF4E1 in each fraction was used as a loading control. **(D)** PTP-tagged EIF4E6 or EIF4E1 (control) was pulled down from 1×10^8 BSFs. Presence of CFB2 protein in input (In), unbound (Unb), and elution (Elu) fractions, as well as in wildtype (WT) BSFs and bacterial inclusion bodies was analyzed using anti-CFB2 antiserum.

7. Web resources

ArrayExpress: https://www.ebi.ac.uk/arrayexpress/

TriTrypDB: http://tritrypdb.org

GeneDB: http://www.genedb.org

BLAST NCBI: http://blast.ncbi.nlm.nih.gov/Blast.cgi

TrypTag: http://tryptag.org/?pageType=landing

YourGenome: https://www.yourgenome.org/facts/what-is-african-sleeping-sickness

8. References

1. Shapiro, T.A. and P.T. Englund, *The structure and replication of kinetoplast DNA.* Annu Rev Microbiol, 1995. **49**: p. 117-43.
2. Holmes, P., *Tsetse-transmitted trypanosomes--their biology, disease impact and control.* J Invertebr Pathol, 2013. **112 Suppl**: p. S11-4.
3. Pipkin, A.C., Sr., *Transmission of Trypanosoma cruzi by arthropod vectors: anterior versus posterior route infection.* Int Rev Trop Med, 1969. **3**: p. 1-47.
4. Franco, J.R., et al., *Monitoring the elimination of human African trypanosomiasis: Update to 2016.* PLoS Negl Trop Dis, 2018. **12**(12): p. e0006890.
5. Fevre, E.M., et al., *The burden of human African trypanosomiasis.* PLoS Negl Trop Dis, 2008. **2**(12): p. e333.
6. Kennedy, P.G., *Clinical features, diagnosis, and treatment of human African trypanosomiasis (sleeping sickness).* Lancet Neurol, 2013. **12**(2): p. 186-94.
7. Welburn, S.C., I. Maudlin, and P.P. Simarro, *Controlling sleeping sickness - a review.* Parasitology, 2009. **136**(14): p. 1943-9.
8. Welburn, S.C., et al., *Crisis, what crisis? Control of Rhodesian sleeping sickness.* Trends Parasitol, 2006. **22**(3): p. 123-8.
9. Connor, R.J., *The impact of nagana.* Onderstepoort J Vet Res, 1994. **61**(4): p. 379-83.
10. Lidani, K.C.F., et al., *Chagas Disease: From Discovery to a Worldwide Health Problem.* Front Public Health, 2019. **7**: p. 166.
11. Torres-Guerrero, E., et al., *Leishmaniasis: a review.* F1000Res, 2017. **6**: p. 750.
12. Heddergott, N., et al., *Trypanosome motion represents an adaptation to the crowded environment of the vertebrate bloodstream.* PLoS Pathog, 2012. **8**(11): p. e1003023.
13. Overath, P. and M. Engstler, *Endocytosis, membrane recycling and sorting of GPI-anchored proteins: Trypanosoma brucei as a model system.* Mol Microbiol, 2004. **53**(3): p. 735-44.
14. Field, M.C. and M. Carrington, *The trypanosome flagellar pocket.* Nat Rev Microbiol, 2009. **7**(11): p. 775-86.
15. Michels, P.A., et al., *Metabolic functions of glycosomes in trypanosomatids.* Biochim Biophys Acta, 2006. **1763**(12): p. 1463-77.

16. Opperdoes, F.R. and P. Borst, *Localization of nine glycolytic enzymes in a microbody-like organelle in Trypanosoma brucei: the glycosome.* FEBS Lett, 1977. **80**(2): p. 360-4.

17. Bringaud, F., L. Riviere, and V. Coustou, *Energy metabolism of trypanosomatids: adaptation to available carbon sources.* Mol Biochem Parasitol, 2006. **149**(1): p. 1-9.

18. Grunfelder, C.G., et al., *Endocytosis of a glycosylphosphatidylinositol-anchored protein via clathrin-coated vesicles, sorting by default in endosomes, and exocytosis via RAB11-positive carriers.* Mol Biol Cell, 2003. **14**(5): p. 2029-40.

19. Ziegelbauer, K. and P. Overath, *Surface antigen change during differentiation of Trypanosoma brucei.* Biochem Soc Trans, 1990. **18**(5): p. 731-3.

20. Matthews, K.R., *The developmental cell biology of Trypanosoma brucei.* J Cell Sci, 2005. **118**(Pt 2): p. 283-90.

21. McWilliam, K.R., et al., *Developmental competence and antigen switch frequency can be uncoupled in Trypanosoma brucei.* Proc Natl Acad Sci U S A, 2019. **116**(45): p. 22774-22782.

22. Hovel-Miner, G., et al., *A Host-Pathogen Interaction Reduced to First Principles: Antigenic Variation in T. brucei.* Results Probl Cell Differ, 2015. **57**: p. 23-46.

23. Horn, D., *Antigenic variation in African trypanosomes.* Mol Biochem Parasitol, 2014. **195**(2): p. 123-9.

24. Reuner, B., et al., *Cell density triggers slender to stumpy differentiation of Trypanosoma brucei bloodstream forms in culture.* Mol Biochem Parasitol, 1997. **90**(1): p. 269-80.

25. Matthews, K.R., *Trypanosome Signaling-Quorum Sensing.* Annu Rev Microbiol, 2021. **75**: p. 495-514.

26. Rojas, F., et al., *Oligopeptide Signaling through TbGPR89 Drives Trypanosome Quorum Sensing.* Cell, 2019. **176**(1-2): p. 306-317 e16.

27. Rojas, F. and K.R. Matthews, *Quorum sensing in African trypanosomes.* Curr Opin Microbiol, 2019. **52**: p. 124-129.

28. MacGregor, P. and K.R. Matthews, *Identification of the regulatory elements controlling the transmission stage-specific gene expression of PAD1 in Trypanosoma brucei.* Nucleic Acids Res, 2012. **40**(16): p. 7705-17.

29. Dean, S., et al., *A surface transporter family conveys the trypanosome differentiation signal.* Nature, 2009. **459**(7244): p. 213-7.

30. Vanhollebeke, B., et al., *Cellular and molecular remodeling of the endocytic pathway during differentiation of Trypanosoma brucei bloodstream forms.* Eukaryot Cell, 2010. **9**(8): p. 1272-82.

31. Nolan, D.P., et al., *Slender and stumpy bloodstream forms of Trypanosoma brucei display a differential response to extracellular acidic and proteolytic stress.* Eur J Biochem, 2000. **267**(1): p. 18-27.

32. Rico, E., et al., *Bloodstream form pre-adaptation to the tsetse fly in Trypanosoma brucei.* Front Cell Infect Microbiol, 2013. **3**: p. 78.

33. Knusel, S. and I. Roditi, *Insights into the regulation of GPEET procyclin during differentiation from early to late procyclic forms of Trypanosoma brucei.* Mol Biochem Parasitol, 2013. **191**(2): p. 66-74.

34. Vassella, E., et al., *Expression of a major surface protein of Trypanosoma brucei insect forms is controlled by the activity of mitochondrial enzymes.* Mol Biol Cell, 2004. **15**(9): p. 3986-93.

35. Vassella, E., et al., *A major surface glycoprotein of trypanosoma brucei is expressed transiently during development and can be regulated post-transcriptionally by glycerol or hypoxia.* Genes Dev, 2000. **14**(5): p. 615-26.

36. Allmann, S., et al., *Glycerol suppresses glucose consumption in trypanosomes through metabolic contest.* PLoS Biol, 2021. **19**(8): p. e3001359.

37. Nolan, D.P., et al., *Characterization of a novel alanine-rich protein located in surface microdomains in Trypanosoma brucei.* J Biol Chem, 2000. **275**(6): p. 4072-80.

38. Sollelis, L. and M. Marti, *A Major Step towards Defining the Elusive Stumpy Inducing Factor in Trypanosoma brucei.* Trends Parasitol, 2019. **35**(1): p. 6-8.

39. Schuster, S., et al., *Unexpected plasticity in the life cycle of Trypanosoma brucei.* Elife, 2021. **10**.

40. Harashima, H., N. Dissmeyer, and A. Schnittger, *Cell cycle control across the eukaryotic kingdom.* Trends Cell Biol, 2013. **23**(7): p. 345-56.

41. McKean, P.G., *Coordination of cell cycle and cytokinesis in Trypanosoma brucei.* Curr Opin Microbiol, 2003. **6**(6): p. 600-7.

42. Woodward, R. and K. Gull, *Timing of nuclear and kinetoplast DNA replication and early morphological events in the cell cycle of Trypanosoma brucei.* J Cell Sci, 1990. **95 (Pt 1)**: p. 49-57.

43. Ogbadoyi, E., et al., *Architecture of the Trypanosoma brucei nucleus during interphase and mitosis.* Chromosoma, 2000. **108**(8): p. 501-13.

44. Berriman, M., et al., *The genome of the African trypanosome Trypanosoma brucei.* Science, 2005. **309**(5733): p. 416-22.

45. Clayton, C., *Regulation of gene expression in trypanosomatids: living with polycistronic transcription.* Open Biol, 2019. **9**(6): p. 190072.

46. Wedel, C., et al., *GT-rich promoters can drive RNA pol II transcription and deposition of H2A.Z in African trypanosomes.* EMBO J, 2017. **36**(17): p. 2581-2594.

47. Clayton, C., et al., *Control of mRNA degradation in trypanosomes.* Biochem Soc Trans, 2008. **36**(Pt 3): p. 520-1.

48. Gilinger, G. and V. Bellofatto, *Trypanosome spliced leader RNA genes contain the first identified RNA polymerase II gene promoter in these organisms.* Nucleic Acids Res, 2001. **29**(7): p. 1556-64.

49. Siegel, T.N., et al., *Four histone variants mark the boundaries of polycistronic transcription units in Trypanosoma brucei.* Genes Dev, 2009. **23**(9): p. 1063-76.

50. Hernandez, R. and A.M. Cevallos, *Ribosomal RNA gene transcription in trypanosomes.* Parasitol Res, 2014. **113**(7): p. 2415-24.

51. Michaeli, S., *Trans-splicing in trypanosomes: machinery and its impact on the parasite transcriptome.* Future Microbiol, 2011. **6**(4): p. 459-74.

52. Ullu, E., K.R. Matthews, and C. Tschudi, *Temporal order of RNA-processing reactions in trypanosomes: rapid trans splicing precedes polyadenylation of newly synthesized tubulin transcripts.* Mol Cell Biol, 1993. **13**(1): p. 720-5.

53. Siegel, T.N., et al., *Genome-wide analysis of mRNA abundance in two life-cycle stages of Trypanosoma brucei and identification of splicing and polyadenylation sites.* Nucleic Acids Res, 2010. **38**(15): p. 4946-57.

54. Nilsson, D., et al., *Spliced leader trapping reveals widespread alternative splicing patterns in the highly dynamic transcriptome of Trypanosoma brucei.* PLoS Pathog, 2010. **6**(8): p. e1001037.

55. Preusser, C., N. Jae, and A. Bindereif, *mRNA splicing in trypanosomes.* Int J Med Microbiol, 2012. **302**(4-5): p. 221-4.

56. Mishra, A., et al., *Selective nuclear export of mRNAs is promoted by DRBD18 in Trypanosoma brucei.* Mol Microbiol, 2021. **116**(3): p. 827-840.

57. Li, H. and C. Tschudi, *Novel and essential subunits in the 300-kilodalton nuclear cap binding complex of Trypanosoma brucei.* Mol Cell Biol, 2005. **25**(6): p. 2216-26.

58. Dostalova, A., et al., *The nuclear mRNA export receptor Mex67-Mtr2 of Trypanosoma brucei contains a unique and essential zinc finger motif.* Mol Microbiol, 2013. **88**(4): p. 728-39.

59. Lueong, S., et al., *Gene expression regulatory networks in Trypanosoma brucei: insights into the role of the mRNA-binding proteome.* Mol Microbiol, 2016. **100**(3): p. 457-71.

60. Clery, A., M. Blatter, and F.H. Allain, *RNA recognition motifs: boring? Not quite.* Curr Opin Struct Biol, 2008. **18**(3): p. 290-8.

61. De Gaudenzi, J., A.C. Frasch, and C. Clayton, *RNA-binding domain proteins in Kinetoplastids: a comparative analysis.* Eukaryot Cell, 2005. **4**(12): p. 2106-14.

62. Mugo, E. and C. Clayton, *Expression of the RNA-binding protein RBP10 promotes the bloodstream-form differentiation state in Trypanosoma brucei.* PLoS Pathog, 2017. **13**(8): p. e1006560.

63. Kolev, N.G., et al., *Developmental progression to infectivity in Trypanosoma brucei triggered by an RNA-binding protein.* Science, 2012. **338**(6112): p. 1352-3.

64. Kolev, N.G., E. Ullu, and C. Tschudi, *The emerging role of RNA-binding proteins in the life cycle of Trypanosoma brucei.* Cell Microbiol, 2014. **16**(4): p. 482-9.

65. Mugo, E., F. Egler, and C. Clayton, *Conversion of procyclic-form Trypanosoma brucei to the bloodstream form by transient expression of RBP10.* Mol Biochem Parasitol, 2017. **216**: p. 49-51.

66. Kramer, S., N.C. Kimblin, and M. Carrington, *Genome-wide in silico screen for CCCH-type zinc finger proteins of Trypanosoma brucei, Trypanosoma cruzi and Leishmania major.* BMC Genomics, 2010. **11**: p. 283.

67. Hendriks, E.F. and K.R. Matthews, *Disruption of the developmental programme of Trypanosoma brucei by genetic ablation of TbZFP1, a differentiation-enriched CCCH protein.* Mol Microbiol, 2005. **57**(3): p. 706-16.

68. Hendriks, E.F., et al., *A novel CCCH protein which modulates differentiation of Trypanosoma brucei to its procyclic form.* EMBO J, 2001. **20**(23): p. 6700-11.

69. Droll, D., et al., *Post-transcriptional regulation of the trypanosome heat shock response by a zinc finger protein.* PLoS Pathog, 2013. **9**(4): p. e1003286.

70. Singh, A., et al., *Trypanosome MKT1 and the RNA-binding protein ZC3H11: interactions and potential roles in post-transcriptional regulatory networks.* Nucleic Acids Res, 2014. **42**(7): p. 4652-68.

71. Subota, I., et al., *ALBA proteins are stage regulated during trypanosome development in the tsetse fly and participate in differentiation.* Mol Biol Cell, 2011. **22**(22): p. 4205-19.

72. Mani, J., et al., *Alba-domain proteins of Trypanosoma brucei are cytoplasmic RNA-binding proteins that interact with the translation machinery.* PLoS One, 2011. **6**(7): p. e22463.

73. Coller, J.M., et al., *The DEAD box helicase, Dhh1p, functions in mRNA decapping and interacts with both the decapping and deadenylase complexes.* RNA, 2001. **7**(12): p. 1717-27.

74. Wang, X., et al., *Modular recognition of RNA by a human pumilio-homology domain.* Cell, 2002. **110**(4): p. 501-12.

75. Archer, S.K., et al., *Trypanosoma brucei PUF9 regulates mRNAs for proteins involved in replicative processes over the cell cycle.* PLoS Pathog, 2009. **5**(8): p. e1000565.

76. Droll, D., et al., *The trypanosome Pumilio-domain protein PUF7 associates with a nuclear cyclophilin and is involved in ribosomal RNA maturation.* FEBS Lett, 2010. **584**(6): p. 1156-62.

77. Schumann Burkard, G., et al., *Nucleolar proteins regulate stage-specific gene expression and ribosomal RNA maturation in Trypanosoma brucei.* Mol Microbiol, 2013. **88**(4): p. 827-40.

78. Cassola, A., J.G. De Gaudenzi, and A.C. Frasch, *Recruitment of mRNAs to cytoplasmic ribonucleoprotein granules in trypanosomes.* Mol Microbiol, 2007. **65**(3): p. 655-70.

79. Cassola, A., *RNA Granules Living a Post-transcriptional Life: the Trypanosomes' Case.* Curr Chem Biol, 2011. **5**(2): p. 108-117.

80. Kramer, S., *RNA in development: how ribonucleoprotein granules regulate the life cycles of pathogenic protozoa.* Wiley Interdiscip Rev RNA, 2014. **5**(2): p. 263-84.

81. Gingras, A.C., B. Raught, and N. Sonenberg, *eIF4 initiation factors: effectors of mRNA recruitment to ribosomes and regulators of translation.* Annu Rev Biochem, 1999. **68**: p. 913-63.

82. Jackson, R.J., C.U. Hellen, and T.V. Pestova, *The mechanism of eukaryotic translation initiation and principles of its regulation.* Nat Rev Mol Cell Biol, 2010. **11**(2): p. 113-27.

83. Browning, K.S. and J. Bailey-Serres, *Mechanism of cytoplasmic mRNA translation.* Arabidopsis Book, 2015. **13**: p. e0176.

84. Furuichi, Y., *Discovery of m(7)G-cap in eukaryotic mRNAs.* Proc Jpn Acad Ser B Phys Biol Sci, 2015. **91**(8): p. 394-409.

85. Freire, E.R., et al., *The Role of Cytoplasmic mRNA Cap-Binding Protein Complexes in Trypanosoma brucei and Other Trypanosomatids.* Pathogens, 2017. **6**(4).

86. Pereira, M.M., et al., *The eIF4E subunits of two distinct trypanosomatid eIF4F complexes are subjected to differential post-translational modifications associated to distinct growth phases in culture.* Mol Biochem Parasitol, 2013. **190**(2): p. 82-6.

87. Niedzwiecka, A., et al., *Biophysical studies of eIF4E cap-binding protein: recognition of mRNA 5' cap structure and synthetic fragments of eIF4G and 4E-BP1 proteins.* J Mol Biol, 2002. **319**(3): p. 615-35.

88. Umenaga, Y., et al., *Identification and function of the second eIF4E-binding region in N-terminal domain of eIF4G: comparison with eIF4E-binding protein.* Biochem Biophys Res Commun, 2011. **414**(3): p. 462-7.

89. Marcotrigiano, J., et al., *Cap-dependent translation initiation in eukaryotes is regulated by a molecular mimic of eIF4G.* Mol Cell, 1999. **3**(6): p. 707-16.

90. Kamenska, A., C. Simpson, and N. Standart, *eIF4E-binding proteins: new factors, new locations, new roles.* Biochem Soc Trans, 2014. **42**(4): p. 1238-45.

91. Frydryskova, K., et al., *Distinct recruitment of human eIF4E isoforms to processing bodies and stress granules.* BMC Mol Biol, 2016. **17**(1): p. 21.

92. Rom, E., et al., *Cloning and characterization of 4EHP, a novel mammalian eIF4E-related cap-binding protein.* J Biol Chem, 1998. **273**(21): p. 13104-9.

93. Hernandez, G., et al., *Functional analysis of seven genes encoding eight translation initiation factor 4E (eIF4E) isoforms in Drosophila.* Mech Dev, 2005. **122**(4): p. 529-43.

94. Cho, P.F., et al., *A new paradigm for translational control: inhibition via 5'-3' mRNA tethering by Bicoid and the eIF4E cognate 4EHP.* Cell, 2005. **121**(3): p. 411-23.

95. Zoltner, M., et al., *Comparative proteomics of the two T. brucei PABPs suggests that PABP2 controls bulk mRNA.* PLoS Negl Trop Dis, 2018. **12**(7): p. e0006679.

96. da Costa Lima, T.D., et al., *Functional characterization of three leishmania poly(a) binding protein homologues with distinct binding properties to RNA and protein partners.* Eukaryot Cell, 2010. **9**(10): p. 1484-94.

97. Freire, E.R., et al., *The four trypanosomatid eIF4E homologues fall into two separate groups, with distinct features in primary sequence and biological properties.* Mol Biochem Parasitol, 2011. **176**(1): p. 25-36.

98. Freire, E.R., et al., *eIF4F-like complexes formed by cap-binding homolog TbEIF4E5 with TbEIF4G1 or TbEIF4G2 are implicated in post-transcriptional regulation in Trypanosoma brucei.* RNA, 2014. **20**(8): p. 1272-86.

99. Freire, E.R., et al., *Trypanosoma brucei translation initiation factor homolog EIF4E6 forms a tripartite cytosolic complex with EIF4G5 and a capping enzyme homolog.* Eukaryot Cell, 2014. **13**(7): p. 896-908.

100. Terrao, M., et al., *The suppressive cap-binding complex factor 4EIP is required for normal differentiation.* Nucleic Acids Res, 2018. **46**(17): p. 8993-9010.

101. Zinoviev, A., et al., *A novel 4E-interacting protein in Leishmania is involved in stage-specific translation pathways.* Nucleic Acids Res, 2011. **39**(19): p. 8404-15.

102. Meleppattu, S., et al., *Structural basis for LeishIF4E-1 modulation by an interacting protein in the human parasite Leishmania major.* Nucleic Acids Res, 2018. **46**(7): p. 3791-3801.

103. Freire, E.R., et al., *Trypanosoma brucei EIF4E2 cap-binding protein binds a homolog of the histone-mRNA stem-loop-binding protein.* Curr Genet, 2018. **64**(4): p. 821-839.

104. Erkmann, J.A., et al., *Nuclear import of the stem-loop binding protein and localization during the cell cycle.* Mol Biol Cell, 2005. **16**(6): p. 2960-71.

105. Thelie, A., et al., *An oocyte-preferential histone mRNA stem-loop-binding protein like is expressed in several mammalian species.* Mol Reprod Dev, 2012. **79**(6): p. 380-91.

106. Marzluff, W.F., E.J. Wagner, and R.J. Duronio, *Metabolism and regulation of canonical histone mRNAs: life without a poly(A) tail.* Nat Rev Genet, 2008. **9**(11): p. 843-54.

107. Dhalia, R., et al., *Translation initiation in Leishmania major: characterisation of multiple eIF4F subunit homologues.* Mol Biochem Parasitol, 2005. **140**(1): p. 23-41.

108. Moura, D.M., et al., *Two related trypanosomatid eIF4G homologues have functional differences compatible with distinct roles during translation initiation.* RNA Biol, 2015. **12**(3): p. 305-19.

109. Erben, E.D., et al., *A genome-wide tethering screen reveals novel potential post-transcriptional regulators in Trypanosoma brucei.* PLoS Pathog, 2014. **10**(6): p. e1004178.

110. Klein, C., et al., *Polysomes of Trypanosoma brucei: Association with Initiation Factors and RNA-Binding Proteins.* PLoS One, 2015. **10**(8): p. e0135973.

111. Kramer, S., et al., *Differential localization of the two T. brucei poly(A) binding proteins to the nucleus and RNP granules suggests binding to distinct mRNA pools.* PLoS One, 2013. **8**(1): p. e54004.

112. Dejung, M., et al., *Quantitative Proteomics Uncovers Novel Factors Involved in Developmental Differentiation of Trypanosoma brucei.* PLoS Pathog, 2016. **12**(2): p. e1005439.

113. Melo do Nascimento, L., et al., *The RNA-associated proteins MKT1 and MKT1L form alternative PBP1-containing complexes in Trypanosoma brucei.* J Biol Chem, 2020. **295**(32): p. 10940-10955.

114. Fadda, A., et al., *Transcriptome-wide analysis of trypanosome mRNA decay reveals complex degradation kinetics and suggests a role for co-transcriptional degradation in determining mRNA levels.* Mol Microbiol, 2014. **94**(2): p. 307-26.

115. Schwede, A., et al., *A role for Caf1 in mRNA deadenylation and decay in trypanosomes and human cells.* Nucleic Acids Res, 2008. **36**(10): p. 3374-88.

116. Estevez, A.M., T. Kempf, and C. Clayton, *The exosome of Trypanosoma brucei.* EMBO J, 2001. **20**(14): p. 3831-9.

117. Li, C.H., et al., *Roles of a Trypanosoma brucei 5'->3' exoribonuclease homolog in mRNA degradation.* RNA, 2006. **12**(12): p. 2171-86.

118. Kramer, S., *The ApaH-like phosphatase TbALPH1 is the major mRNA decapping enzyme of trypanosomes.* PLoS Pathog, 2017. **13**(6): p. e1006456.

119. Ernst, N.L., et al., *TbMP57 is a 3' terminal uridylyl transferase (TUTase) of the Trypanosoma brucei editosome.* Mol Cell, 2003. **11**(6): p. 1525-36.

120. Aphasizhev, R., I. Aphasizheva, and L. Simpson, *Multiple terminal uridylyltransferases of trypanosomes.* FEBS Lett, 2004. **572**(1-3): p. 15-8.

121. Lim, J., et al., *Uridylation by TUT4 and TUT7 marks mRNA for degradation.* Cell, 2014. **159**(6): p. 1365-76.

122. Falk, F., K. Kamanyi Marucha, and C. Clayton, *The EIF4E1-4EIP cap-binding complex of Trypanosoma brucei interacts with the terminal uridylyl transferase TUT3.* PLoS One, 2021. **16**(11): p. e0258903.

123. Tyanova, S., et al., *The Perseus computational platform for comprehensive analysis of (prote)omics data.* Nat Methods, 2016. **13**(9): p. 731-40.

124. Melo do Nascimento, L., et al., *Functional insights from a surface antigen mRNA-bound proteome.* Elife, 2021. **10**.

125. Dillon, L.A., et al., *Transcriptomic profiling of gene expression and RNA processing during Leishmania major differentiation.* Nucleic Acids Res, 2015. **43**(14): p. 6799-813.

126. Mabille, D., et al., *4E Interacting Protein as a Potential Novel Drug Target for Nucleoside Analogues in Trypanosoma brucei.* Microorganisms, 2021. **9**(4).

127. Mackey, Z.B., et al., *High-throughput analysis of an RNAi library identifies novel kinase targets in Trypanosoma brucei.* Chem Biol Drug Des, 2011. **78**(3): p. 454-63.

128. Tupperwar, N., et al., *A newly identified Leishmania IF4E-interacting protein, Leish4E-IP2, modulates the activity of cap-binding protein paralogs.* Nucleic Acids Res, 2020. **48**(8): p. 4405-4417.

129. Baron, N., et al., *Distinct features of the Leishmania cap-binding protein LeishIF4E2 revealed by CRISPR-Cas9 mediated hemizygous deletion.* PLoS Negl Trop Dis, 2021. **15**(3): p. e0008352.

130. Ruscica, V., et al., *Direct role for the Drosophila GIGYF protein in 4EHP-mediated mRNA repression.* Nucleic Acids Res, 2019. **47**(13): p. 7035-7048.

131. Amaya Ramirez, C.C., et al., *4EHP-independent repression of endogenous mRNAs by the RNA-binding protein GIGYF2.* Nucleic Acids Res, 2018. **46**(11): p. 5792-5808.

132. Yoffe, Y., et al., *Binding specificities and potential roles of isoforms of eukaryotic initiation factor 4E in Leishmania.* Eukaryot Cell, 2006. **5**(12): p. 1969-79.

133. Labrecque, R., et al., *Chromatin remodelling and histone m RNA accumulation in bovine germinal vesicle oocytes.* Mol Reprod Dev, 2015. **82**(6): p. 450-62.

134. Sheader, K., et al., *Variant surface glycoprotein RNA interference triggers a precytokinesis cell cycle arrest in African trypanosomes.* Proc Natl Acad Sci U S A, 2005. **102**(24): p. 8716-21.

135. Ooi, C.P., et al., *Blocking variant surface glycoprotein synthesis alters endoplasmic reticulum exit sites/Golgi homeostasis in Trypanosoma brucei.* Traffic, 2018. **19**(6): p. 391-405.

136. Maudlin, I.E., et al., *VSG mRNA levels are regulated by the production of functional VSG protein.* Mol Biochem Parasitol, 2021. **241**: p. 111348.

137. Liu, D., et al., *Faster growth with shorter antigens can explain a VSG hierarchy during African trypanosome infections: a feint attack by parasites.* Sci Rep, 2018. **8**(1): p. 10922.